***Final Report***

# INVESTIGATION OF THE IMPACT OF MILLING AND CONSTRUCTION ON THE BOND STRENGTH OF REMAINING THIN (SCAB) LAYERS

UF Project No.: AWD05456
Contact No.: BDV31 977-104

*Submitted to:*

Florida Department of Transportation
605 Suwannee Street MS-30
Tallahassee, FL, 32399

Dr. Jian Zou
Dr. Reynaldo Roque, P.E.
George Lopp

Department of Civil and Coastal Engineering
College of Engineering
365 Weil Hall, P.O. Box 116580
Gainesville, FL, 32611-6580
Tel: (352) 294-7799
Fax: (352) 392-3394

**November 2022**

DISCLAIMER

The option, findings, and conclusions expressed in this publication are those of the authors and not necessarily those of the State of Florida Department of Transportation.

Prepared in cooperation with the State of Florida Department of Transportation.

# SI* (MODERN METRIC) CONVERSION FACTORS

## APPROXIMATE CONVERSIONS TO SI UNITS

| SYMBOL | WHEN YOU KNOW | MULTIPLY BY | TO FIND | SYMBOL |
|---|---|---|---|---|
| | | **LENGTH** | | |
| in | inches | 25.4 | millimeters | mm |
| ft | feet | 0.305 | meters | m |
| yd | yards | 0.914 | meters | m |
| mi | miles | 1.61 | kilometers | km |
| | | **AREA** | | |
| $in^2$ | square inches | 645.2 | square millimeters | $mm^2$ |
| $ft^2$ | square feet | 0.093 | square meters | $m^2$ |
| $yd^2$ | square yard | 0.836 | square meters | $m^2$ |
| ac | acres | 0.405 | hectares | ha |
| $mi^2$ | square miles | 2.59 | square kilometers | $km^2$ |
| | | **VOLUME** | | |
| fl oz | fluid ounces | 29.57 | milliliters | mL |
| gal | gallons | 3.785 | liters | L |
| $ft^3$ | cubic feet | 0.028 | cubic meters | $m^3$ |
| $yd^3$ | cubic yards | 0.765 | cubic meters | $m^3$ |
| | NOTE: volumes greater than 1000 L shall be shown in $m^3$ | | | |
| | | **MASS** | | |
| oz | ounces | 28.35 | grams | g |
| lb | pounds | 0.454 | kilograms | kg |
| T | short tons (2000 lb) | 0.907 | megagrams (or "metric ton") | Mg (or "t") |
| | | **TEMPERATURE (exact degrees)** | | |
| °F | Fahrenheit | 5 (F-32)/9<br>or (F-32)/1.8 | Celsius | °C |
| | | **ILLUMINATION** | | |
| fc | foot-candles | 10.76 | lux | lx |
| fl | foot-Lamberts | 3.426 | $candela/m^2$ | $cd/m^2$ |
| | | **FORCE and PRESSURE or STRESS** | | |
| lbf | poundforce | 4.45 | newtons | N |
| $lbf/in^2$ | poundforce per square inch | 6.89 | kilopascals | kPa |

## APPROXIMATE CONVERSIONS FROM SI UNITS

| SYMBOL | WHEN YOU KNOW | MULTIPLY BY | TO FIND | SYMBOL |
|---|---|---|---|---|
| | | **LENGTH** | | |
| mm | millimeters | 0.039 | inches | in |
| m | meters | 3.28 | feet | ft |
| m | meters | 1.09 | yards | yd |
| km | kilometers | 0.621 | miles | mi |
| | | **AREA** | | |
| $mm^2$ | square millimeters | 0.0016 | square inches | $in^2$ |
| $m^2$ | square meters | 10.764 | square feet | $ft^2$ |
| $m^2$ | square meters | 1.195 | square yards | $yd^2$ |
| ha | hectares | 2.47 | acres | ac |
| $km^2$ | square kilometers | 0.386 | square miles | $mi^2$ |
| | | **VOLUME** | | |
| mL | milliliters | 0.034 | fluid ounces | fl oz |
| L | liters | 0.264 | gallons | gal |
| $m^3$ | cubic meters | 35.314 | cubic feet | $ft^3$ |
| $m^3$ | cubic meters | 1.307 | cubic yards | $yd^3$ |
| | | **MASS** | | |
| g | grams | 0.035 | ounces | oz |
| kg | kilograms | 2.202 | pounds | lb |
| Mg (or "t") | megagrams (or "metric ton") | 1.103 | short tons (2000 lb) | T |
| | | **TEMPERATURE (exact degrees)** | | |
| °C | Celsius | 1.8C+32 | Fahrenheit | °F |
| | | **ILLUMINATION** | | |
| lx | lux | 0.0929 | foot-candles | fc |
| $cd/m^2$ | $candela/m^2$ | 0.2919 | foot-Lamberts | fl |
| | | **FORCE and PRESSURE or STRESS** | | |
| N | newtons | 0.225 | poundforce | lbf |
| kPa | kilopascals | 0.145 | poundforce per square inch | $lbf/in^2$ |

*SI is the symbol for the International System of Units. Appropriate rounding should be made to comply with Section 4 of ASTM E380.

(Revised March 2003)

| 1. Report No. | 2. Government Accession No. | 3. Recipient's Catalog No. | |
|---|---|---|---|
| 4. Title and Subtitle<br>Investigation of the Impact of Milling and Construction on the Bond Strength of Remaining Thin (Scab) Layers | | 5. Report Date<br>November 2022<br>6. Performing Organization Code | |
| 7. Author(s)<br>Jian Zou, Reynaldo Roque, and George Lopp | | 8. Performing Organization Report No. | |
| 9. Performing Organization Name and Address<br>University of Florida<br>Department of Civil and Coastal Engineering<br>365 Weil Hall, PO Box 116580<br>Gainesville, FL 32611-6580 | | 10. Work Unit No. (TRAIS)<br>11. Contract or Grant No.<br>BDV31-977-104 | |
| 12. Sponsoring Agency Name and Address<br>Florida Department of Transportation<br>Research Center, MS 30<br>605 Suwannee Street<br>Tallahassee, FL, 32399-0450 | | 13. Type of Report and Period Covered<br>Draft Final<br>12/20/18-11/30/22<br>14. Sponsoring Agency Code | |
| 15. Supplementary Notes | | | |
| 16. Abstract: Field investigation in Florida indicated that there was a potential link between weakly-bonded scabbed areas and slippage failure in the braking zones. Also, evidence from NCAT test track studies suggested that localized interface debonding might lead to surface cracking under free-rolling traffic. The primary objective of this research was to determine critical responses and potential distress in asphalt overlay with scabbing. To achieve the objective, both conventional analysis assuming a global interface representation and finite element analysis with a hybrid interface representation were conducted to evaluate the effect of weakly-bonded scabbed layer on pavement responses and potential distress. Furthermore, impact analysis was performed to investigate whether compaction of overlay would weaken the bond below the scabbed layer. This research revealed that under the free-rolling condition, the presence of weakly-bonded scabbed area has the potential to cause near-surface cracking initiated at the upper interface for intermediate and large size scabs, and reflective cracking at the lower interface and further interface debonding at the edge of the scab for intermediate size scab. Under the braking condition, the presence of poorly-bonded scabbed area would most likely cause slippage at the overlay surface for intermediate and large size scabs. It would increase the potential of further interface debonding for intermediate size scab. Also, it would increase the potential of near-surface cracking and reflective cracking regardless of scab size. Roller compaction would likely weaken the bond below the scabbed area. Vibratory rollers would induce more critical conditions than oscillatory rollers. Therefore, the following guidelines are provided for dealing with scabbed sections: i) Make every effort to set the milling depth to minimize scabbing during resurfacing; ii) Loose scabbing should be removed prior to resurfacing; and iii) Consider removing isolated scabbed areas or scabbed areas adjacent to critical locations such as intersections and other braking areas. | | | |
| 17. Key Words: Scabbing, full bond, global partial bond, localized partial, hybrid interface representation, interface reaction modulus, slippage, near-surface cracking, interface debonding. | | 18. Distribution Statement<br>No restrictions | |
| 19. Security Classif. (of this report)<br>Unclassified | 20. Security Classif. (of this page)<br>Unclassified | 21. No of Pages<br>112 | 22. Price |

Form DOT F 1700.7 (8-72)

ACKNOWLEDGEMENT

The authors would like to acknowledge and thank the Florida Department of Transportation (FDOT) for providing technical and financial support and materials for this project. Special thanks go to project manager Wayne Rilko and engineers and technicians of the Bituminous Section of the State Materials Office for their contributions throughout the various phases of this project. The authors also would like to acknowledge and thank former graduate students at the University of Florida: Dr. Ziqian Han, Zhengyu Wu, and Junyi Duan for their help in completing this project.

# EXECUTIVE SUMMARY

Milling is used to remove existing pavement distresses prior to resurfacing. The milled surface generally provides a better bond with the new overlay than a non-milled surface (Sholar et al., 2004, Tashman et al., 2008, Das et al., 2017). However, if the depth of milling is close to the interface between previously paved HMA lifts, a thin layer of the upper lift may be left behind, which is referred to as a scabbed layer or scabbing.

Field investigation in Florida indicated there was a potential link between weakly-bonded scabbed areas and slippage failure, which was likely caused by high lateral stresses from braking condition. Furthermore, evidence from NCAT test track studies suggested that localized interface debonding might lead to surface cracking (Willis and Timm, 2007). While slippage is a local distress that primarily appears in braking zones, bending-induced surface cracking under free-rolling traffic could potentially be more prevalent on highways and represent a greater concern. This study focused on responses and potential distress, including slippage and surface longitudinal cracking in asphalt overlay, associated with the presence of partially or fully debonded scabbed areas. In addition, Muench and Moomaw (2008) reported that compaction of overlay, especially by vibratory roller, may weaken the bond below or even break up the scabbed areas. In other words, even if the bond below scabbed area remains strong after milling, it may be weakened by roller compaction during overlay construction. Therefore, the impact of roller compaction on stresses near the scabbed area was also investigated.

The primary objective of this research was to determine critical responses and potential distress in asphalt overlay associated with the presence of scabbing. To achieve the objective, both conventional analysis assuming a global interface representation and finite element analysis with a hybrid interface representation were conducted to evaluate the effect of weakly-bonded scabbed layer on pavement responses and potential distress. Furthermore, impact analysis was performed to investigate whether compaction of overlay would weaken the bond below the scabbed layer. It was found that the conventional analysis with the global interface (scabbing) representation provided an efficient tool to access the effect of weakly-boned scabbed layer on

pavement responses without considering scab size. Results showed that a higher AC-to-base stiffness ratio and a thinner underlying AC generally resulted in more critical responses. The finite element analysis with the hybrid interface representation allowed more comprehensive evaluation of the effect of weakly-bonded scabbed layer on pavement responses. Results showed that a localized partial bond condition clearly led to more critical responses than a global partial bond condition. Results from both conventional analysis and finite element analysis showed that a weak bond led to more critical responses. The addition of a horizontal load in the braking zones consistently resulted in significantly higher tension at the surface of the overlay and higher tension and shear at the interface.

Further analysis with the finite element approach showed an intermediate scab size (with a radius in the range of one to two times the radius of the load) appeared to induce the most critical responses. When the scab size increased to about five times the radius of the load, the stress distributions became almost identical to those from the global partial bond condition under both free-rolling and braking loads. Increasing overlay thickness generally resulted in lower tension at the lower interface and at the surface of the overlay. A thicker overlay had slightly higher shear at the edge of the scab. A less stiff overlay mixture resulted in slightly lower tension at the surface of the overlay and lower shear at the edge of the scab. Lower overlay stiffness generally led to higher tension at the lower interface. The approach using drum impact successfully reproduced the rocking motion of compaction associated with oscillatory rollers. Further analysis with drum impact showed that compaction of asphalt overlay with scabbing induced critical stress states that may lead to debonding at the interface between the scabbed layer and the underlying AC layer.

Based on the findings of this study, it was concluded that under the free-rolling condition, the presence of weakly-bonded scabbed area has the potential to cause near-surface cracking initiated at the upper interface below the center of the load for intermediate and large size scabs, and reflective cracking at the lower interface below the edge of the scab and further interface debonding at the edge of the scab for intermediate size scab. Under the braking condition, the presence of poorly-bonded scabbed area would most likely cause slippage at the overlay surface behind the back edge of the wheel load for intermediate and large size scabs. It would increase

the potential of further interface debonding ahead of the front edge of the scabbed area for intermediate size scab. Also, it would increase the potential of near-surface cracking at the upper interface below the center of the load and reflective cracking at the lower interface below the edge of the scab regardless of scab size. Roller compaction would likely weaken the bond below the scabbed area if it was fully bonded to the underlying AC layer before the compaction. Vibratory rollers would induce more critical conditions than oscillatory rollers. It is important to note that although this study showed a small size scab (2.5-inch radius and 0.25-inch thickness) did not cause critical responses under free-rolling condition, a recent HVS study (Kwon et al., 2022) reported that surface cracks were observed in pavement sections with moderate scabbing involving multiple scattered small scabs (0.25-inch thickness). Therefore, the following guidelines are provided for dealing with scabbed sections: i) Make every effort to set the milling depth to minimize scabbing during resurfacing; ii) Loose scabbing should be removed prior to resurfacing; and iii) Consider removing isolated scabbed areas or scabbed areas adjacent to critical locations such as intersections and other braking areas.

Regarding future work, it is recommended that in addition to a single scabbed area, the existence of multiple weakly-bonded scabs should be considered for further modeling and analysis to have a better understanding of the effect of scabbing on pavement responses and potential distress. Furthermore, simulation of the milling operation is recommended to determine whether the remaining scabbed layer would potentially have a weaker bond than prior to the milling process.

TABLE OF CONTENTS

LIST OF TABLES

LIST OF FIGURES

# CHAPTER 1
# INTRODUCTION

## 1.1 Problem Statement

Milling is typically used to remove pavement exhibiting top-down cracking (near-surface longitudinal cracking), which is the most common distress in asphalt pavement due for rehabilitation in Florida. Top-down cracks typically have a wider opening near the surface and get narrower with depth (Roque et al., 2011). Although in a few cases top-down cracks were observed to propagate through all asphalt layers, most cracks stopped at the top layer of HMA. Milling helps remove the aged and cracked top asphalt layer, and a milled surface generally provides a better bond with the new overlay than a non-milled surface (Sholar et al., 2004, Tashman et al., 2008, Das et al., 2017). However, if the depth of milling is close to the interface between previously paved HMA lifts, a thin layer of the upper lift may be left behind, which is referred to as a scabbed layer or scabbing (Figure 1-1).

In their case studies for interface debonding in Washington State (Figure 1-2), Muench and Moomaw (2008) reported that weakly bonded thin layers (scabbing) remained after milling. They speculated the weak bond between the scabbed layer and the underlying layer might be caused by either poor tack coat adhesion or water infiltration through surface cracking or an inadequately compacted surface layer. If these scabbed layers were not removed, any HMA paved over them would not be properly bonded to the pavement structure. Therefore, a sweeper, motor grader blade or loader bucket were recommended to loosen and remove these thin layers. In a nationwide study on best practices for RAP management, West et al. (2013) recommended adjusting the milling depth to remove the scabbed area if scabbing was observed at the milling surface. They suspected performance of the overlay would severely diminish if such a weakly bonded area was allowed to remain in place.

(a) 2″ milling

(b) 1-3/4″ milling

Figure 1-1 Milled surfaces showing scabbing in Florida (Photos courtesy of FDOT district engineers).

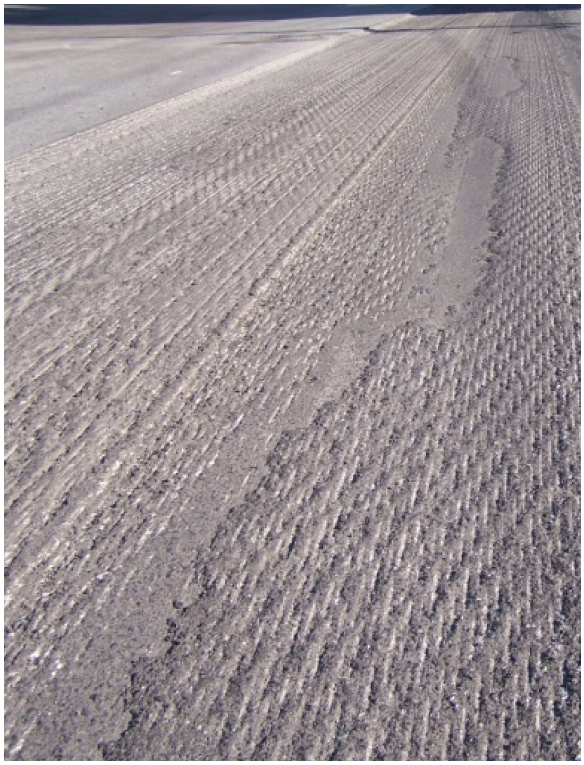

(a) Milled surface of SR 28

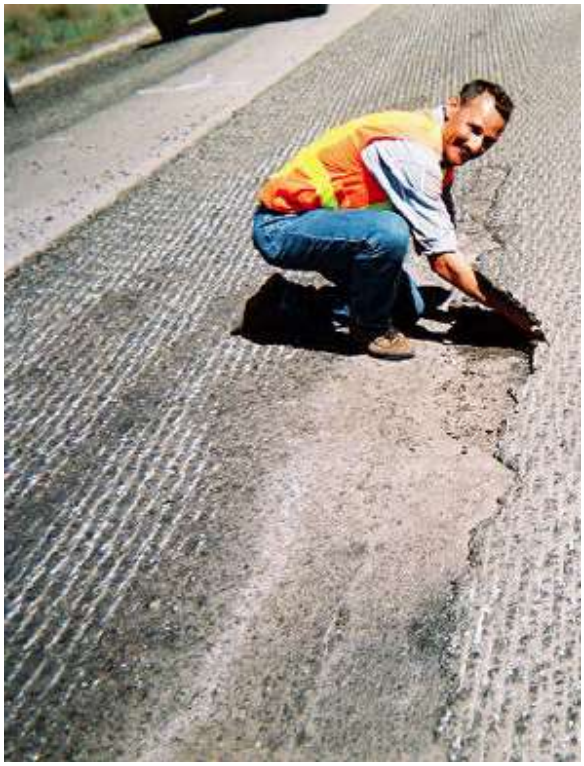

(b) Milled surfare of SR 97A

Figure 1-2 Milled surface showing weakly bonded scabbed layers (Muench and Moomaw, 2008).

Recently, slippage failures were observed in several locations within a one-mile section of roadway placed on the Westbound I-4 exit ramp to SR-536 (Figure 1-3). The typical section for this ramp consists of a milling depth of 2.25 inch and resurfacing with 1.5-inch Type SP structural course (Traffic C, PG 76-22 PMA) and 0.75-inch friction course FC-5 (PG 76-22 PMA). Placement of more than 23 lane miles of the structural course began in April 2014 and was completed in November 2014. Areas of slippage were discovered in December 2014. Based on field observations and interlayer bond strength test results, an investigation effort led by the FDOT concluded the slippage problem could be associated with a weak bond at or near the interface of the interlayer below the milled surface. Figure 1-4 shows two cores taken from areas near one slippage location. Both indicated debonding below the scabbed layer.

(a) Slippage at Location 1 (b) Slippage at Location 2

Figure 1-3 Slippage failure observed on the Westbound I-4 single-lane exit ramp (Photos courtesy of FDOT district engineers).

(a) Core 1 (b) Core 2

Figure 1-4 Cores taken from areas near Slippage Location 2 (Photos courtesy of FDOT district engineers).

As shown in Figure 1-5, it appeared a weak bond existed between the scabbed layer and the underlying asphalt layer. As opposed to full bond condition, the localized weak bond (partial bond) will lead to stress redistribution in the overlay, which may result in pavement distress such as slippage cracking under braking condition or surface longitudinal cracking due to bending-induced tension. However, the mechanisms of potential distress have not been fully investigated. Therefore, further research is needed to evaluate the impact of scabbing on stress redistribution in the overlay and its potential effect on overlay performance.

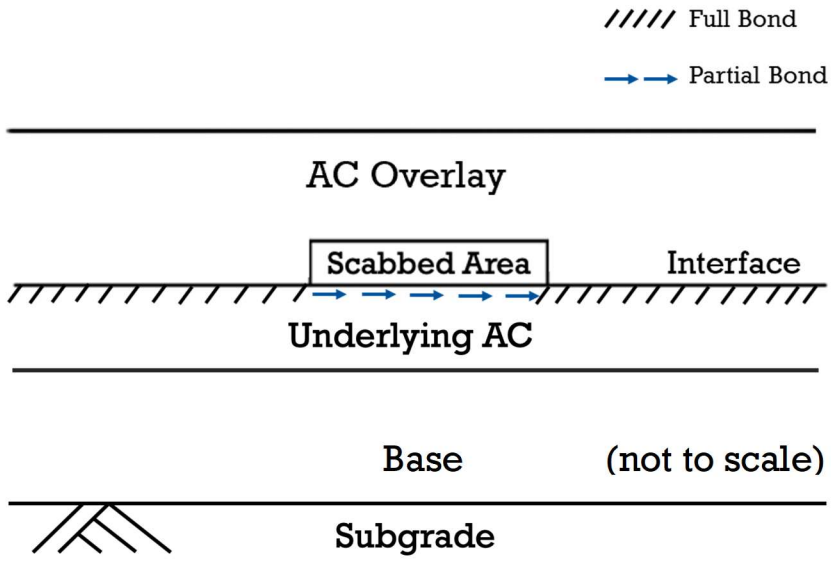


Figure 1-5 Schematic of localized weak bond under the scabbed layer along with full bond elsewhere for a hybrid interface bonding condition.

## 1.2 Scope

Field investigation in Florida indicated there was a potential link between weakly-bonded scabbed areas and slippage failure, which is likely caused by high lateral stresses from braking condition. Furthermore, evidence from NCAT test track studies suggested that localized interface debonding might lead to surface cracking (Willis and Timm, 2007). While slippage is a local distress that appears in braking zones, bending-induced surface cracking under free-rolling traffic could potentially be more prevalent on highways and represent a greater concern. Therefore, this study will focus on responses and potential distress, including slippage and surface longitudinal cracking in asphalt overlay, associated with the presence of partially or fully debonded scabbed areas. In addition, Muench and Moomaw (2008) reported that compaction of overlay, especially by vibratory roller, may weaken the bond below or even break up the scabbed areas. In other words, even if the bond below scabbed areas remains strong after milling, it may be weakened by roller compaction during overlay construction. Therefore, an investigation of the impact of roller compaction on stresses near the scabbed area is also warranted.

## 1.3 Objectives

The primary objective of this research is to determine the potential effect of scabbing on overlay performance. Detailed objectives of this project are:

- Evaluate the effect of relevant factors, e.g., size and thickness of partially or fully debonded scabbed areas, on potential pavement distress.
- Investigate whether compaction of overlay may weaken the bond below the scabbed area.
- Provide guidelines for dealing with scabbed pavement sections.

## 1.4 Research Approach

The proposed research approach is illustrated in Figure 1-6. It involves development of models to evaluate the potential effect of a weakly bonded scabbed area on pavement distress, as well as models to determine the effect of compaction on the bond below the scabbed area. Analyses and interpretation of simulation results will be performed to establish guidelines for dealing with scabbed pavement sections.

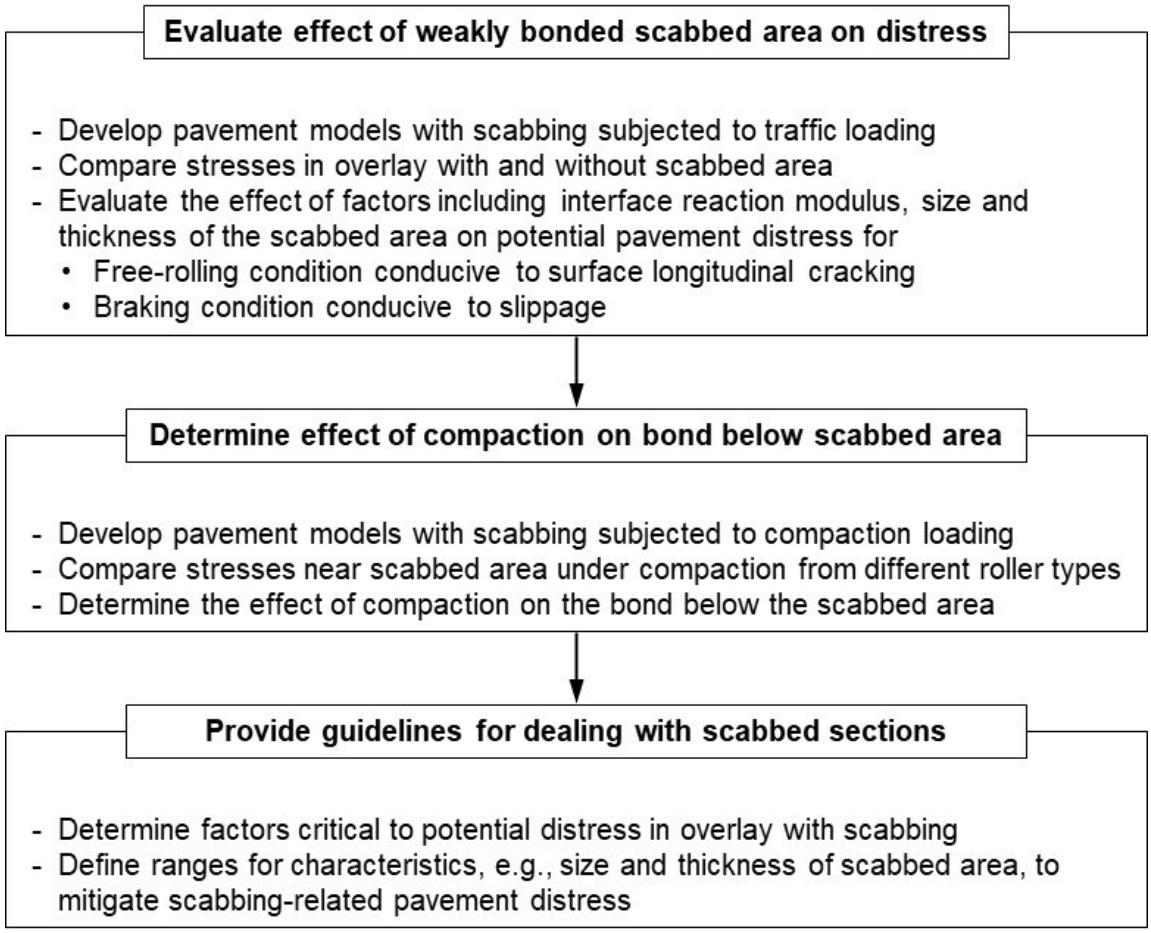


Figure 1-6 Overall research approach for this project.

# CHAPTER 2
# LITERATURE REVIEW

Very few studies have been carried out to evaluate the effect of scabbing on pavement responses and/or performance. Therefore, a literature review was conducted to explore a broader topic, i.e., the effect of interface bond on pavement performance, including interface bond characterization tests, field evaluation, and interface modeling efforts.

## 2.1 Interface Material and Bond Characterization

Three interface materials (asphalt cement, cutback asphalt and emulsified asphalt) have been used as tack coats to bond the interfaces of asphalt layers. However, both asphalt cement and cutback asphalts have disadvantages associated with their use. Asphalt cement requires excessive heating to achieve proper viscosity for spraying purposes and it cools rapidly when placed in the field. Cutback asphalts are not typically used due to environmental concern. A recent survey conducted as part of the NCHRP Project 9-40 (Mohammad et al., 2012) showed asphalt emulsions, asphalt cement, and asphalt cutbacks were used by 100%, 26%, and 21% of the agencies that responded, respectively.

Emulsions are practical applications for tack coats as they flow easily and provide a uniform application when sprayed (Leng et al., 2008). Emulsions are classified based on the electronic charge surrounding the asphalt binder particles (i.e., anionic, cationic, and nonionic) and on how quickly the asphalt droplets will coalesce (e.g., slow-setting and rapid-setting). Emulsions are further identified by a series of numbers and letters related to the viscosity of the emulsions (the number 2 is for higher viscosity than the number 1), the hardness of the base asphalt binders (the letter h indicates a harder base binder), and the presence of polymer modification (indicated by the letter P). Through a vast literature review and a worldwide survey, Mohammad et al. (2012) found that slow-setting emulsions are the most frequently used tack coat materials, either anionic or cationic, followed at a great distance by rapid-setting emulsions. The use of a slow-setting emulsion may be counterintuitive since this type of emulsion takes a long time to set and is considered the preferable choice for prime coats. However, slow-setting emulsions can be diluted, which brings the advantage of better flow and more uniform spray application (Asphalt

Institute 2001, 2008; Mohammad et al., 2012). With respect to application rates, residual binder application typically varies from 0.09 to 0.36 L/m$^2$ (0.02 to 0.08 gal/yd$^2$) depending on surface conditions (new, old, milled, etc.).

Recently, non-tracking emulsions were designed to mitigate tracking problems associated with traditional tacks. A significant variety of proprietary emulsions or additives are available and marketed as non-tracking. However, it is more accurate to call these emulsions "reduced-tracking," because they still require at least some time to set, even though the time is reduced from traditional emulsions (Gierhart and Johnson, 2018). They typically use a harder base asphalt binder that leaves a less tacky finish at ambient temperatures for reduced tracking while achieving good bond strengths when reactivated at overlay construction temperatures. FDOT has criteria for trackless properties and bond strength when approving reduced-tracking tack coats, i.e., the material must show little to no tracking and have a minimum bond strength value of 100 psi tested at a loading rate of 2 in/min and 25°C for approval (FDOT, 2016). Reduced-tracking materials do not currently have an AASHTO specification (Gierhart and Johnson, 2018).

### 2.1.1 Interface shear bond tests

Tests in shear, tension, and torque modes have been developed and employed by various researchers and engineers to characterize interface bond (Mohammad et al., 2012). Shear mode is most widely used because it is more representative of stress states experienced by tack coat materials at the interface. Interface shear bond tests generally have two loading types: monotonic loading and cyclic loading. Monotonic loading shear bond tests are commonly used to rank tack coat materials based on shear strength values. A wide range of loading rates (0.02 to 2 in/min) have been used to characterize shear bond of interface materials for both laboratory-compacted samples and field cores. Due to the viscoelastic nature of asphalt material, interface reaction modulus and shear strength generally increase with increasing loading rate. The most common loading rate used in the U.S. and Europe is 2.0 in/min (Table 2-1). This is the displacement rate at which the Marshall apparatus is geared to operate. Compared to monotonic loading, cyclic/repeated loading is more consistent with field loading conditions and the resulting progressive debonding mechanism. However, cyclic loading has only been employed in research-grade tests on laboratory-compacted samples due to more sophisticated equipment,

technician training, and a longer testing time (Diakhaté et al., 2011, Tozzo et al., 2014, and Isailovic et al., 2017).

Table 2-1 Monotonic interface shear bond tests with varying loading rates.

| Loading Type | Loading Rate | Location (Reference) |
|---|---|---|
| Monotonic | 2.0 in./min | United Kingdom (Sangiorgi et al., 2002) |
| | | Florida (Sholar et al., 2004) |
| | | Switzerland (Raab and Partl, 2004) |
| | | Alabama (West et al., 2005) |
| | | Virginia (McGhee et al., 2009) |
| | | North Carolina (Cho et al., 2017) |
| | 0.5 in./min | Louisiana (Romanoschi and Metcalf, 2001a) |
| | 0.3 in./min | Illinois (Hasiba, 2012) |
| | 0.2 in./min | Texas (Wilson et al., 2016) |
| | | North Carolina (Cho et al., 2017) |
| | 0.1 in./min | Israel (Uzan et al., 1978) |
| | | Italy (Canestrari and Santagata, 2005) |
| | | Louisiana (Mohammad et al., 2012) |
| | 0.02 in./min | North Carolina (Cho et al., 2017) |

### 2.1.2 Factors affecting bond strength

A summary of findings in terms of factors affecting bond strength based on results of monotonic loading shear bond tests reported in the literature is presented as follows:

- Interface shear strength decreases with increasing temperature. Asphalt is highly susceptible to temperature, showing a reduction in strength as temperature rises.
- Interface shear strength increases with increasing normal pressure (i.e., confinement). Asphalt materials follow a Mohr-Coulomb type failure criterion and, as such, shear resistance increases with the level of confinement. For a given shear stress level, a stress state with lower normal pressure will fall closer to the failure criterion and will be potentially more susceptible to interface failure.
- According to the results of Mohammad et al. (2012), interface shear strength increased with viscosity (both rotational and absolute viscosity) and hardness (measured from penetration test) of binder residue. Three emulsions were evaluated in their study, i.e.,

CRS-1 (cationic rapid-setting), SS-1h (anionic slow-setting with a hard binder), and NTSS-1hM (non-tracking anionic slow-setting with hard binder and modification).

- The effect of application rate on shear strength may be confounded by varying loading rates applied by different researchers. Using a loading rate of 2 in./min, Sholar et al. (2004) observed a slight effect of application rate on shear strength within the range of 0.09 to 0.36 L/m$^2$ (0.02 to 0.08 gal/yd$^2$). However, Willis and Timm (2007) pointed out in their forensic study that a slower loading rate might differentiate better the shear strength between cores from areas with and without debonding. Based on test results at a loading rate of 0.1 in./min, Mohammad et al. (2012) reported that all tack coat materials used produced the highest interface shear strength when they were applied at the highest application rates within the range of 0.14 to 0.70 L/m$^2$ (0.03 to 0.15 gal/yd$^2$).
- Tashman et al. (2008) reported that tack coat curing (i.e., a curing time of 2.5-hour as opposed to 3.0-min) was an insignificant factor based on results of field cores taken right after construction. However, curing may have a long-term effect on shear strength. Das et al. (2017) tested field cores taken at several service times (0, 4, and 12 months in Louisiana and Florida projects and 0, 7, and 12 months in Missouri project). They found shear strength increased with service time in all field projects and for all surface types as a result of long-term curing. Similar observations were reported by Sholar et al. (2004).
- Muench and Moomaw (2008) reported that dilution of asphalt emulsions can help achieve a more uniform application and could potentially reduce tack tracking. However, they also indicated dilution can cause issues such as excessively low residual application rate, premature emulsion break (due to thermal shock if cold water is added), and extended curing time.
- Dirt (dust) has always been an issue. Water has become even more of an issue due to the 'silica rule' of Occupational Safety and Health Administration (OSHA). Milling operations are using water to minimize fugitive dust. Some of this water ends up on the milled surface mixing with the dust produced by the milling machine and forming a mud-like surface coating. The surface coating is difficult to broom off, leaving a dirty surface for tack application, which results in lower shear bond strength. The presence of water (e.g., rainwater) on an existing surface also has the effect of reducing bond strength.

- As for surface roughness, Sholar et al. (2004), West et al. (2005), Tashman et al. (2008) and Mohammad et al. (2012) obtained higher shear strengths on specimens in which the sheared interface contained a milled surface.
- The gradation of the layers surrounding the interface affects shear strength. Coarse-graded layers provided higher strength values because of better interlocking (Sholar et al., 2004).

In addition to the factors discussed above, the actual surface condition in the field during the construction process, which can greatly differ from that in a laboratory, is a key variable to interface bond strength. According to Muench and Moomaw (2008), one of the most common problems encountered in the field is a non-uniform tack coat application due to clogged nozzles in the spray bar of the distributor truck. Clogged nozzles result in streaky or spotty coverage, which in turn cause areas of poor or even no bond between asphalt layers. In addition, haul trucks drive on the tack coat and pick it up with their rubber tires in the wheelpath, which eventually results in tack tracking. As a result, a wide variety of trackless tack materials have been developed to mitigate the tack tracking issue (Wilson et al., 2016). Furthermore, milling in a rehabilitation process sometimes leaves thin layers in the pavement surface, known as scabbing. Muench and Moomaw (2008) speculated that thin scabbed areas may be broken up by compaction of the asphalt overlay (particularly when vibratory compaction is used), which can result in debonding as well as areas of low density where water can get trapped and promote moisture damage.

## 2.2 Field Evaluation

Although it is widely acknowledged that pavement distress, such as fatigue cracking and slippage failure, may be associated with poor bonding, only a few studies (see Sections 2.2.1 to 2.2.3) have collected field performance along with bond strength data and attempted to address the link between interface bond strength and pavement distress. In addition, due to the great effort associated with coring, laboratory samples were sometimes prepared to replicate field cores. Observations regarding whether laboratory prepared specimens may adequately reproduce bonding conditions in the field are summarized in Section 2.2.4.

### 2.2.1 Florida study

Sholar et al. (2004) performed a field study using the FDOT shear tester developed to determine the effects of moisture (presence of rainwater), tack coat application rate, mixture gradation, and surface condition (milled vs. non-milled) on interface bond strength. All tests were conducted on field cores at a loading rate of 2 inch/min at 25°C. The results showed that water applied to the surface of the tack coat significantly reduced the interface shear strength of the pavement sections when compared to equivalent sections without water. Tack coat application rate within the FDOT's specified range (0.09 to 0.36 L/m$^2$) had a slight effect on shear strength. Generally, shear strength increased slightly as the tack coat application rate was increased. As weeks passed, the strengths essentially equalized regardless of the application rate. Mixture gradation played a critical role in the shear strengths achieved shortly after construction. Coarse-graded mixtures exhibited higher shear strength than fine-graded mixtures. Milling increased the shear strength at the interface and reduced the effect of the application rate.

Recently, a field investigation was conducted by the FDOT (2015) to identify the cause of slippage failure observed in several locations within a one-mile section of roadway placed on the Westbound I-4 exit ramp to SR-536. The typical section for this ramp consists of a milling depth of 2.25 inch and resurfacing with 1.25-inch Type SP structural course (Traffic C, PG 76-22 PMA) and 0.75 inch friction course FC-5 (PG 76-22 PMA). Placement of more than 23 lane miles of the structural course began in April 2014 and was completed in November 2014. Areas of slippage were discovered in December 2014 (Figure 1-3). Cores were taken from areas near slippage locations and tested using the FDOT shear tester. Based on field observations and the failure pattern of the cores (Figure 1-4), it was concluded that the slippage problem could be associated with a weak bond at or near the interface of the interlayer below the milled surface. In other words, there was a potential link between weakly bonded scabbed areas and slippage failure.

### 2.2.2 Alabama study

West et al. (2005) conducted a field study using the NCAT bond strength test developed to determine the effects of tack coat material, application rate, and surface condition on the

interface bond strength. For pavement sections using an emulsified asphalt tack coat material, the residual application rates were 0.15, 0.23, and 0.30 L/m$^2$. For sections using a paving grade binder as the tack coat material, the target application rates were 0.15, 0.25, and 0.35 L/m$^2$. Three types of receiving surfaces (new AC, milled AC, and old Portland cement concrete) were evaluated. All tests were conducted on field cores at a loading rate of 2 inch/min at 25°C. The results showed milled HMA surfaces appeared to significantly enhance bond strength with the subsequent asphalt layer. Although a few field sections with paving grade tack coat had good bond strengths, there was not sufficient evidence to conclude that paving grade asphalt is superior to asphalt emulsion tack coats. Overall, the field data suggested that an average interface shear strength of 100 psi was representative of a good bond. The range of bond strengths between 50 to 100 psi was considered marginal. However, these preliminary ranges were based on results of cores taken right after construction (i.e., the initial pavement condition). The link between a minimum bond strength and pavement distress (e.g., slippage failure) was not established.

In a follow-up field study, Tran et al. (2012) tested cores taken from the same group of pavement sections as those of West et al. (2005) after four years in service. All these sections showed no sign of failure related to debonding. The interface shear strength of all sections generally increased over time, especially for two sections with polymer modified emulsion (CQS-1HP) at high application rates. A minimum bond strength of 100 psi appeared to be responsible for good performance in these pavement sections. In addition, Tran et al. (2012) investigated test sections exhibiting slippage failure. Cores were taken from both failed areas and nearby areas without slippage. The bond strengths of the cores obtained from the intact areas were greater than 87 psi. For cores from the failed areas, the bond strengths were much lower than 87 psi. Based on results from sections with no sign of debonding and sections exhibiting slippage, Tran et al. (2012) recommended a preliminary minimum bond strength requirement of 100 psi for evaluating the interface bond between the wearing and underlying layers.

Willis and Timm (2007) performed forensic investigation of interface debonding in rich bottom pavement in the NCAT test track. Through a comparison of theoretical and measured strain ratios, a double debonding at both the SMA-HMA interface (located 1-inch below the surface)

and the HMA-rich bottom interface (5-inch below) was identified in pavement section N8, which exhibited fatigue cracking. The double debonding failure was indicated by a drop in the strain ratios, which occurred about 3 months before fatigue cracking was noticed in section N8. In other words, the loss of bond was likely the cause of fatigue cracking in section N8. For a companion section N7 without cracking, a full bond condition between all layers was determined as no drop in the strain ratios was observed. In addition, trenches were cut at three locations in section N8 for physical examination of debonding. Trenches 1 and 2 were located in the area of N8 where fatigue cracking occurred. Debonding at the SMA-HMA interface was clearly observed from both trenches. Trench 3 was cut near the N7-N8 joint where virtually no surface damage had been noticed. No debonding was observed from Trench 3. Further study showed the cores taken from the N8 debonded area exhibited similar interface shear strengths as those from N7. However, the cores from the N8 debonded area failed right along the layer interfaces, while N7 cores failed around the aggregates, resulting in a rough edge. In addition, N7 cores were able to carry a much higher residual stress than cores from the N8 debonded area after they reached the maximum shear load. Willis and Timm (2007) speculated that the results of shear strength were confounded by the high loading rate (2 in/min) employed in the laboratory bond strength test. In the test track, the bond in section N7 resisted many more load cycles than N8 because a lower shear stress level was applied to both sections. Therefore, a cyclic shear loading at a lower stress level was recommended to better differentiate the shear resistance between the cores from N7 and N8 sections in the laboratory testing.

### 2.2.3 Louisiana study

Mohammad et al. (2012) conducted a field study using the Louisiana interlayer shear strength tester (LISST) to investigate factors affecting interface bond using five types of tack coat materials (SS-1h, SS-1, CRS-1, Trackless, and PG 64-22 asphalt binder) and four surface types (milled HMA, new HMA, existing HMA, and PCC). Each tack coat material was applied at four residual application rates (0.00, 0.14, 0.28, and 0.70 L/m$^2$). All tests were conducted on 4-in diameter field cores at a loading rate of 0.1 inch/min at 25°C. The results showed that all tack coat materials produced the highest interface shear strength (ISS) when they were applied at the highest application rates. The trackless tack coat provided the highest bond strength, whereas CRS-1 yielded the lowest bond strength. Milled HMA surface yielded the highest ISS value,

followed by PCC, existing HMA, and new HMA. A stress ratio, defined as the ratio of interface shear stress calculated using a finite element modeling approach to the ISS measured by the LISST, was used to assess the potential of fatigue failure at the interface. The stress ratio of 0.5 was identified as the failure criterion. As a result, an ISS of 40 psi was recommended to prevent failure at the interface. It should be noted that this minimum shear strength requirement (40 psi) was more conservative compared to the requirement (100 psi) proposed by Tran et al. (2012). However, the general trend of reducing shear strength with decreased loading rate (from 2.0 in/min to 0.1 in/min) was expected.

As a follow-up study, the effects of interface bonding on short-term pavement performance were evaluated by Das et al. (2017). Cores were taken several times within the first in-service year (0, 4, and 12 months in Louisiana and Florida projects and 0, 7, and 12 months in Missouri project) and tested using the LISST. The results showed milled HMA surface yielded the greatest ISS, followed by new HMA, existing HMA, and PCC surface types. Trackless tack coat resulted in greater ISS than SS-1 and SS-1H due to the stiffer base asphalt cement used. ISS increased with service time in all field projects and for all surface types, which is consistent with observations reported by Sholar et al. (2004). Finally, all test sections performed satisfactorily with regard to cracking, except for those that did not meet the minimum ISS requirement of 40 psi proposed by Mohammad et al. (2012). Specifically, sections in the Missouri project, where the average ISS dropped below the minimum ISS threshold, exhibited moderate surface cracking.

### 2.2.4 Washington and Texas studies

Based on an extensive review of literature and core logs, Muench and Moomaw (2008) observed that laboratory-prepared specimens with no tack coat yielded substantial shear resistance, whereas field cores without tack coat could not even be tested in many instances. Therefore, they questioned whether laboratory prepared specimens adequately reproduce bonding conditions in the field. Muench and Moomaw (2008) speculated that field cores may have been subjected to additional factors that helped weaken the bond, including compaction with construction equipment, non-uniform application rate, and forces created by the core drilling machine.

Recently, Wilson et al. (2016) evaluated effects of trackless tack materials, application rates, and surface types on ISS in three field projects using the Texas shear bond strength test conducted at a loading rate of 0.2 in/min at 25°C on field cores and laboratory-prepared specimens. The laboratory specimens were fabricated using materials collected in the field, i.e., cores of the existing surface, tack and overlay mixture. The results showed bond strengths from field cores (15-95 psi) were considerably lower than for laboratory-prepared specimens (100-200 psi). This observation supported the speculation of Muench and Moomaw (2008) that laboratory prepared specimens may not adequately reproduce field bonding conditions.

### 2.2.5 Wisconsin study

Mehta and Siraj (2007) used backcalculated stiffness (from FWD test data) and field-observed distresses to understand the factors critical to slippage cracking, and to develop guidelines for pavement design to minimize the slippage cracking due to interlayer bonding failure. It was found that the stiffness ratio ($E_1/E_2$) appeared to inversely correlate with observed distress. Higher stiffness ratio (i.e., greater than 10) consistently showed less distress, indicating a better interlayer bonding performance. It was concluded that if the stiffness ratio between the top HMA layer and the second layer is greater than 10 during the design and if the second layer stiffness is greater than 20 ksi, the pavement will resist slippage more effectively than that when the stiffness ratio is less than 10. Based on limited cases, this study demonstrated that by increasing the thickness of the surface layer, the structural capacity of the slipped pavement with a stiffness ratio of 2 can be increased to reach an equivalent capacity of the pavement with a stiffness ratio of 10. The additional top layer thicknesses were 2 in for an existing 2-in top layer and 4 in for an existing 3-in top layer. In other words, a thicker surface layer with the lower stiffness ratio needs to be modified more significantly than for a thinner layer to change the structural capacity measured by surface deflection.

## 2.3 Interface Modelling Efforts

Interface modeling efforts have primarily focused on evaluation of the potential effects of smeared interface conditions on the stress and strain distribution in the pavement structure and its potential impact on pavement performance. Note that a smeared interface condition represents the condition where identical material properties (e.g., reaction modulus and shear strength) are enforced throughout the interface. Interface compliance models and strength models derived from monotonic loading tests were widely used to characterize the response of the interface in the pavement structure. Interface compliance describes the relationship between relative displacement and shear stress at the interface. Interface shear strength is the maximum shear stress. Interface failure was typically determined when shear stress was equal to shear strength for a critical load scenario or when shear stress ratio (defined as the ratio of shear stress to shear strength) reached a specified value for a repeated load scenario. This section explores the literature for compliance models, strength models and associated failure criteria developed and implemented (Table 2-2). In addition, a hybrid interface bonding condition recently proposed by UF researchers to investigate the link between localized interface debonding and longitudinal cracking will be introduced. As opposed to a smeared interface bonding condition, a hybrid interface bonding condition allows different material properties at different portions of the interface. Field evidence indicated a weak bond existed below local scabbed areas. Therefore, hybrid interface bonding condition composed of partial bond for scabbed areas along with full bond elsewhere may be more representative of field conditions.

### 2.3.1 Interface compliance model

One of the first documented studies on the effect of interface conditions on pavement response was performed by Uzan (1976). He proposed a linear model to simulate the behavior of partially rough interfaces based on Goodman's constitutive law. He assumed the interface to be a layer of finite thickness (h). A shear stress ($\tau$) was applied at the interface, which resulted in a relative displacement ($\Delta u$) between the two sides of the interface (Figure 2-1).

Table 2-2 Interface models and failure criteria.

| Model / Criterion | Type | Location (Reference) |
|---|---|---|
| Compliance model | Goodman's Law | Israel (Uzan et al., 1976) |
| | | Netherland (De Jong et al., 1979) |
| | | South Africa (Maina et al., 2007) |
| | Thin layer assumption | Texas (Wilson et al., 2016) |
| Strength model | Confinement independent | Louisiana (Romanoschi and Metcalf, 2001a) |
| | Confinement dependent | Louisiana (Romanoschi and Metcalf, 2001a) |
| | | Illinois (Ozer et al., 2008) |
| | Shear rate and confinement dependent | Italy (Canestrari et al., 2013) |
| | | North Carolina (Cho et al., 2017) |
| Failure criterion | Single load event | Louisiana (Romanoschi and Metcalf, 2001b) |
| | Fatigue failure | Louisiana (Mohammad et al., 2012) |
| | | North Carolina (Karshenas et al., 2014) |

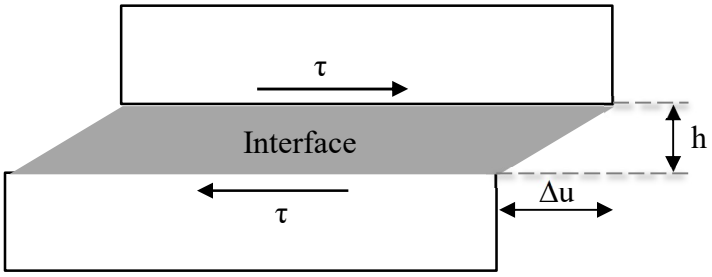


Figure 2-1 Schematic of an interface bonded between two surfaces.

The shear strain γ for an elastic material can be related to the shear stress τ:

$$\tau = G \cdot \gamma \tag{2.1}$$

where G is the shear modulus of the interface material. For small displacements, shear strain is defined as:

$$\gamma = \frac{\Delta u}{h} \tag{2.2}$$

Substituting Eq. 2.2 into Eq. 2.1 gives:

$$\tau = \frac{G}{h} \cdot \Delta u = K \cdot \Delta u \tag{2.3}$$

where K is defined as the reaction modulus of the interface.

This model was employed by Uzan (1976) to perform a sensitivity analysis on the effect of various interface conditions, as represented by different K values, on the responses of a four layer pavement structure (two asphalt layers, base and subgrade). Only the interface between the two asphalt layers was modeled using Eq. 2.3; the other two interfaces were assumed fully bonded. The interface between asphalt layers was located at a depth equal to half the radius of the load, which for a typical load radius of 5 to 6 in results in a depth of 2.5 to 3 in. Three elastic moduli were considered for the upper asphalt layer. For the purpose of the analysis, K was assumed to be an intrinsic interface property, independent of interface thickness, normal load and relative displacement rate, which seemed to be appropriate in the context of linear elastic layered systems. Uzan (1976) found that most of the change in the radial stress (and strain) at the bottom of the upper asphalt layer occurred when K varied between 1 and 100 N/mm$^3$ (100-10,000 kgf/cm$^3$). When K was less than 1 N/mm$^3$ or greater than 100 N/mm$^3$, the results were within 10% of those for slip and full bond conditions, respectively.

Field experiences discussed by Uzan et al. (1978) suggested that the state of adhesion in actual pavement is somewhere between full adhesion and zero adhesion, depending on material properties and construction quality. In other words, there is some inherent compliance associated with the interface. In fact, Uzan et al. (1978) recommended a K value of 10 N/mm$^3$ to model an interface in the upper part of an asphalt pavement subjected to a tire pressure of 75-100 psi at normal highway speed and 25 ºC.

In the multilayer linear elastic program Bitumen Stress Analysis in Roads (BISAR) developed by De Jong et al. (1979), the interface between any two pavement layers is represented by an infinitely thin layer characterized by a shear spring compliance parameter AK. AK describes the relative horizontal displacement induced by a unit shear stress at the interface:

$$AK = \frac{Relative\ horizontal\ displacement}{Interface\ shear\ stress} = \frac{\Delta u}{\tau} \tag{2.4}$$

Note that shear spring compliance AK is the inverse of the reaction modulus K. The relationship described in Eq. 2.4 is treated mathematically through the slip parameter α, expressed as:

$$AK = \frac{\Delta u}{\tau} = \frac{\alpha}{1-\alpha} \cdot \frac{1+\nu}{E} \cdot a \tag{2.5}$$

where E and ν are the elastic modulus and the Poisson's ratio of the layer above the interface, and a is the radius of the load. The slip parameter α varies from 0 (full bond) to 1 (full slip). Note that, for a given interface compliance value AK, α depends on the radius of the applied load. Thus, α is not a pure material property and should not be considered to be a 'classic' friction coefficient.

Maina et al. (2007) utilized a similar concept to that implemented in BISAR in order to model interface slip and evaluate its influence on the critical responses of an airport pavement. The relationship between relative horizontal displacement and shear stress was defined as follows:

$$\frac{\Delta u}{\tau} = \frac{\alpha}{1-\alpha} \cdot \beta \tag{2.6}$$

in which α is a slip parameter and β is a parameter that allows consideration of different shear compliance models shown below:

$$\beta_1 = a^* \cdot \left(\frac{1+v_i}{E_i} + \frac{1+v_{i+1}}{E_{i+1}}\right) \tag{2.7a}$$

$$\beta_2 = 2a^* \cdot \left(\frac{1+v_i}{E_i}\right) \tag{2.7b}$$

$$\beta_3 = 2a^* \cdot \sqrt{\left(\frac{1+v_i}{E_i}\right) \cdot \left(\frac{1+v_{i+1}}{E_{i+1}}\right)} \tag{2.7c}$$

where a* was selected as the maximum radius among the surface loads; and $E_i$, $E_{i+1}$ and $\nu_i$, $\nu_{i+1}$ are the elastic modulus and Poisson's ratio of the $i^{th}$ and $(i+1)^{th}$ layers, respectively.

Maina et al. (2007) used the three models described by Eq. 2.7 to examine critical interface conditions for a typical airport flexible pavement subjected to vertical and horizontal loads.

Strain energy of distortion (SED) was used to identify critical responses. According to calculations carried out by UF researchers, K values used by Maina et al. (2007) may have ranged from 0.34 N/mm$^3$ (α=0.9) to 12.1 N/mm$^3$ (α=0.2), apart from the full bond case (α=0). SED was found to be maximum at the surface of the pavement structure, regardless of the slip level α. As α increased, SED at the bottom of the top layer (where interface slip was introduced) increased. These results were observed for the three slip models, though the effects were more evident for model 3 (Eq. 2.7c). Based on SED results, it was concluded that slip of the interface between the surface and the binder layer (about 2-in deep in this case) can potentially lead to deterioration from both the top and the bottom of the surface layer.

Hernando et al. (2018) used the BISAR program to determine stress states potentially conducive to interface debonding for a range of interface compliance represented by K value. The study showed the existence of a zone of high horizontal shear coupled with low confinement at a depth of 1 to 3 in below the surface and extending to 2 in outside the tire edge. Given the shear stress magnitude in this zone (full bond condition) was similar to the shear strength (90-100 psi) reported in the literature (Tran et al., 2012) and that the rapid drop in confinement immediately outside the tire edge, it was concluded that the repetition of these critical stress states can cause localized debonding of an interface located about 2 in below the pavement surface.

In addition, Wilson et al. (2015) evaluated the effect of bond conditions on shear stress at the interface by introducing a thin layer (1 mm) of linear elastic material between an asphalt overlay and an existing asphalt layer in their finite element pavement model. It should be noted that the 1-mm interface thickness (h) would correspond to a residual tack coat application rate of 1.0 L/m$^2$ (0.22 gal/yd$^2$), which was much higher than the typical range of residual rate (0.02 to 0.09 gal/yd$^2$) reported in the literature (Mohammad et al., 2012, FDOT, 2016). Three moduli (423, 317, and 212 ksi) were assigned to simulate different interface conditions, corresponding to 100, 75, and 50 percent of the overlay modulus, respectively. According to calculations carried out by UF researchers, K values used by Wilson et al. (2015) may have ranged from 1000 N/mm$^3$ (E=423 ksi) to 500 N/mm$^3$ (E=212 ksi). The study showed that the maximum shear stresses at the interface were the same (40 psi) for all three conditions under a 9-kip vertical load (tire pressure=100 psi). When the load was inclined at an angle of 15° to simulate turning traffic, the

maximum shear stress increased for all three conditions ranging from 110 psi (E=423 ksi) to 120 psi (E=212 ksi).

### 2.3.2 Interface strength model and failure criterion

#### 2.3.2.1 Interface strength model with or without confinement

Romanoschi and Metcalf (2001a) derived a two-stage constitutive model (Figure 2-2) to characterize the interface between two asphalt layers from results of direct shear tests conducted at 0.5 in/min. Laboratory testing included three temperatures (15, 25 and 35 ºC), four normal load levels (20, 40, 60 and 80 psi) and two different interface conditions (tack coat and no tack coat). In the first stage, called stick condition, the relative displacement of the two layers is proportional to shear stress until the shear strength of the interface ($\tau_{max}$) is reached (failure criterion). The relationship between shear stress and relative displacement is given by the interface reaction modulus (K). Relative displacement is elastic and recoverable in this first stage. In the second stage (post-failure), a simple frictional model defined by a coefficient of friction ($\mu$) is used to represent the behavior of the interface (friction condition). The friction coefficient relates vertical normal stress (i.e., confinement) to shear stress. Romanoschi and Metcalf (2001a) reported that interface reaction modulus values varied from 0.2 to 1.2 N/mm$^3$ and shear strength was between 0.5 and 2.5 MPa (72.5 to 362.5 psi).

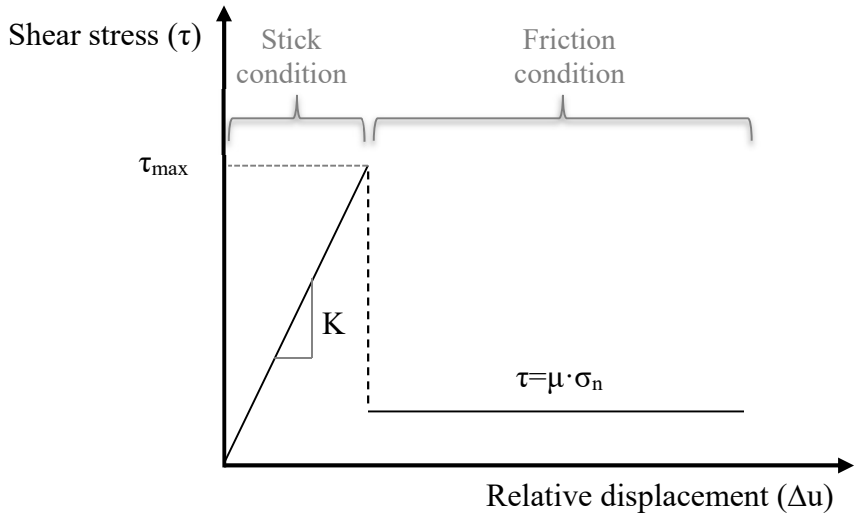


Figure 2-2 Constitutive interface model (Romanoschi and Metcalf, 2001a).

Romanoschi and Metcalf (2001b) employed the constitutive model developed and conducted a theoretical study for evaluation of the effect of interface conditions on the life of flexible pavements. For the interface between the surface course and the binder course, the following conditions were modeled by the contact interaction feature available in the finite element (FE) program ABAQUS:

- Full bond condition (stick condition): each node of a slave surface was tied to the nearest node on a master surface.
- Interface with tack coat: the relative displacement at the interface was proportional to shear stress. In this case, shear strength and interface reaction modulus were defined as independent of normal stress; values of 1.415 MPa (205 psi) and 0.885 N/mm$^3$ were selected for $\tau_{max}$ and K, respectively, based on direct shear test results at 25 ºC.
- Interface without tack coat: the relative displacement at the interface was also proportional to shear stress. However, $\tau_{max}$ and K were defined as normal stress dependent:

$$\tau_{max}[kPa] = 842.5 + 7.66 \cdot \sigma[kPa] \quad (2.8)$$

$$K[N/mm^3] = 0.361 + 0.2307 \cdot \sigma[MPa] \quad (2.9)$$

- Friction condition: the resistance to movement was proportional to the normal stress at the interface (Coulomb's friction law) characterized by a friction coefficient μ=0.7.

The maximum tensile strain was used to estimate pavement life in terms of fatigue cracking. The full bond condition exhibited the highest number of cycles to failure. Regarding critical depth, the maximum tensile strain was found at the bottom of the binder asphalt course for the full bond condition and at the bottom of the surface course for the other three conditions. In other words, the introduction of an interface model to account for some level of compliance at the interface between the surface and binder layers moved the maximum tensile strain location to the bottom of the surface course. The horizontal loads acting at the pavement surface led to significantly increased tensile strains at the top and bottom of the surface course and at the top of the binder course.

Mohammad et al. (2012) employed the constitutive model developed by Romanoschi and Metcalf (2001a) to predict interface shear stress of six different pavement structures. Results from direct shear tests (25 °C) on four different tack coats at three residual application rates (0.14, 0.28 and 0.70 L/m$^2$) were used to determine the interface reaction modulus K and interface shear strength (ISS). The following observations can be made from their results: i) shear stress is directly proportional to the level of bending; thus, sections with thicker asphalt layer exhibited lower shear stress; ii) predicted interface shear stress exceeded measured shear strength for only two out of 72 combinations; and iii) interface shear stress was barely sensitive to tack coat type and application rate. It should be pointed out K values obtained from testing were between 0.1 and 0.3 N/mm$^3$. The UF researchers are of the opinion that these low K values may have been the result of the low displacement rate used for testing (0.1 in/min). According to the sensitivity analysis performed by Uzan (1976), K values below 1 N/mm$^3$ yield similar results to those provided by a slip condition. Therefore, low interface shear stress is expected for low interface reaction modulus. In addition, a stress ratio, defined as the ratio of calculated interface shear stress to measured shear strength was used to assess the potential for fatigue failure at the interface. The stress ratio of 0.5 was selected as the failure criterion. As a result, a minimum shear strength of 40 psi was recommended to prevent failure at the interface.

Ozer et al. (2008) implemented a hyperbolic Mohr-Coulomb frictional model to describe the behavior of tack coat interfaces. The hyperbolic yield function is defined by Equations 2.10 and 2.11 and is illustrated in Figure 2-3.

$$F = \tau_{eq}^2 - (c - \sigma_{nn} \cdot \tan \Phi)^2 + (c - s \cdot \tan \Phi)^2 \tag{2.10}$$

$$\tau_{eq} = \sqrt{\tau_{ns}^2 + \tau_{nt}^2} \tag{2.11}$$

where $\tau_{eq}$ is the equivalent tangential traction calculated based on two tangential components ($\tau_{ns}$ and $\tau_{nt}$) on the interface plane; $\sigma_{nn}$ is the normal traction; s is the tensile strength; c is the cohesion, and $\Phi$ is the friction angle. The c and $\Phi$ parameters can be measured from shear tests at various normal pressures, while s can be obtained from a pullout test. If pullout data is not readily available, s could be assumed equal to cohesion. Shear test results are also used to

characterize the initial elastic behavior of the interface, which is governed by the interface reaction modulus K.

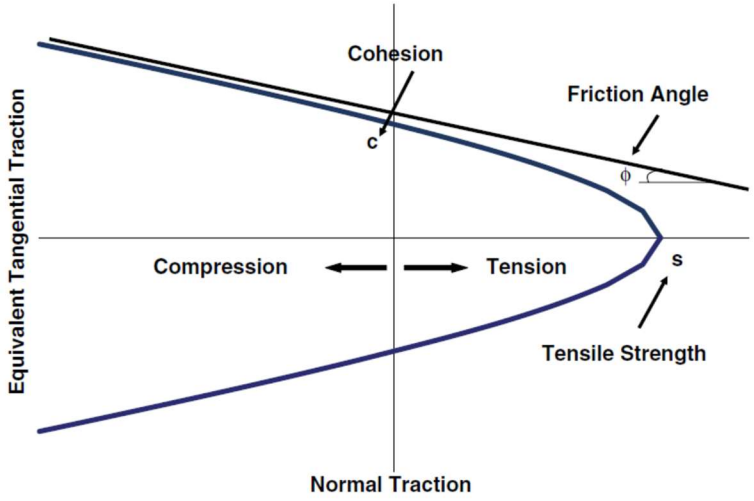


Figure 2-3 Hyperbolic Mohr-Coulomb frictional model (Ozer et al., 2008).

Ozer et al. (2012) employed results of direct shear tests on specimens composed of a 2.2-in thick asphalt overlay on a smooth concrete surface to determine input parameters for the hyperbolic interface model. A rapid curing cutback asphalt (RC-70) at three application rates (0.09, 0.23 and 0.41 L/m$^2$; or 0.02, 0.05 and 0.09 gal/yd$^2$) was used to tack the asphalt overlay to the PCC surface. A total of six interface conditions (Table 2-3) were simulated using the FE program Abaqus, which considered the viscoelastic characteristics of asphalt mixture and moving traffic loading. Interface reaction modulus in the two tangential directions ($K_{ns}$ and $K_{nt}$) and shear strength values (ISS) were selected based on shear test results without confinement. Additional assumptions included a friction angle of 35º, and a tensile strength (s) and a cohesion (c) equal to the shear strength. Note that while Cases I and II are the parameter sets representing experimental test results, Cases III-VI were used to perform a sensitivity analysis.

The FE models were used by Ozer et al. (2012) to evaluate the effect of interface conditions on fatigue cracking by examining the transverse strain at the bottom of the asphalt layer. The transverse strain distribution under single wide-base and dual tire configurations with K values lower than 1.0 N/mm$^3$ agreed with the no bond condition. Likewise, a K value of 100 N/mm$^3$

yielded similar response to the full bond scenario. Furthermore, they investigated the potential for instability rutting based on the octahedral shear stress distribution at tire edge through the depth of the asphalt layer. The maximum octahedral shear stress was found at approximately 0.5 in below the surface of the pavement due to the combined effect of bending and lateral tangential stresses at the tire-pavement contact, regardless of interface reaction modulus. However, the magnitude of the maximum octahedral stress did increase as K decreased. K values below 0.1 $N/mm^3$ yielded almost identical results to the no bond condition whereas a K value of 100 $N/mm^3$ matched the full bond condition.

Table 2-3 Interface characteristics used by Ozer et al. (2012) based on shear test results.

| Parameter | Unit | Case | | | | | |
|---|---|---|---|---|---|---|---|
| | | I | II | III | IV | V | VI |
| $K_{nn}$ | $N/mm^3$ | 15,000 | 15,000 | 15,000 | 15,000 | N/A | N/A |
| $K_{ns}$ | $N/mm^3$ | 0.01 | 0.1 | 1 | 100 | Full bond | No bond |
| $K_{nt}$ | $N/mm^3$ | 0.01 | 0.1 | 1 | 100 | Full bond | No bond |
| ISS | MPa | 0.05 and 0.2 | | | | | |
| Φ | º | 35 | | | | | |

In addition, Ozer et al. (2013) investigated critical interface conditions between asphalt layers under a moving load with a combination of three load magnitudes and three rolling conditions (rolling, braking, and cornering). A 3D FE pavement model composed of a 10-in HMA layer on top of stabilized subgrade was built to predict shear stresses at an interface located 2 in below the surface. Results from direct shear tests (0.3 in/min at 25 °C) on two overlay mixtures and two tack coat materials (at an application rate of 0.18 $L/m^2$) under three confinement levels were used to determine input parameters for the hyperbolic interface model (Figure 2-4). A stress ratio was defined as the ratio of calculated shear stress to shear strength predicted using the hyperbolic interface model based on calculated confinement. The stress ratio was used to identify critical interface conditions for different mixtures and tack coat materials. The results showed that interface failure was more likely to occur in SS-1hp tack coat than in SS-1vh (also known as trackless tack coat) for both overlay mixtures at room-temperature.

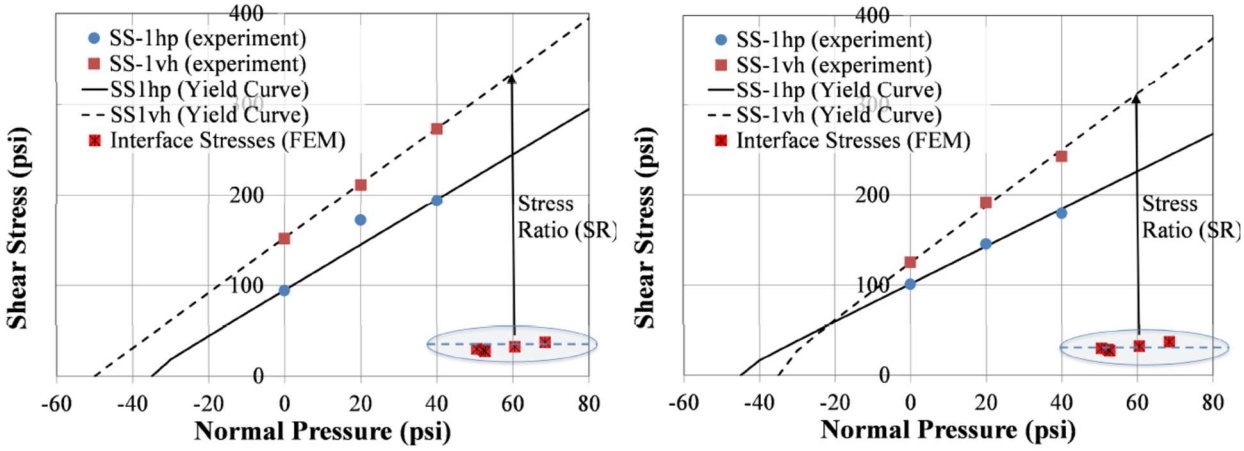


(a) 4.75-mm mix (b) 9.5-mm mix

Figure 2-4 Interface shear strength yield curves and calculated interfacial stress at 2 in below pavement surface (Ozer et al., 2013).

#### 2.3.2.2 Shear rate and confinement-dependent interface strength model

Canestrari et al. (2013) developed a shear rate and confinement-dependent interface shear strength model shown in the equations below, based on results from direct shear tests on two tack coat materials at an application rate of 0.15 L/m$^2$ for three normal confinements, six loading rates and five temperatures.

$$\tau_{Tx} = 10^{a \cdot T_x + b} \tag{2.12}$$

$$\tau_{\sigma n} = (1 + 0.38\sigma_n) \cdot \tau_{\sigma 0} + 0.74\sigma_n \tag{2.13}$$

$$\tau_{vx} = \tau_{v1} \cdot \left(\frac{v_x}{v_1}\right)^{0.22} \tag{2.14}$$

where, $\tau_{Tx}$ is the shear strength at temperature $T_x$, $\tau_{\sigma 0}$ is the shear strength without normal stress, $\tau_{\sigma n}$ is the shear strength under normal stress $\sigma_n$, $\tau_{v1}$ is shear strength at loading rate $v_1$ and $\tau_{vx}$ is shear strength at loading rate $v_x$, a and b are fitting coefficients.

Karshenas et al. (2014) employed the shear strength model of Canestrari et al. (2013) to investigate the interface shear failure mechanism. A 3D viscoelastic FE pavement model was used to predict shear stresses and vertical normal stresses developed at the interface (1.5 inch

below the surface of the pavement) under an 18-kip axle load moving at a speed of 5 mph and at 60 °C. The wheel was assumed to be in the braking status with a friction coefficient of 0.66. A stress ratio was defined as the ratio of calculated shear stresses to shear strength predicted using the strength model (Equations 2.12 to 2.14). The stress ratio was used to identify the location for interface shear failure. The critical location was found to be along the central longitudinal axis slightly in front of the tire edge, where the maximum stress ratio was 1.01, and the corresponding shear stress and normal stress were 31.9 psi (0.22 MPa) and 18.8 psi (0.13 MPa), respectively. Of note, the peak shear stress of 58.0 psi (0.40 MPa) was located about 2 inch from the critical location toward the center of the tire. The greater normal stress of 85.5 psi (0.59 MPa) prevented this location from being the critical location.

In a follow-up study to Karshenas et al. (2014), Cho et al. (2017) developed an interface shear strength model based on their results of laboratory shear tests on four types of tack coat materials at a residual application rate of 0.18 L/m$^2$ typically used in North Carolina. Three normal confining stresses, three loading rates, and four temperatures were employed in the testing program. The resulting shear strength model (Equation 2.15) is a function of reduced shear strain rate ($\dot{\gamma_R}$) and normal confining stress ($\sigma_c$).

$$\tau_f = a \cdot (\dot{\gamma_R})^b \cdot \sigma_c + c \cdot (\dot{\gamma_R})^d + e \cdot \sigma_c \quad (2.15)$$

where a, b, c, d, e are fitting coefficients. Furthermore, Cho et al. (2017) conducted viscoelastic finite element analyses to predict interface shear stresses for three pavement structures under a moving load at four temperatures. Three vehicle speeds, three axle loads, and two rolling conditions (free-rolling and braking) were employed in the analysis. A stress ratio, defined as the ratio of calculated shear stresses to shear strength predicted using the strength model (Equation 2.15) was employed to assess the potential of interface debonding. A higher potential of shear failure was associated with a shear ratio closer to 1.0 (failure criterion). The critical location was found to be on the central longitudinal axis under the braking condition, while it was on the central transverse axis under the free-rolling condition. The interface with no tack coat exhibited the highest potential to debonding, while trackless emulsion tacked interface had the lowest potential. Further results showed that higher temperature, lower speed and heavier axle load led

to more critical condition for interface debonding, and a thinner pavement structure was more vulnerable to interface failure.

### 2.3.3 Hybrid interface bonding condition

Field evidence showed debonding was a local phenomenon, which started at a critical location and gradually progressed through a portion of the interface. Therefore, Roque et al. (2017) introduced a localized debonding approach, i.e., a hybrid interface bonding condition to identify a potential mechanism connecting debonding and near-surface longitudinal cracking. The hybrid interface bonding condition included no bond along a debonded strip (2 in below the surface and extended from the center of the load up to 2 in from the outside edge of the tire) and full bond elsewhere. The contact faces of the debonded strip were frictionless and no penetration of the faces was allowed in the normal direction under a normal pressure load. Results of the study showed bending caused by repeated traffic loads applied at the center of the wheel path can initiate a crack below the tip of the debonded strip that can reflect to the surface as a result of thermal cycles, differential aging and wheel load wander. Furthermore, a vertical crack can initiate above the tip of the debonded strip and propagate upward due to the lateral movement of traffic loads within the lane (traffic wander).

## 2.4 Concluding Remarks

Generally, monotonic loading shear bond tests have been used to determine interface bond strength and to rank tack coat materials. Due to the viscoelastic nature of tack coat materials, both interface bond strength and reaction modulus increase with increasing loading rate. The loading rate of 2 in/min was most commonly employed due to short testing time and wide availability of the Marshall apparatus associated with this loading. Compared to the results from laboratory prepared samples, bond strength data from field cores were considerably lower and may be more suitable for use as input parameters for evaluation of pavement performance in the field. Accordingly, reaction modulus data from field cores should be used as input parameters for field evaluation.

Field investigation in Florida indicated there was a potential link between weakly bonded scabbed areas and slippage failure, which is likely caused by high lateral stresses from braking. Furthermore, evidence from the NCAT test track studies suggested that localized interface debonding might lead to surface cracking. While slippage is a local distress that appears in braking zones, bending-induced surface cracking under normal-rolling traffic could potentially be much more prevalent on highways and represent a greater concern. Therefore, this study will focus on responses and potential distress, including slippage and surface longitudinal cracking in asphalt overlay, associated with the presence of partially or fully debonded scabbed areas.

With respect to modeling of interface response, most studies have employed a global interface representation where material properties were assumed the same throughout the interface. Several shear strength models have been developed mainly dependent on whether normal confining stress (confinement) was considered or not. While shear strength without confinement may be acceptable for tacking materials for quality control or quality assurance purposes, confinement-dependent shear strength is more realistic and better represents field conditions. A reaction modulus K has typically been used to represent the compliance associated with the interface between two asphalt layers, ranging from no compliance ($K=\infty$) to full compliance ($K=0$). Field evidence has shown a weak bond existed below localized scabbed areas. Therefore, global interface representation does not appear to be representative of field conditions. A hybrid interface representation composed of a partial bond for scabbed areas along with a full bond elsewhere seems more appropriate for determination of the potential effect of scabbing on overlay performance.

CHAPTER 3

PAVEMENT SCABBING ANALYSIS WITH CONVENTIONAL APPROACH

## 3.1 Introduction

Conventional pavement analysis was carried out using the multilayer linear elastic program Bitumen Stress Analysis in Roads (BISAR) developed by De Jong et al. (1979). Figure 3-1 shows the coordinate system for BISAR analysis. The depth (z-direction) is a layer input, and the length (x-direction) and width (y-direction) are infinite. Tension is positive following the sign convention of BISAR.

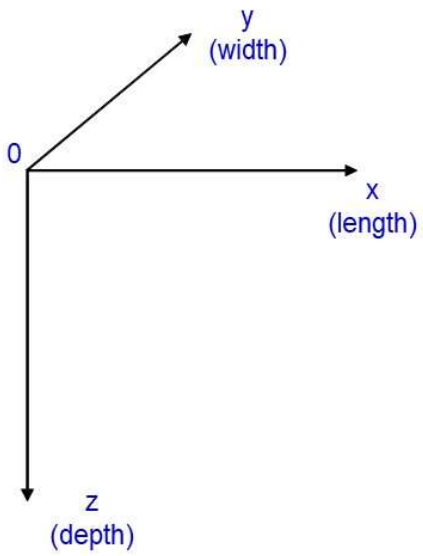


Figure 3-1 Coordinate system for BISAR analysis.

### 3.1.1 Pavement structure and layer properties

In order to determine the effects of presence of scabbing on stress redistribution in asphalt overlay, two typical asphalt pavement structural designs were selected for analysis and evaluation, including a thin AC layer (i.e., 4-inch) on top of a 12-inch granular base layer, and a thicker AC layer (i.e., 8-inch) on a 12-inch base layer as shown in Figures 3-2a and 3-2b, respectively. Two levels of stiffness were considered for AC layer (200 and 800 ksi), two for base (25 and 40 ksi), and one for subgrade (15 ksi). This resulted in a combination of four AC-

to-base stiffness ratio (SR): 5, 8, 20, and 32 for each pavement structure. Poisson's ratio values of 0.35, 0.40 and 0.45 were assumed for AC, base, and subgrade, respectively.

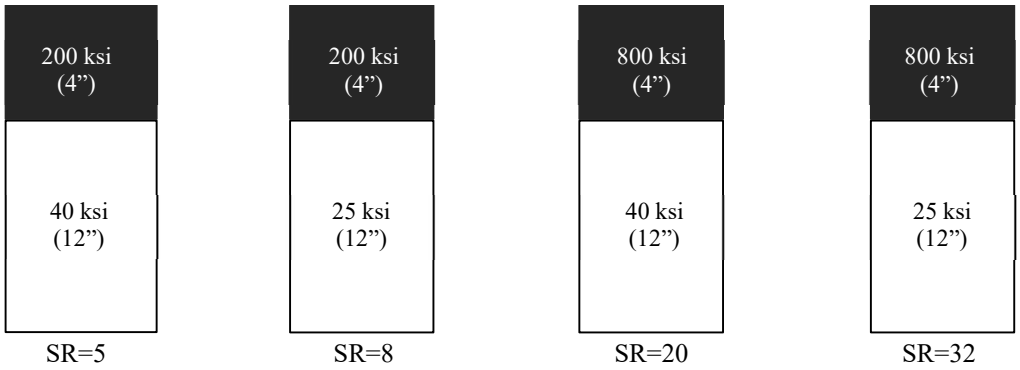


(a) Thin Asphalt Sections

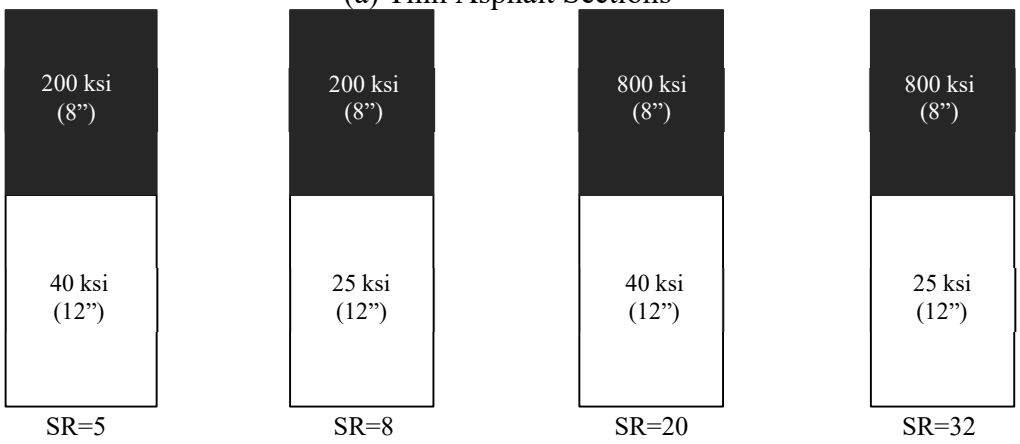


(b) Thick Asphalt Sections

Figure 3-2 Pavement sections with varying structural characteristics.

### 3.1.2 Global Interface representation

As shown in Figure 3-3, the global interface representation assumes that the interface is continuous and homogeneous, i.e., the interface has the same bonding condition (full bond or partial bond) throughout. This presentation is relatively simple for implementation and there are analytical solutions available. Therefore, it has been widely used in conventional approaches investigating the effects of interface bonding conditions on pavement responses (Uzan, 1976, Tran et al., 2012, and Hernando et al., 2018).

The BISAR computer program includes an interface model to account for the effect of slip (i.e., a weak bond) between the layers at the interface using a compliance parameter AK, which is defined as the relative horizontal displacement at the interface induced by a unit shear stress:

$$AK = \frac{Relative\ horizontal\ displacement}{Interface\ shear\ stress} = \frac{\Delta u}{\tau} \tag{3.1}$$

The interface reaction modulus K is the reciprocal of the compliance parameter AK. Several researchers have characterized reaction modulus using interface shear bond tests (Uzan et al., 1978, Romanoschi and Metcalf, 2001a, Mohammad et al., 2012). According to Uzan (1976), most of the change in the radial stress (and strain) at the bottom of the upper asphalt layer occurred when K varied between 1 and 100 N/mm$^3$. When K was less than 1 N/mm$^3$ or greater than 100 N/mm$^3$, the results were within 10% of those for no bond condition and full bond condition, respectively. A range of five K values were considered in this part of the study to evaluate the effect of reaction modulus on pavement stress distribution near the interface, including 0.1, 1, 10, 100 N/mm$^3$ (for partial bond condition) and infinite (for full bond condition).

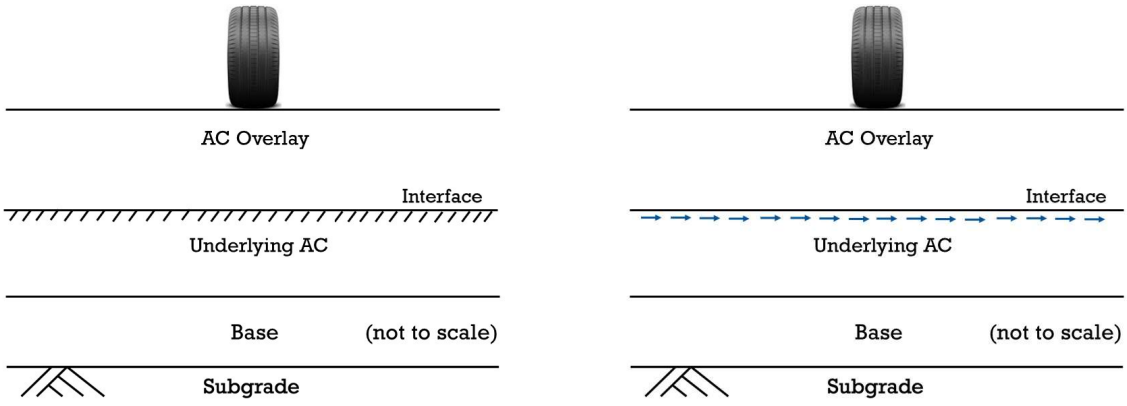


(a) Fully-bonded interface (b) Partially-bonded interface (scabbing)

Figure 3-3 Global interface representations for pavement analysis.

### 3.1.3 Rolling conditions

Two rolling conditions were considered, including the free-rolling condition conducive to longitudinal cracking and the braking condition conducive to slippage in asphalt overlays on scabbed areas.

It was shown by Michelin (2012) that the rolling resistance coefficient for large truck tires under the free-rolling condition ranged from 0.0045 to 0.008. Cho et al. (2017) compared two cases of

rolling resistance coefficients, i.e., 0 and 0.008 for a range of axle loads and pavement structures. No meaningful difference was found in normal and shear stress distributions throughout the pavement depth. Therefore, a 9-kip vertical load (with a uniform pressure of 100 psi and a radius of 5.35 inch) was applied to the pavement structures under the free-rolling condition.

It is well known that a portion of the vertical load is mobilized in the horizontal direction when a vehicle brakes. Several coefficients of friction were reported in the literature for use between a rubber tire and dry asphalt pavement surface in braking zones. In an effort of developing bond strength criteria, Tran et al. (2012) adopted coefficients of friction in the range of 0.5 to 0.8 for the braking condition. More recently, Cho et al. (2017) utilized three coefficients of friction, i.e., 0.35, 0.45, and 0.55 in a study for evaluating the potential of debonding distress in asphalt pavements. A friction coefficient of 0.8 was employed in this study to represent the worst lateral loading scenario where 80% of the vertical load was mobilized in the horizontal direction.

## 3.2 Effects of Stiffness Ratio and Existing AC Thickness

A total of sixteen cases were simulated for this part of the study, including four levels of AC-to-base stiffness ratio (5, 8, 20, and 32), two levels of underlying AC thickness (post milling: 2 and 6 inch), and two rolling conditions (free-rolling and braking). Intermediate values of overlay thickness (1.5 inch) and interface reaction modulus (10 $N/mm^3$) were selected and kept constant throughout this analysis.

### 3.2.1 Results of analysis for free-rolling condition

Figure 3-4 presents the results of stress distribution for thin AC layer sections with a varying AC-to-base stiffness ratio (SR) under the free-rolling condition. Increasing SR value resulted in an increase in tension at the surface of the overlay from 8 to 27 psi (Figure 3-4a), at the bottom of the underlying AC from 85 to 388 psi (Figure 3-4b), as well as at the upper interface from 51 to 70 psi (Figure 3-4c). Also, a greater SR led to higher shear stresses. The peak horizontal shear of 68 psi occurred at about 2.5 inch below the edge of the wheel load in the pavement section with a SR of 32 (Figure 3-4d).

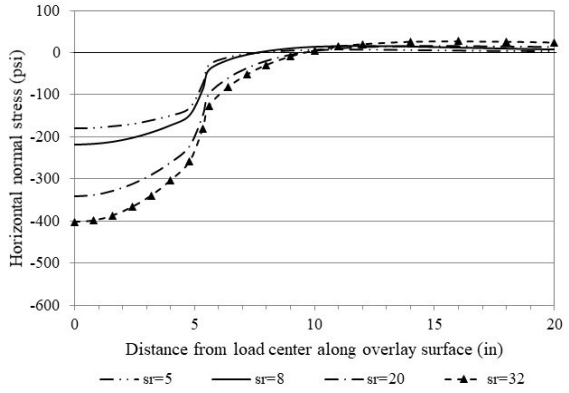


(a) Along surface of overlay

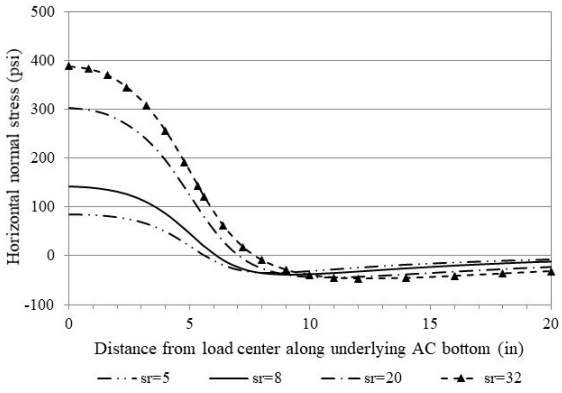


(b) Along bottom of underlying AC

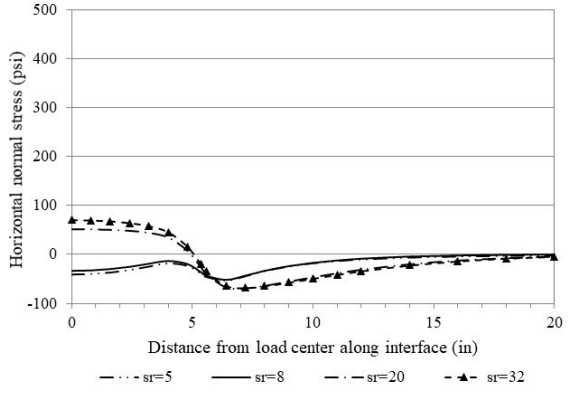


(c) Along interface

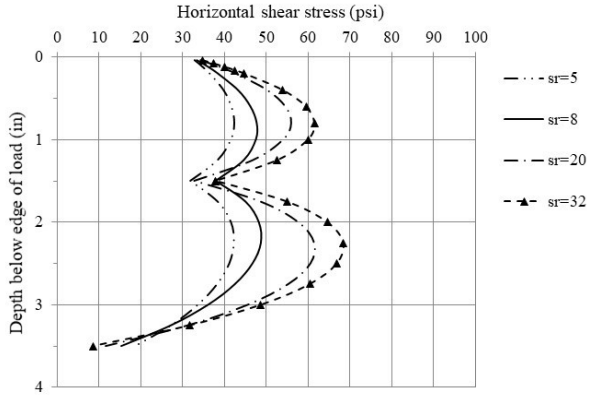


(d) Shear below edge of the wheel load

Figure 3-4 Effect of stiffness ratio on stress distribution in thin AC layer (free-rolling).

Compared to the results from the thin AC layer sections, an increase in underlying AC layer thickness greatly reduced horizontal tensile and shear stresses as shown in Figure 3-5. There was no tension at the surface of the overlay (Figure 3-5a) and at the upper interface (Figure 3-5c) regardless of AC-to-base stiffness ratio. The tension at the bottom of the underlying AC and shear stress remained proportional to SR. The peak tension (resulting from a SR of 32) reduced to 170 psi (Figure 3-5b). The peak horizontal shear reduced to 44 psi, which occurred at about 3.5 inch below the edge of the wheel load in the section with a SR of 32 (Figure 3-5d).

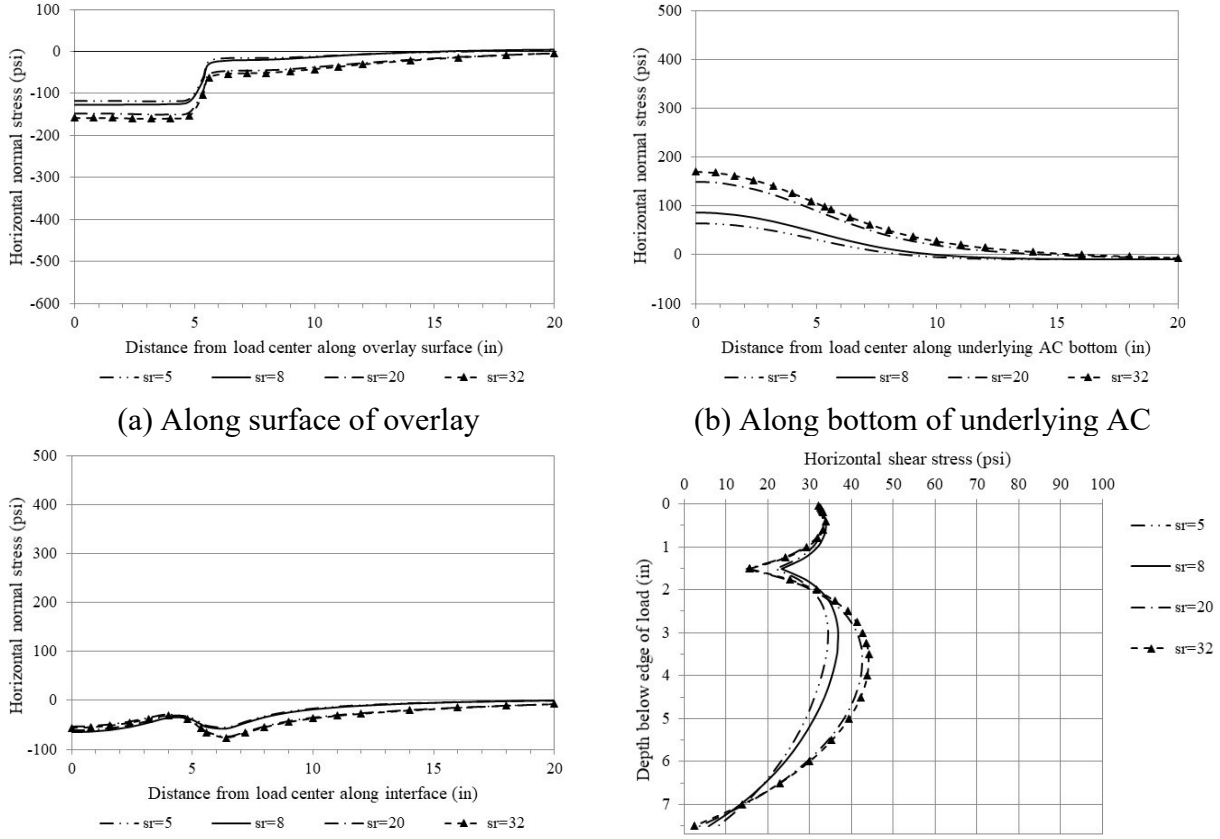


(a) Along surface of overlay (b) Along bottom of underlying AC

(c) Along interface (d) Shear below edge of the wheel load

Figure 3-5 Effect of stiffness ratio on stress distribution in thick AC layer (free-rolling).

### 3.2.2 Results of analysis for braking condition

Figure 3-6 presents the results of stress distribution for thin AC layer sections with a varying SR under the braking condition. Compared to the results under the free-rolling condition, the addition of a horizontal load at pavement surface in the braking zones resulted in higher tension at the surface of the overlay and at the upper interface as well as higher shear stresses. There was almost no change in tension at the bottom of the underlying AC (Figure 3-6b). The increase in surface tension was most significant. The peak value in the range of 143 to 206 psi occurred right behind the wheel load (Figure 3-6a). The peak tension at the upper interface increased to 123 psi, which occurred below the back edge of the load in the section with a SR of 32 (Figure 3-6c). The peak horizontal shear increased to 90 psi, which was only about 0.5 inch below the front edge of the wheel load in the high SR section (Figure 3-6d).

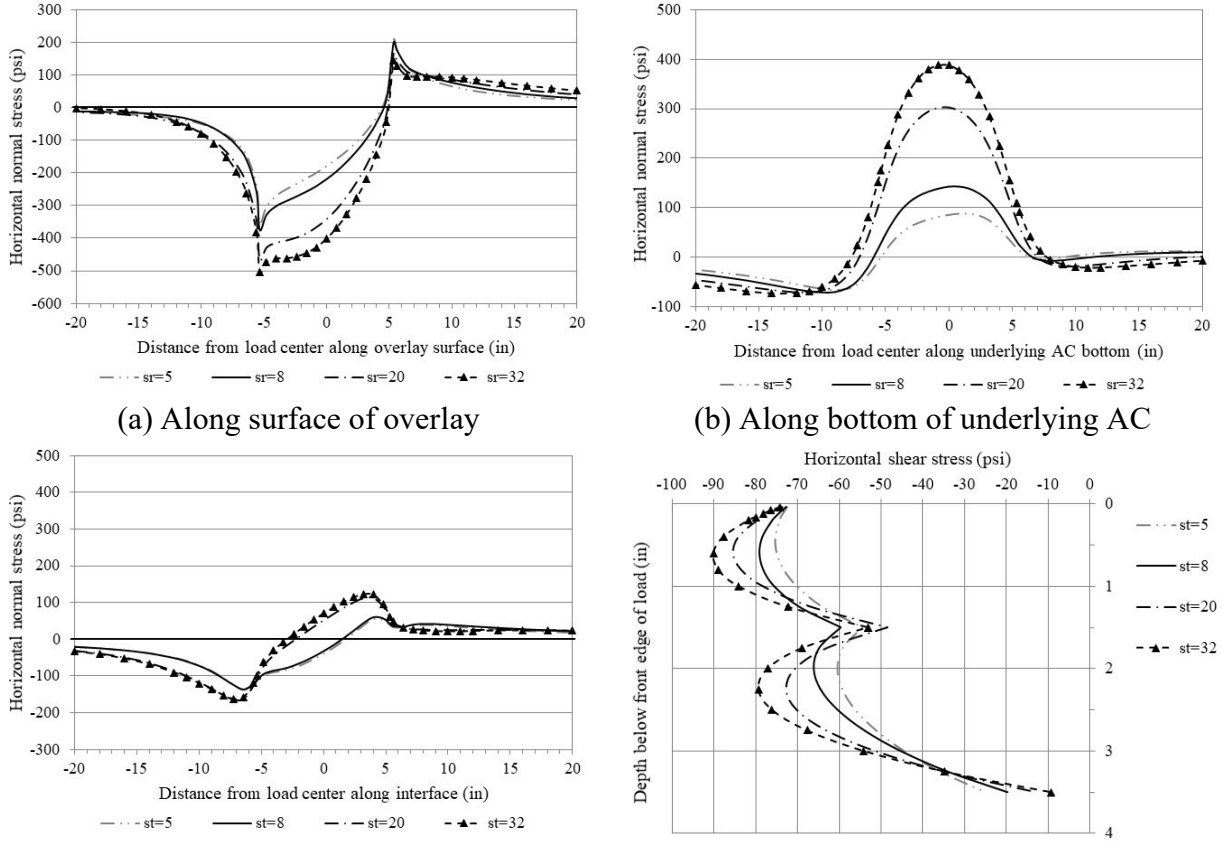


(a) Along surface of overlay (b) Along bottom of underlying AC

(c) Along interface (d) Shear below front edge of the wheel load

Figure 3-6 Effect of stiffness ratio on stress distribution in thin AC layer (braking).

Like the results from the free-rolling conditions, an increase in underlying AC layer thickness greatly reduced tension at the bottom of the underlying AC and at the upper interface as well as shear stresses under the braking loading (Figure 3-7). The peak tension at the bottom of the underlying AC (Figure 3-7b) and at the upper interface (Figure 3-7c) reduced to 171 psi and 60 psi, respectively. The peak horizontal shear reduced to 72 psi, which occurred at the front edge of the wheel load (Figure 3-7d). However, the surface tension remained very high. The peak value in the range of 179 to 197 psi occurred right behind the wheel load (Figure 3-7a).

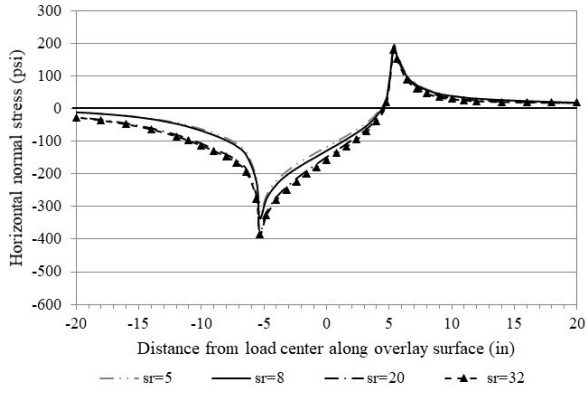


(a) Along surface of overlay

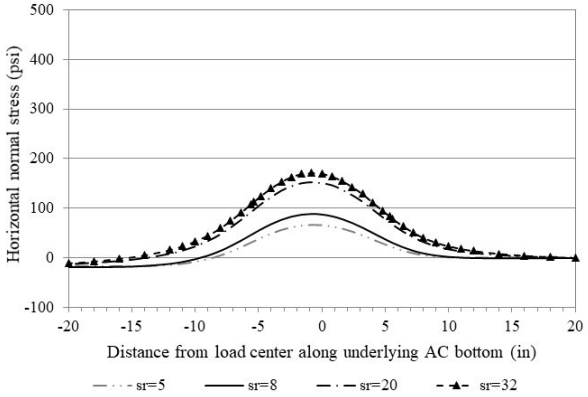


(b) Along bottom of underlying AC

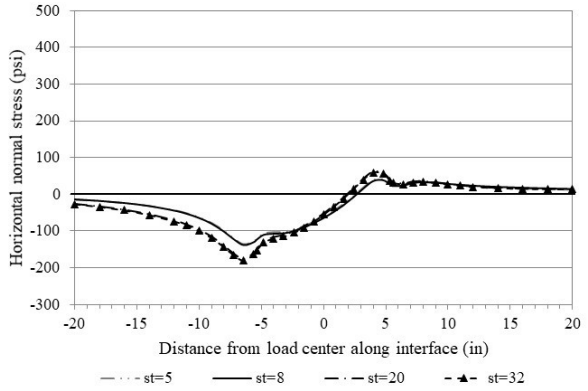


(c) Along interface

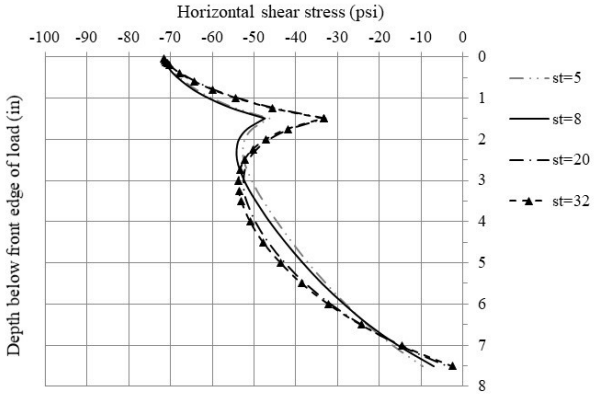


(d) Shear below front edge of the wheel load

Figure 3-7 Effect of stiffness ratio on stress distribution in thick AC layer (braking).

### 3.3 Effect of Overlay Thickness

The study presented in Section 3.2 revealed that a higher AC-to-base stiffness ratio and a thinner underlying AC thickness generally resulted in more critical stress states under both free-rolling and braking loads. Therefore, a high SR of 32 and a low underlying AC thickness of 2 inch were selected and kept constant for evaluating the effect of overlay thickness. An intermediate value of interface reaction modulus (10 $N/mm^3$) was employed to represent a weak bond condition. In total, ten cases were simulated for this part of the study, including five levels of overlay thickness (1.0, 1.25, 1.5, 2.0, and 2.5 inch) and two rolling conditions (free-rolling and braking).

Figure 3-8 presents the resulting stress distribution for pavement sections with varying overlay thickness under the free-rolling condition. Increasing overlay thickness resulted in a reduction in tension at the surface of the overlay from 30 to 20 psi (Figure 3-8a) and at the bottom of the

underlying AC from 432 to 292 psi (Figure 3-8b). However, an increased overlay thickness resulted in higher tension at the upper interface. Specifically, it increased from zero for a 1-in overlay to 148 psi for a 2.5-in overlay (Figure 3-8c). In addition, a greater overlay thickness led to reduction in peak shear stress from 82 to 65 psi (Figure 3-8d). It is important to note that horizonal shear stress peaked below the interface for overlays with a thickness no greater than 1.5 inch, while it peaked above the interface for thicker overlays.

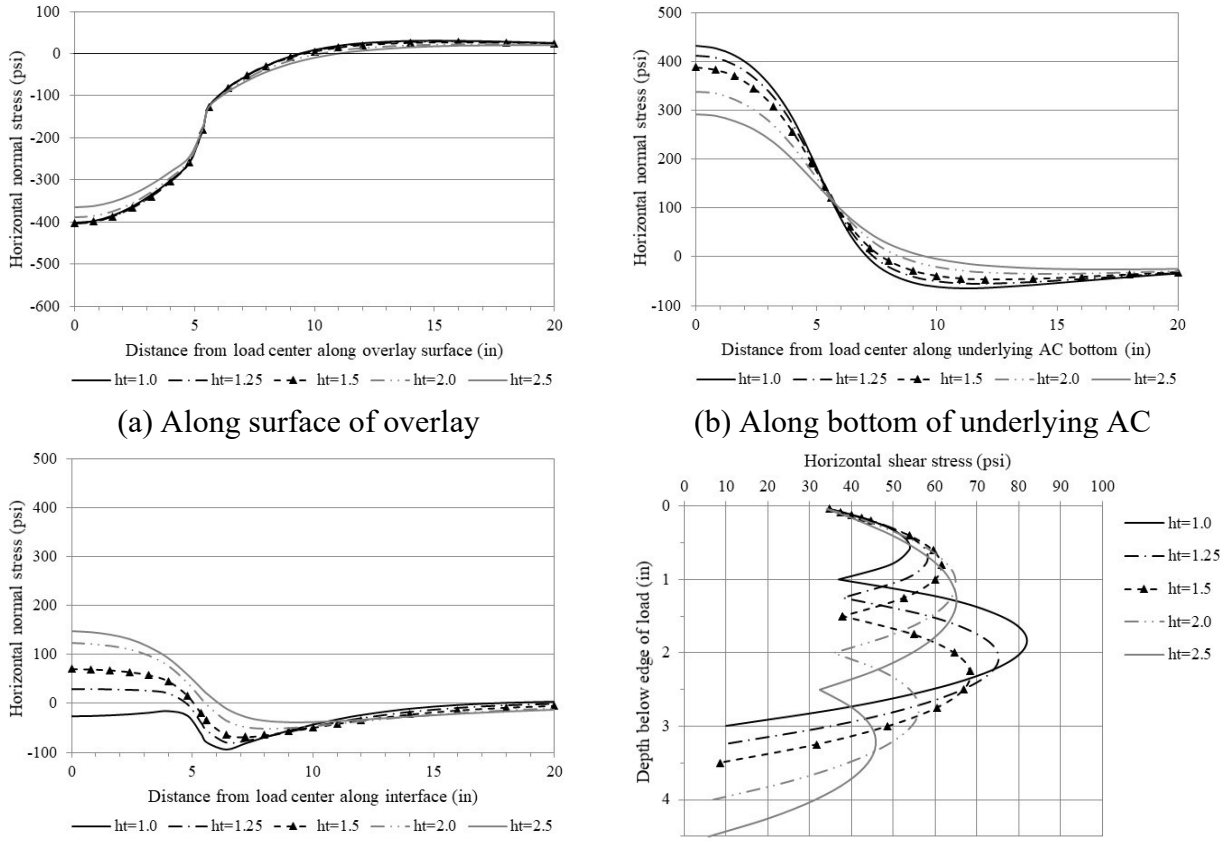


(a) Along surface of overlay

(b) Along bottom of underlying AC

(c) Along interface

(d) Shear below edge of the wheel load

Figure 3-8 Effect of overlay thickness on stress distribution (free-rolling).

Figure 3-9 presents the resulting stress distribution for the same pavement sections under the braking condition. Compared to the results under the free-rolling condition, the addition of a horizontal load in the braking zones resulted in higher tension at the surface of the overlay and at the upper interface as well as higher shear stresses. As expected, there was almost no change in tension at the bottom of the underlying AC (figure 3-9b). The increase in surface tension was most significant. The peak value in the range of 125 to 168 psi occurred right behind the wheel

load (Figure 3-9a). The peak tension at the upper interface increased to 154 psi, which occurred below the load in the section with an overlay thickness of 2.5 inch (Figure 3-9c). The peak horizontal shear increased to 95 psi, which was about 1.5 inch below the front edge of the wheel load in the thin overlay section (Figure 3-9d).

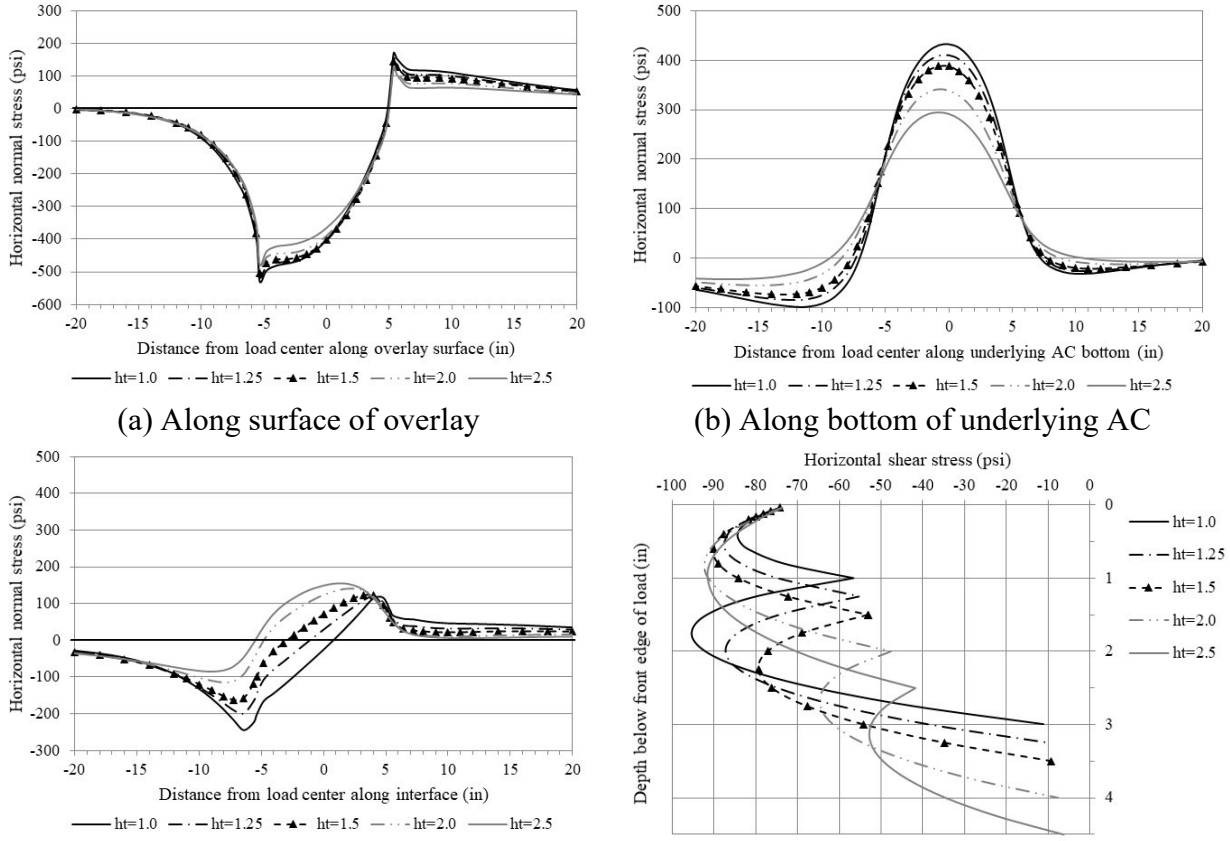


(a) Along surface of overlay (b) Along bottom of underlying AC

(c) Along interface (d) Shear below front edge of the wheel load

Figure 3-9 Effect of overlay thickness on stress distribution (braking).

## 3.4 Effect of Reaction Modulus

Like the study presented in Section 3.3, a high SR of 32 and a low underlying AC thickness of 2 inch were selected and kept constant for evaluating the effect of interface reaction modulus. An intermediate value of overlay thickness (1.5 inch) was used. A total of ten cases were simulated, including five levels of interface reaction modulus (K = 0.1, 1, 10, and 100 N/mm$^3$ representing a wide range of weak bond conditions under scabbing, and K = infinite representing a full bond condition), and two rolling conditions (free-rolling and braking).

Figure 3-10 presents the resulting stress distribution for pavement sections with varying interface reaction modulus under the free-rolling condition. Compared to the full bond condition, an increase in the degree of weakness in the bond condition (i.e., a reduction in K value) resulted in an increase in tension at the surface of the overlay from 30 to 49 psi (Figure 3-10a), at the bottom of the underlying AC from 348 to 415 psi (Figure 3-10b), and at the upper interface from 0 to 342 psi (Figure 3-10c). A decreased reaction modulus resulted in slightly lower shear. Specifically, peak shear reduced from 76 to 68 psi (Figure 3-10d). It is important to note that horizonal shear stress peaked below the interface for all weak bond conditions.

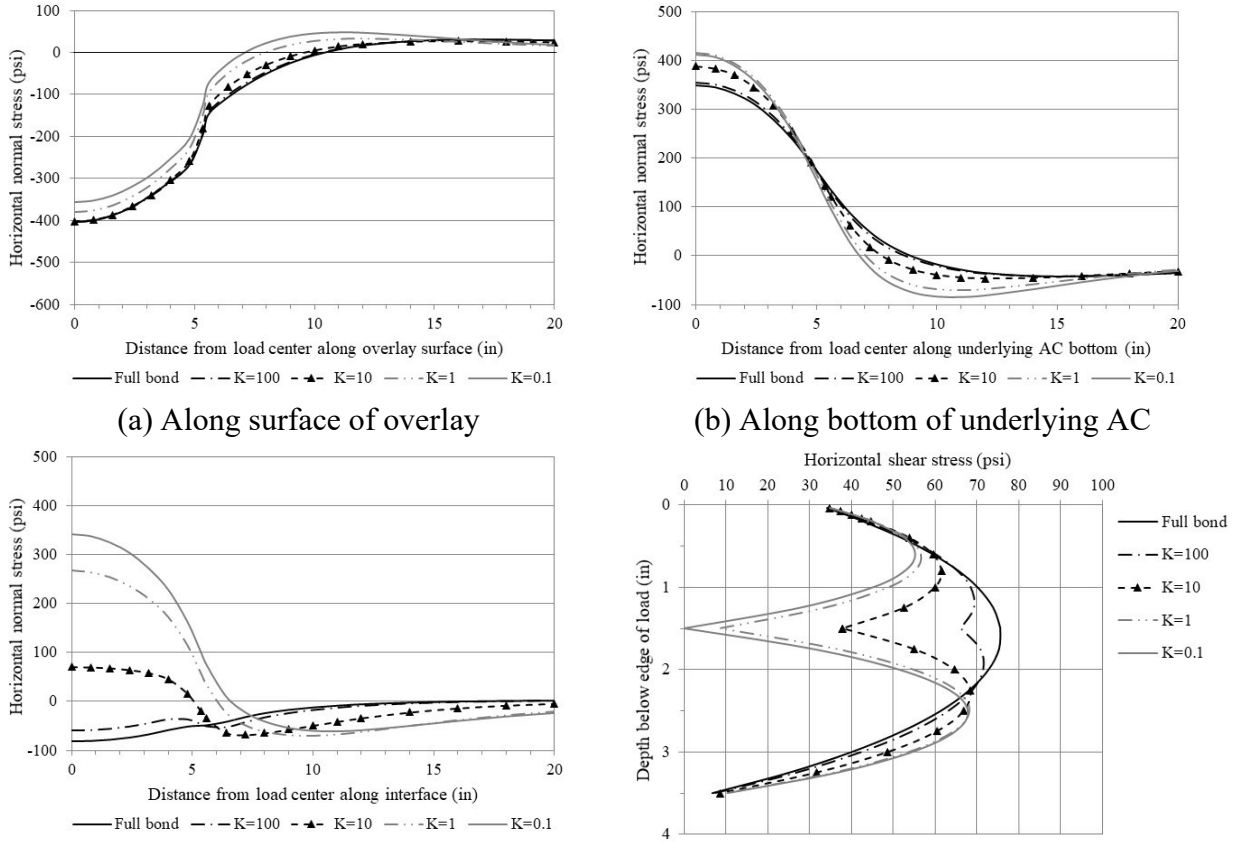


(a) Along surface of overlay

(b) Along bottom of underlying AC

(c) Along interface

(d) Shear below edge of the wheel load

Figure 3-10 Effect of reaction modulus on stress distribution (free-rolling).

The resulting stress distribution for the same pavement sections under the braking condition are shown in Figure 3-11. Compared to the results under the free-rolling condition, the addition of a horizontal load in the braking zones resulted in higher tension at the surface of the overlay and at

the upper interface as well as higher shear stresses. As expected, there was almost no change in tension at the bottom of the underlying AC (figure 3-11b). The increase in surface tension was most significant. The peak value in the range of 112 to 218 psi occurred right behind the wheel load (Figure 3-11a). The peak tension at the upper interface increased to 351 psi, which occurred below the load in the section with a K of 0.1 N/mm$^3$ (Figure 3-11c). The peak horizontal shear increased to 99 psi, which was about 1.5 inch below the front edge of the wheel load (Figure 3-11d).

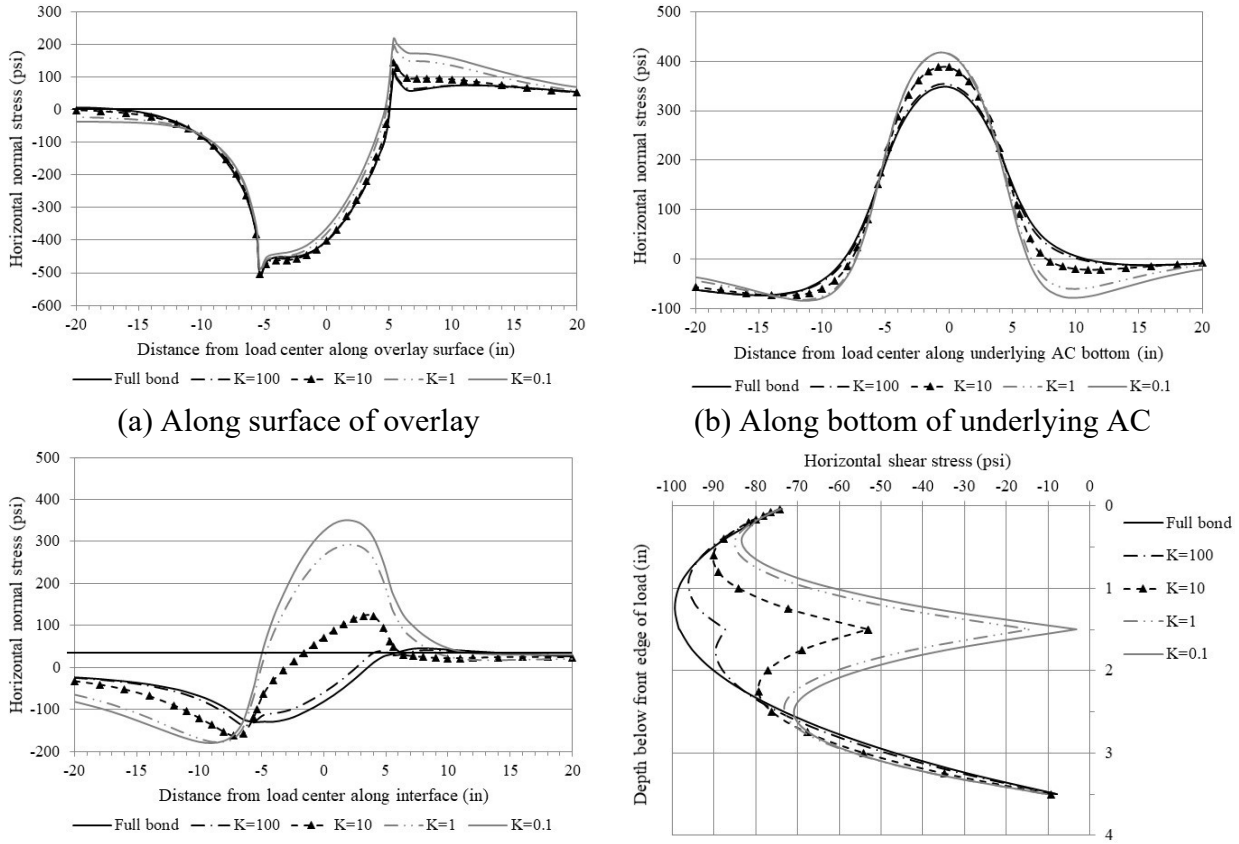


(a) Along surface of overlay

(b) Along bottom of underlying AC

(c) Along interface

(d) Shear below front edge of the wheel load

Figure 3-11 Effect of reaction modulus on stress distribution (braking).

## 3.5 Concluding Remarks

Pavement scabbing analysis was conducted with the global interface (scabbing) representation for a combination of 36 cases based on five key factors: AC-to-base stiffness ratio, underlying AC thickness, overlay thickness, interface reaction modulus, and rolling condition. A summary of key findings regarding effects of these factors on stress distribution near the scabbed area is presented as follows.

- A higher AC-to-base stiffness ratio and a thinner underlying AC generally resulted in more critical stress states.
- Increasing overlay thickness reduced tension at the surface of the overlay and at the bottom of the underlying AC as well as peak shear stress, although it resulted in higher tension at the upper interface.
- An increase in the degree of weakness in the bond condition led to significant increase in tension at the upper interface. Also, a weaker bond resulted in an increase in tension at the surface of the overlay and at the bottom of the underlying AC.
- The addition of a horizontal load in the braking zones consistently resulted in much higher tension at the surface of the overlay. Also, the brake loading condition led to higher tension at the upper interface as well as higher shear stress.

Overall, the conventional approach with the global interface (scabbing) representation provided insights regarding the effects of a range of key factors on pavement responses. However, it could not consider the effect of the scabbing size (i.e., radius and thickness of the scabbed layer) on stress distribution in the overlay. Therefore, finite element models with a hybrid interface representation were developed for further study as described in Chapter 4.

CHAPTER 4

FINITE ELEMENT MODEL DEVELOPMENT FOR PAVEMENT SCABBING ANALYSIS

## 4.1 Introduction

Finite element pavement models with scabbing were developed using LS-DYNA (2021), which is an advanced general-purpose multi-physics simulation software package. It originated from the three-dimensional finite element analysis program DYNA3D developed primarily for the analysis of structures subjected to impact loads (Hallquist, 1976). Livermore Software Technology Corporation (LSTC) was founded in 1988 to add more capabilities to the software, including a preprocessor LS-PrePost designed to provide an efficient and friendly interface to pre and post process files for the main solver of LS-DYNA.

### 4.1.1 Hybrid interface representation

The global interface representation associated with the conventional approach in BISAR could not consider the effect of scabbing size on stress distribution in the overlay (Figure 4-1a). Therefore, a hybrid interface representation was employed in finite element analysis to represent field conditions more closely, where a partial bond (i.e., a weak bond) existed below localized scabbed areas along with a full bond existed in the remaining area of the interface (Figure 4-1b).

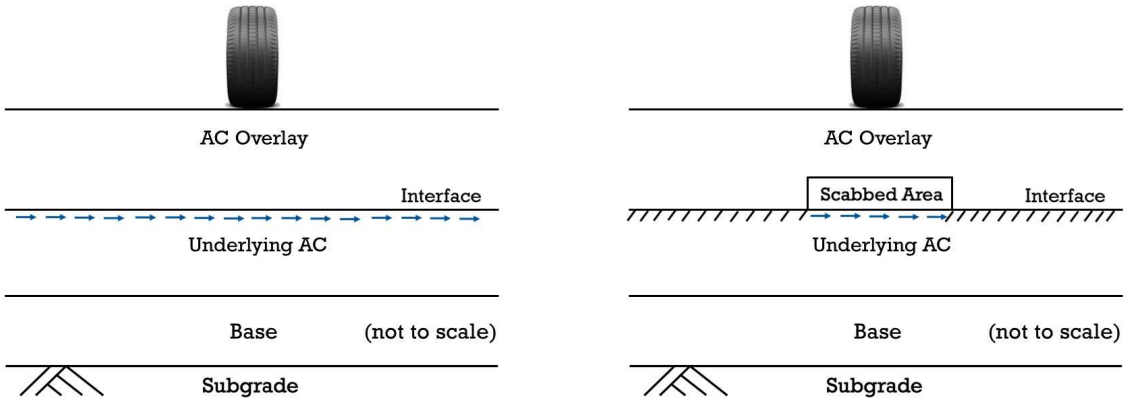


(a) Global interface representation (b) Hybrid interface representation

Figure 4-1 Comparison of global and hybrid interface representations for scabbing analysis.

In LS-DYNA, an interface model was employed by assigning a pair of horizontal springs to connect the upper interface and the lower interface for each pair of elements along the interface (Figure 4-2).

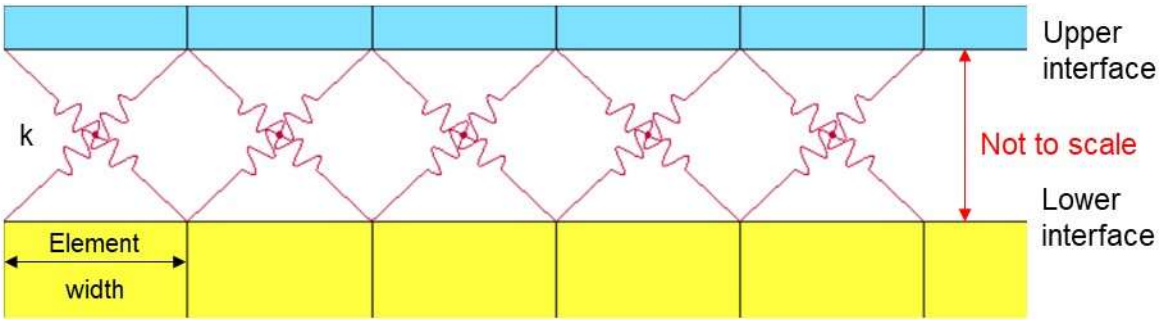


Figure 4-2 Schematic layout for horizontal springs in one-dimensional representation.

The elemental spring constant (k) can be determined as the product of interface reaction modulus and elemental surface area in the horizontal plane using Equation 4.1.

$$k = \frac{Interface\ shear\ force}{Relative\ horizontal\ displacement} = K \cdot Surface\ area \quad (4.1)$$

Where, k is spring constant for each pair of elements and K denotes interface reaction modulus. The surface area equals to the product of element width and element length. An interface reaction modulus in the range of 1 to 100 N/mm$^3$ was used to represent the weak bond below localized scabbed areas.

### 4.1.2 Scab size and milling depth

It was assumed that a lift thickness of 2-inch was used in construction of the asphalt layers of the original pavement sections. Milling and overlay were employed for rehabilitation of these pavements after being in service for several years (e.g., 10 years). Furthermore, it was assumed that a milling depth that is no greater than 1.0 inch would not result in scabbing due to the relatively large thickness in the remaining top lift. Also, a milling depth of 2.0 inch which equals to the lift thickness would not result in scabbing. Scabbing would occur when milling depth was greater than 1.0 and less than 2.0 inch, and a greater milling depth in this range would lead to a thinner and smaller scabbed layer. Based on discussion with the research panel, three sizes of scabbed layers were selected for this study, including a large size (0.75-inch thickness and 25-

inch radius), an intermediate size (0.5-inch thickness and 10-inch radius), and a small size (0.25-inch thickness and 2.5-inch radius) as shown in Table 4-1.

Table 4-1 Thickness and radius selected for scabbed layer after milling

| Milling depth (in.) | Scabbing status | Scabbed layer | |
|---|---|---|---|
| | | Thickness (in.) | Radius (in.) |
| ≤ 1.0 | No | – | – |
| 1.25 | Yes | 0.75 | 25.0 |
| 1.50 | | 0.50 | 10.0 |
| 1.75 | | 0.25 | 2.5 |
| 2.0 | No | – | – |

An asphalt pavement section employed in Chapter 3 was selected for this part of the study. The pavement section (without scabbing) consists of 1.5-inch AC overlay, 2-inch underlying AC layer (after milling), and 12-inch base on top of the subgrade. All materials were assumed to be linear elastic with properties presented in Table 4-2. For a companion pavement section with localized scabbing, a scabbed body of 10-inch radius and 0.5-inch thickness was introduced to sit at the surface of the underlying AC and below the center of the wheel load (100-psi pressure and 5.35-inch radius). The scabbed body had the same material properties as the underlying AC layer. A partial bond with an intermediate K value (10 $N/mm^3$) was used below the scabbed area, while a full bond was applied to the remaining area of the interface.

Table 4-2 Pavement structure and property of layers.

| Pavement layers | Thickness (in.) | Modulus (ksi) | Poisson's ratio |
|---|---|---|---|
| AC overlay | 1.5 | 800 | 0.35 |
| Underlying AC | 2 | 800 | 0.35 |
| Base | 12 | 25 | 0.4 |
| Subgrade | – | 15 | 0.45 |

## 4.2 Axisymmetric Finite Element Pavement Models for Free-Rolling Condition

Axisymmetric finite element pavement models were developed subjected to a vertical load for free-rolling condition. Both the pavement system and the uniformly-distributed circular load are symmetrical with respect to the central axis. Model verification was conducted by comparing results from the finite element model and those from the layered elastic analysis program BISAR, assuming a global interface representation (Figure 4-1a). Example simulations were performed to identify locations of interest in finite element pavement models with localized scabbing, assuming a hybrid interface representation (Figure 4-1b).

### 4.2.1 Model verification for free-rolling condition

A range of three K values was adopted for model verification, including: 1) K = 0 for no bond condition, 2) K = 10 N/mm$^3$ for partial bond condition, and 3) K = infinite for full bond condition. Figures 4-3a and 4-3b show horizontal normal stresses and shear stresses along the interface for three bond conditions, including two extreme conditions (full bond and no bond) and a partial bond condition. When the AC overlay was fully bonded with the underlying AC layer (K = infinite), the horizontal normal stresses were generally in compression and the shear stresses peaked at around 75 psi below the edge of the load. For the no bond condition (K = 0), the horizontal normal stresses peaked at around 330 psi in tension below the center of the load and the shear stresses were about zero throughout the interface. As expected, the horizontal normal stresses and shear stresses along the interface for the partial bond condition stayed in between the results from the two extreme conditions.

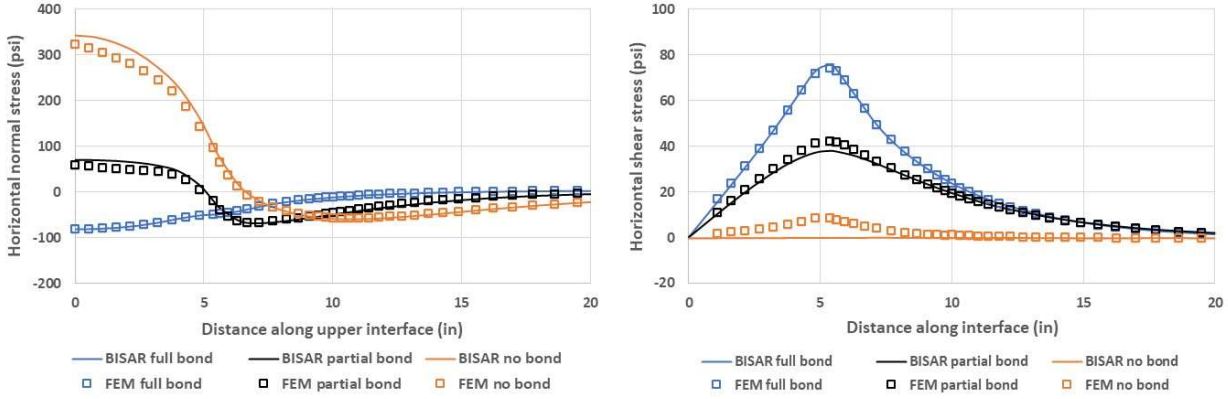


(a) Horizontal normal stress (b) Shear stress

Figure 4-3 Comparison of stresses along the interface.

Horizontal normal stresses below the center of the load and shear stresses below the edge of the load are shown in Figures 4-4a and 4-4b, respectively. When the AC overlay was fully bonded with the underlying AC (K = infinite), the horizontal normal stress varied linearly from around 400 psi (compression) at the surface of AC overlay to around 300 psi (tension) at the bottom of underlying AC layer, while the shear stress peaked at around 75 psi at the interface. For the no bond condition (K = 0), there was a large jump in horizontal normal stress from tension at the bottom of the overlay to compression at the top of the underlying layer, while the shear tress diminished at the interface. The horizontal normal stresses and shear stresses along the depth of AC layers for the partial bond condition stayed in between the results from the two extreme conditions.

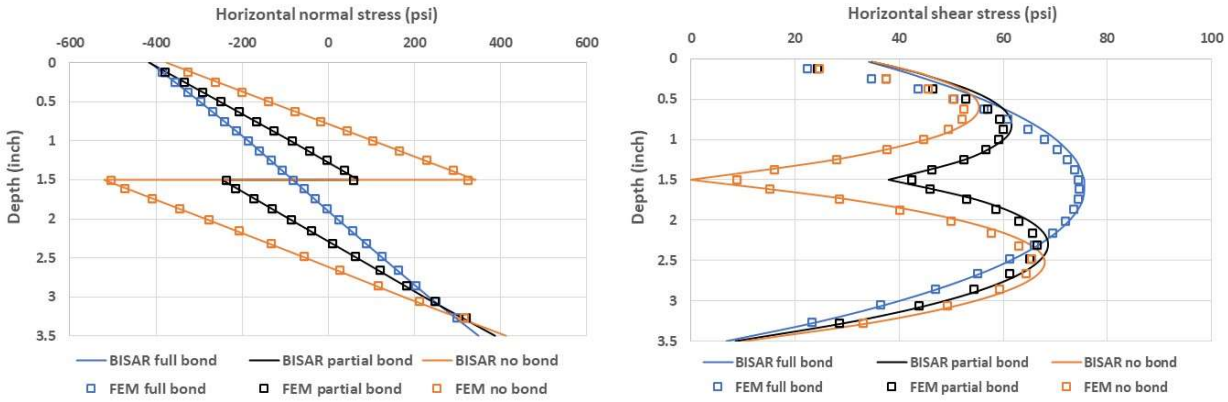


(a) Horizontal normal stress below center of the load

(b) Shear stress below edge of the load

Figure 4-4 Comparison of stresses along the depth of AC layers.

Furthermore, both Figures 4-3 and 4-4 show that results from the axisymmetric finite element model (consisting of four-node elements) agreed well with those from the BISAR program. This agreement demonstrated that the interface model adopted for the axisymmetric pavement model was appropriate for simulating the behavior of a partial bond under the free-rolling condition.

### 4.2.2 Example simulation and results

Figure 4-5 presents the meshes for the axisymmetric finite element pavement model with a hybrid interface representation. As shown in the zoomed-in view (Figure 4-5b), a scabbed body of 10-inch radius and 0.5-inch thickness (in blue) was introduced below the center of the wheel load and sitting at the surface of the underlying AC (in green). A partial bond was used below

the scabbed area (red dashed line), while a full bond was applied to the remaining area of the interface (black continuous line).

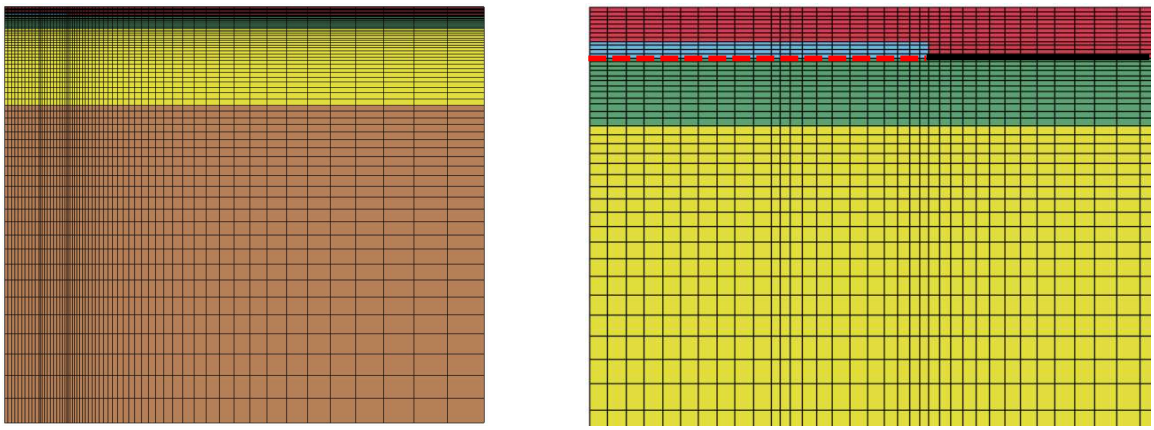

(a) Complete view (b) Zoomed-in view

Figure 4-5 Mesh for the axisymmetric pavement model with scabbing.

Figure 4-6a shows a contour of horizontal normal stress distribution in AC layers for the pavement model without scabbing (full bond condition). A companion stress contour for the pavement model with localized scabbing is presented in Figure 4-6b. The presence of a weak bond below the scabbed area altered the stress distribution and resulted in two new tension zones near the interface between scabbing and underlying AC as described below.

- Zone 1 is above the interface and located at the bottom of the central area of the scab. The tensile stresses in Zone 1 may cause fatigue cracking in the scab under repeated traffic loading.
- Zone 2 is below the interface and located under the edge of the scab. The tensile stresses in Zone 2 tends to initiate a crack in the underlying AC, which may be reflected to the surface under a combination of thermal and traffic loading.

Figure 4-7 compares contours of horizontal shear stress distribution in AC layers for the pavement models with and without scabbing. The presence of a weak bond below the scabbed area resulted in a new shear zone at the edge of the scab. The shear stresses in this zone may weaken the full bond in the interface next to the scabbing and potentially extend the partial bond beyond the scabbed area. Therefore, the upper and lower interfaces (for horizontal normal stresses) and the interface (for horizontal shear stresses) were selected as the locations of interest

for sensitivity study and further evaluation. Also, the overlay surface (for horizontal normal stresses) was included for additional information.

(a)

(b)

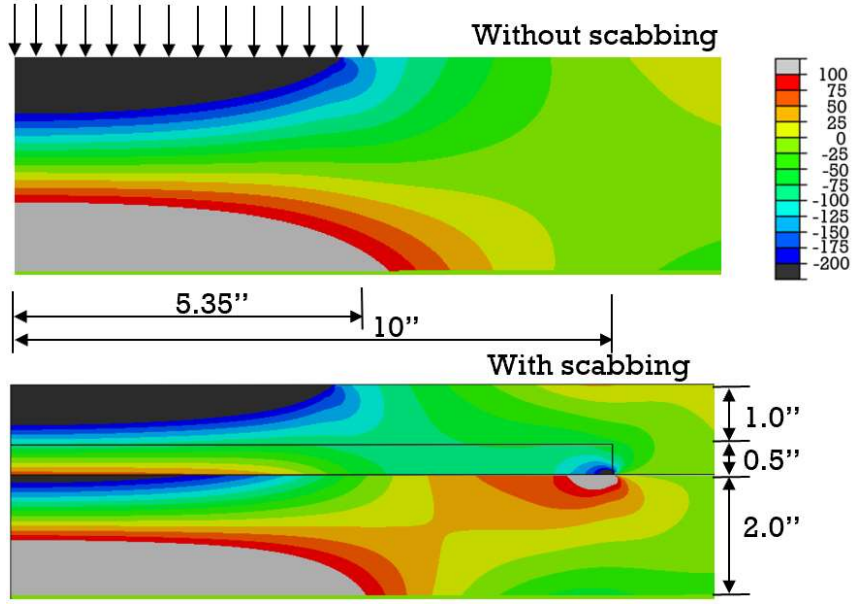


Figure 4-6 Horizontal normal stress: (a) full bond and (b) localized partial bond (free-rolling).

(a)

(b)

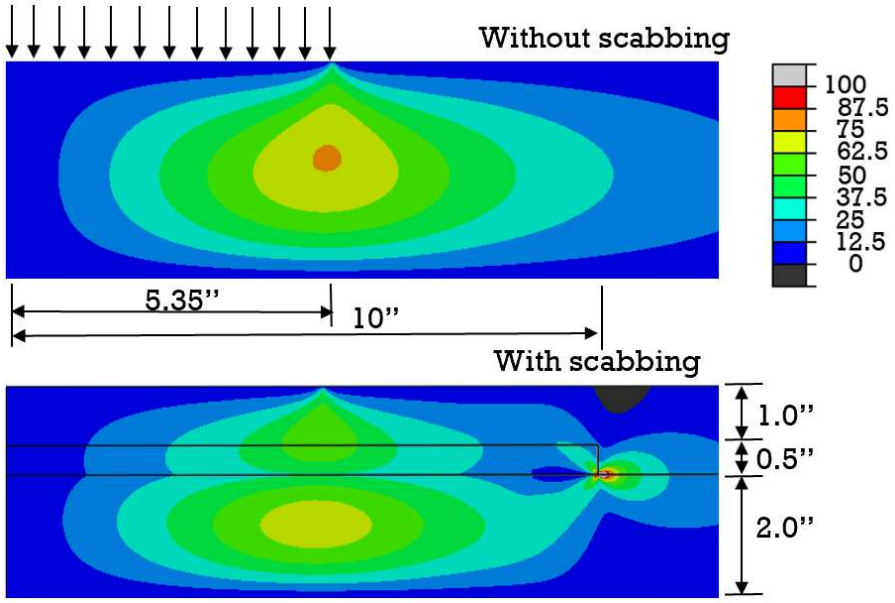


Figure 4-7 Horizontal shear stress: (a) full bond and (b) localized partial bond (free-rolling).

Figure 4-8 presents the results of stress distribution at locations of interest for pavement sections with three interface bond conditions under the free-rolling load, including full bond (no scabbing), global partial bond (global scabbing), and localized partial bond (localized scabbing). Compared to the full bond condition, both global partial bond and localized partial bond resulted in a stress reversal (i.e., change in horizontal normal stress from compression to tension) at the upper interface below the load (Figure 4-8a). A localized partial bond condition led to a significant increase in tension at the lower interface below the edge of the scab (Figure 4-8b) and a mild increase in tension at the surface of the overlay (Figure 4-8c). Shear stress distribution in Figure 4-8d shows that both global partial bond and localized partial bond resulted in lower horizontal shear below the edge of the load. However, the localized partial bond condition led to a significant increase in shear at the edge of the scab.

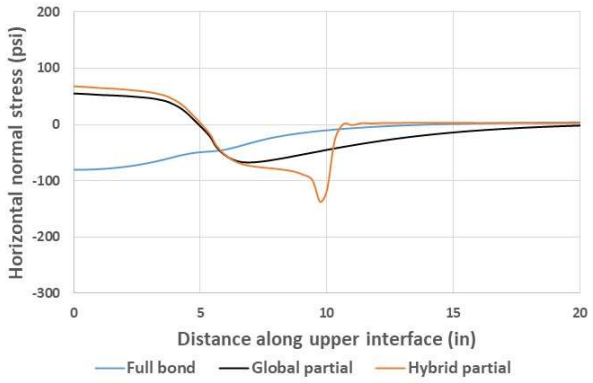


(a) HOR normal stress: upper interface

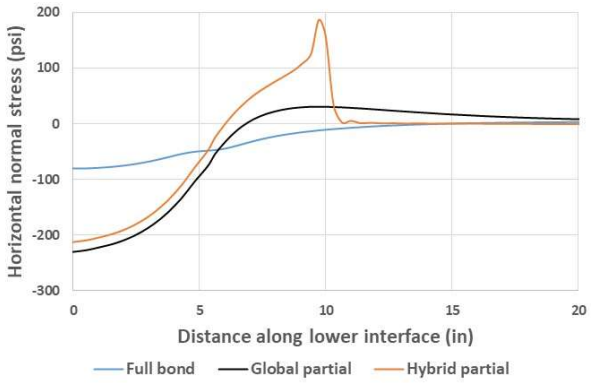


(b) HOR normal stress: lower interface

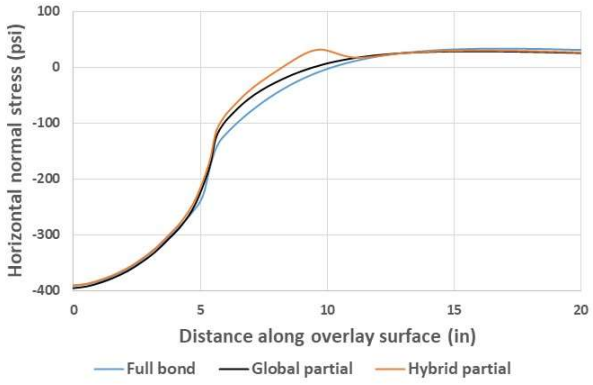


(c) HOR normal stress: overlay surface

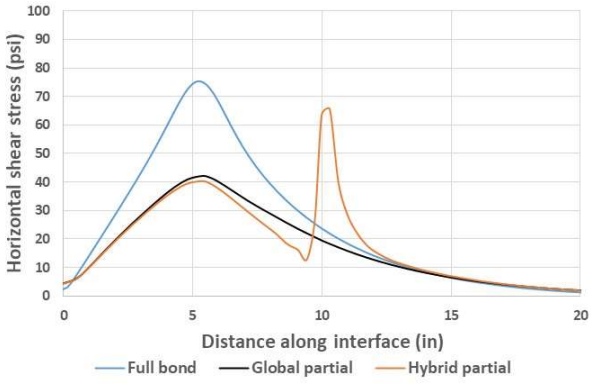


(d) HOR shear stress: interface

(HOR denotes horizontal for brievity.)

Figure 4-8 Effect of scabbing on horizontal stress distribution (free-rolling).

## 4.3 Three-Dimensional Finite Element Pavement Models for Braking Condition

Three-dimensional finite element pavement models were developed subjected to a combination of vertical and horizontal loads for braking condition. Only one half of the pavement system was included in the models because both the system and the load were symmetrical with respect to the central vertical plane parallel to the horizontal load. Like the work performed for free-rolling condition, model verification was conducted for braking condition by comparing results from the finite element model and those from BISAR, assuming a global interface representation. Example simulations were performed to identify locations of interest in finite element pavement models with localized scabbing, assuming a hybrid interface representation.

### 4.3.1 Model verification for braking condition

A range of three K values was adopted for model verification for braking condition, including: 1) K = 0 for no bond condition, 2) K = 10 N/mm$^3$ for partial bond condition, and 3) K = infinite for full bond condition. Figures 4-9a and 4-9b show horizontal normal stresses and shear stresses along the interface under the braking loads for three bond conditions, including two extreme conditions (full bond and no bond) and a partial bond condition. Unlike the results for the free-rolling condition, the stresses are asymmetric with respect to the central axis. When the AC overlay was fully bonded with the underlying AC layer (K = infinite), the horizontal normal stresses were generally in compression and the shear stresses peaked at around 100 psi below the front edge of the load. For the no bond condition (K = 0), the horizontal normal stresses peaked at around 350 psi in tension below the back edge of the load and the shear stresses were about zero throughout the interface. As expected, the horizontal normal stresses and shear stresses along the interface for the partial bond condition stayed in between the results from the two extreme conditions.

Horizontal normal stresses below the center of the load and shear stresses below the front edge of the load are shown in Figures 4-10a and 4-10b. When the AC overlay was fully bonded with the underlying AC layer (K = infinite), the horizontal normal stress varied linearly from around 400 psi (compression) at the surface of overlay to around 300 psi (tension) at the bottom of the underlying AC, while the shear stress peaked at around 100 psi at the interface. For the no bond

condition (K = 0), there was a big jump in horizontal normal stress from tension at the bottom of the overlay to compression at the top of the underlying AC, while the shear stress diminished at the interface. Again, the horizontal normal and shear stresses along the depth of AC layers for the partial bond condition stayed in between the results from the two extreme conditions.

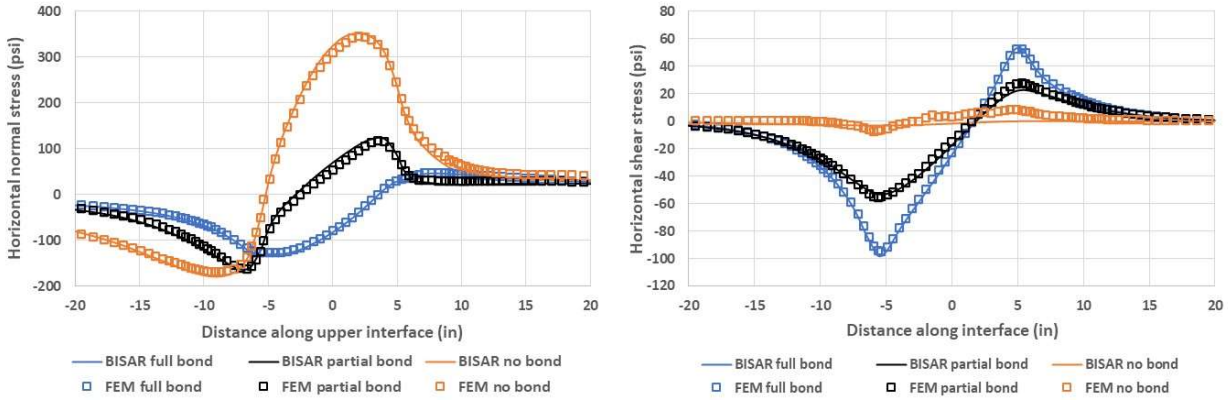


(a) Horizontal normal stress (b) Shear stress

Figure 4-9 Comparison of stresses along the interface under braking condition.

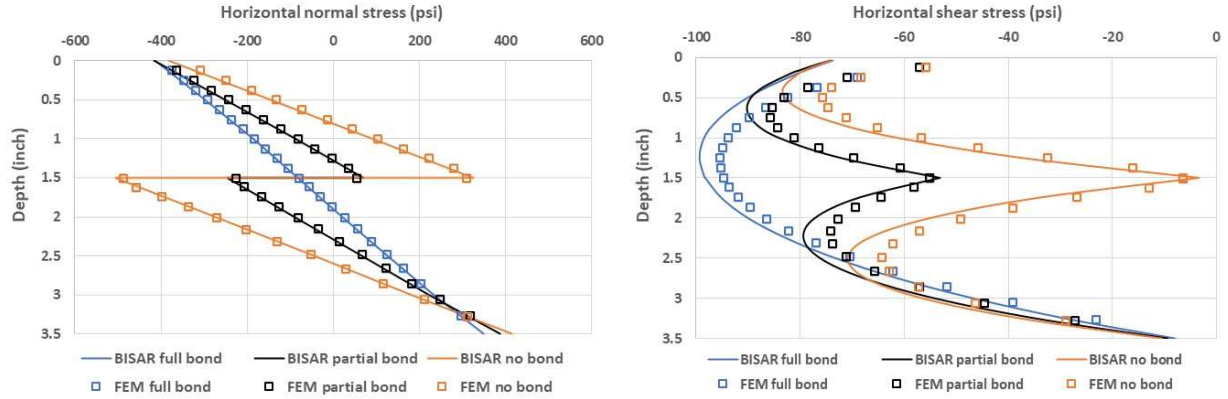


(a) Horizontal normal stress below center of the load

(b) Shear stress below front edge of the load

Figure 4-10 Comparison of stresses along the depth of AC layers under braking condition.

Both Figures 4-9 and 4-10 show that results from the three-dimensional finite element model (consisting of eight-node brick elements) agreed well with those from the BISAR program. This agreement demonstrated that the interface model adopted for the three-dimensional pavement model can be used to properly evaluate the effect of a partial bond under the braking condition. The partial bond is deemed necessary for representation of a weak bond beneath a localized scabbed area.

### 4.3.2 Results of example simulation

Figure 4-11 presents the meshes for the three-dimensional finite element pavement model with localized scabbing. As shown in the zoomed-in view (Figure 4-11b), a scabbed body of 10-inch radius and 0.5-inch thickness (in blue) was introduced below the center of the wheel load and sitting at the surface of the underlying AC (in green). A partial bond was used below the scabbed area (red dashed line), while a full bond was applied to the remaining area of the interface (black continuous line). The pavement was subjected to a wheel load under the braking condition represented by a combination of vertical and horizontal loads. The wheel load was assumed to be heading toward the left side of the pavement structure.

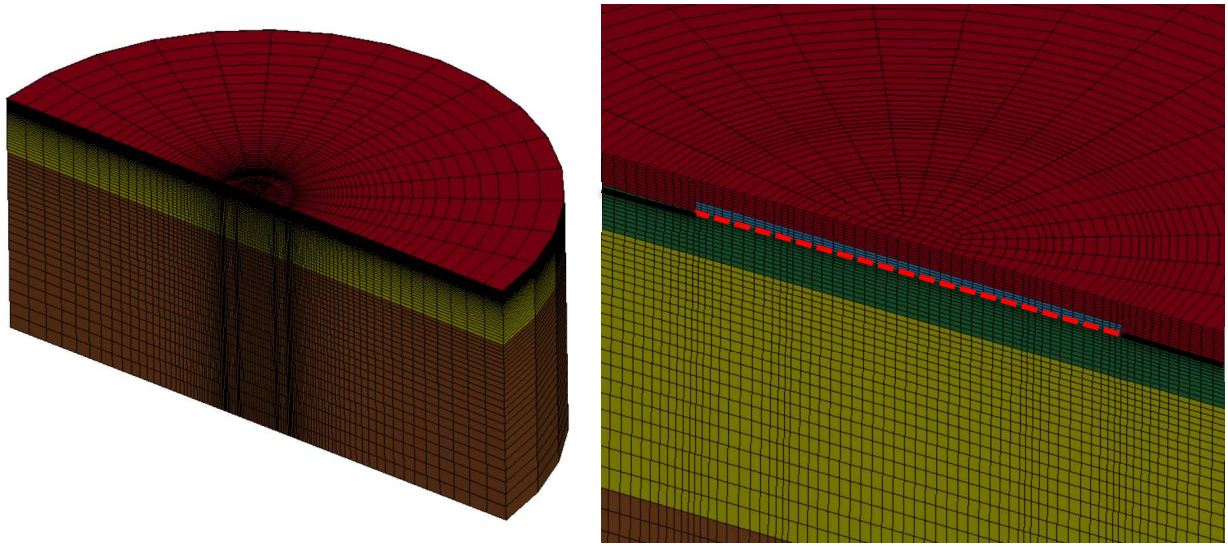

(a) Complete view (b) Zoomed-in view

Figure 4-11 Mesh for the three-dimensional model with scabbing.

Figure 4-12a shows a contour of horizontal normal stress distribution in AC layers for the three-dimensional pavement model without scabbing (full bond condition). A companion stress contour for the pavement model with scabbing (localized partial bond condition) was presented in Figure 4-12b. Under braking condition, the presence of a weak bond below the scabbed area led to a significant increase in tension at the surface of the overlay behind the back edge of the wheel load. High tensile stresses in this location may cause slippage failure under repeated traffic

loading. Also, the weakly-bonded scabbed body resulted in three new tension zones near the interface between scabbing and underlying AC as described below.

- Zone 1 is above the interface and located at the bottom of the scabbed body below the back edge of the wheel load. The tensile stresses in Zone 1 may cause fatigue cracking in the scabbed body under repeated loading.
- Zones 2 and 3 are below the interface and located under the front edge and back edge of the scabbed body, respectively. The tensile stresses in both zones tend to initiate a crack in the underlying AC, which may be reflected to the surface under a combination of thermal and traffic loading.

(a)

(b)

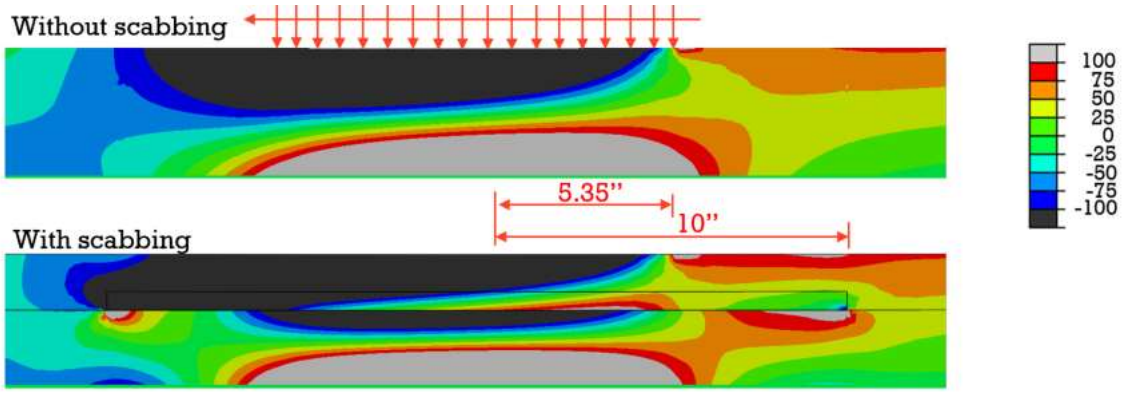


Figure 4-12 Horizontal normal stress: (a) full bond and (b) localized partial bond (braking).

Figure 4-13 compares contours of horizontal shear stress distribution in AC layers for the pavement models with and without scabbing. While the presence of a weak bond below the scabbed area reduced the transfer of shear stresses from the overlay to the underlying AC layer, it led to stress concentration at the edges of the scabbed body, especially at the front edge. The shear stresses in stress concentration zones may weaken the full bond in the interface next to the scabbing and potentially extend the partial bond beyond the scabbed area. Therefore, the overlay surface (for horizontal normal stresses), the upper and lower interfaces (for horizontal normal stresses) and the interface (for horizontal shear stresses) were selected as the locations of interest for sensitivity study and further evaluation.

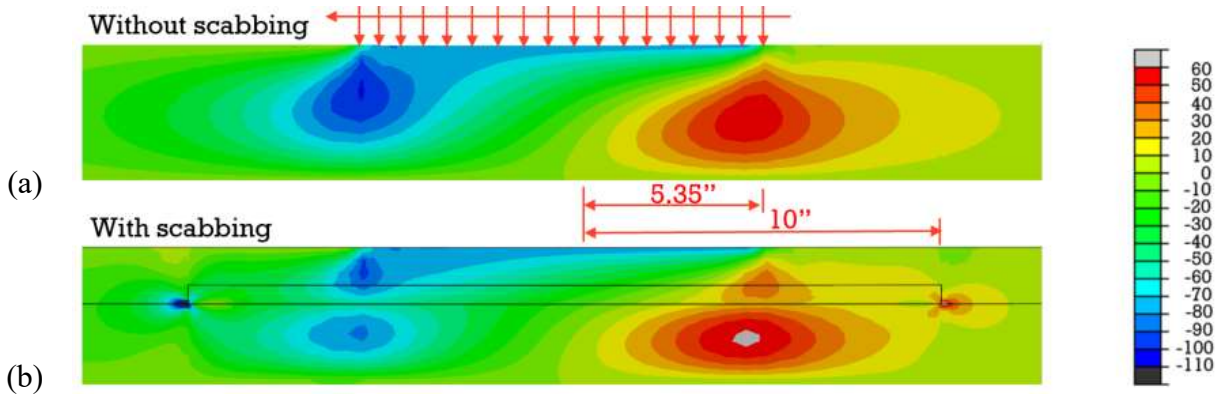

Figure 4-13 Horizontal shear stress: (a) full bond and (b) localized partial bond (braking).

Figure 4-14 presents the results of stress distribution at locations of interest for pavement sections with three interface bond conditions under the braking load: full bond (no scabbing), global partial bond (global scabbing), and localized partial bond (localized scabbing). Compared to the full bond condition, both global partial bond and localized partial bond resulted in a stress reversal (i.e., change in horizontal normal stress from compression to tension) at the upper interface below the load (Figure 4-14a). A localized partial bond condition led to a significant increase in tension at the lower interface below the back edge of the scab (Figure 4-14b) and an increase in tension at the surface of the overlay behind the back edge of the wheel load (Figure 4-14c). Also, it led to tension at the lower interface below the front edge of the scab (Figure 4-14b). Shear stress distribution in Figure 4-14d shows that both global partial bond and localized partial bond resulted in lower horizontal shear below the edge of the load. However, the localized partial bond condition led to a significant increase in shear at both edges of the scab, especially at the front edge. It is important to note that compared to results under free-rolling condition (Figure 4-8), the peak tension at the upper interface shifted from below the center of the load to below the back edge of the load and increased by about two times. The peak tension at overlay surface shifted from the edge of the scab to the back edge of the load and increased by about five times.

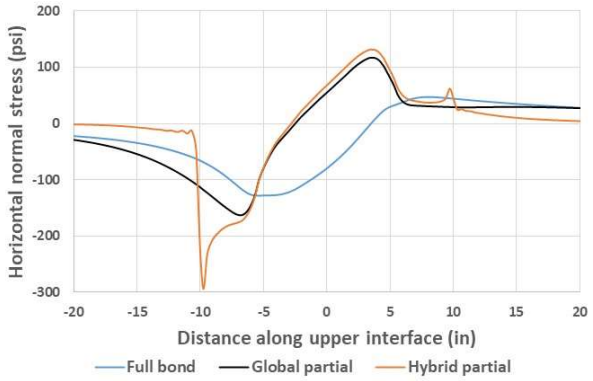


(a) HOR normal stress: upper interface

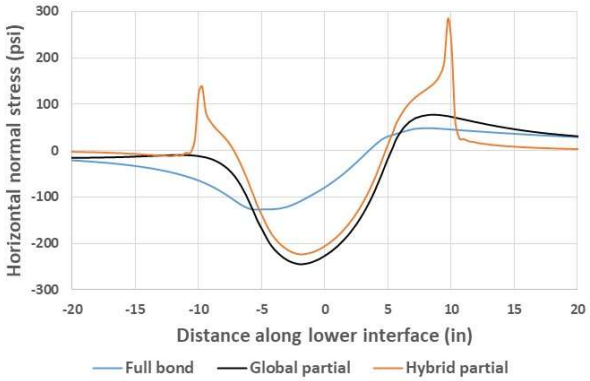


(b) HOR normal stress: lower interface

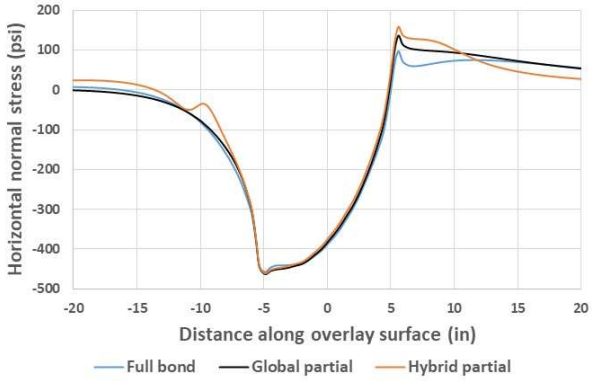


(c) HOR normal stress: overlay surface

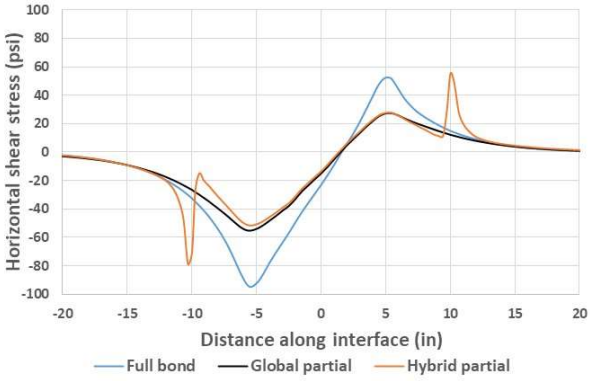


(d) HOR shear stress: interface

Figure 4-14 Effect of scabbing on stress distribution in 3-D models (braking).

### 4.4 Plane Strain Finite Element Pavement Models for Braking Condition

Due to significant effort for developing 3-D finite element pavement models with localized scabbing and long computer running time, 2-D plane strain models were evaluated to serve as a more efficient alternative while retaining sufficient accuracy. Figure 4-15 presents the results of stress distribution for a plane strain pavement model with three interface bond conditions under the braking load: full bond (no scabbing), global partial bond (global scabbing), and localized partial bond (localized scabbing). Compared to the results from 3-D models (Figure 4-14), the plane strain models generally produced similar trends in critical responses at the locations of interest. The main difference was in tension at the surface of the overlay where the shape of load mattered the most (a circular load in 3-D vs. a strip load in plane strain). While the tension at the surface peaked at the back edge of the load and diminished quickly from the 3-D model, the tension from the plane strain model peaked farther away from the load and sustained for a much

longer distance. The same trend can be consistently observed from a more extensive comparison of three-dimensional and plane strain finite element results included in Appendix A.

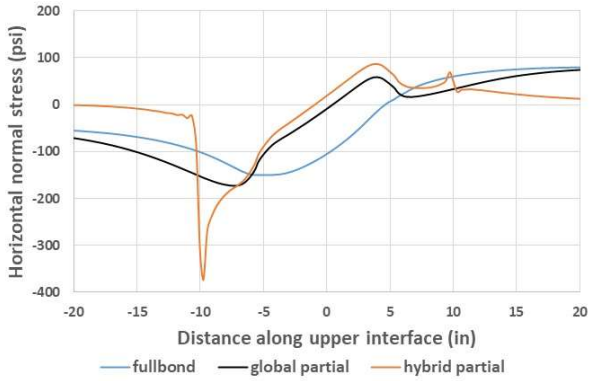


(a) HOR normal stress: upper interface

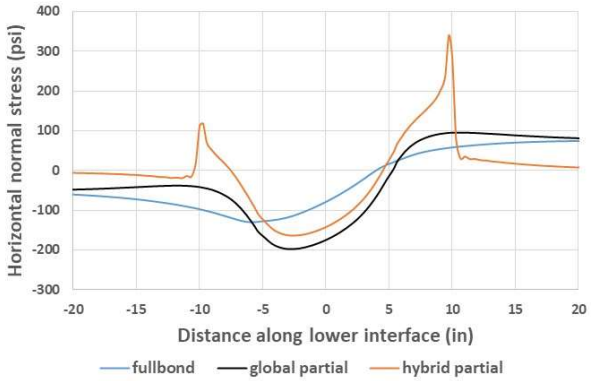


(b) HOR normal stress: lower interface

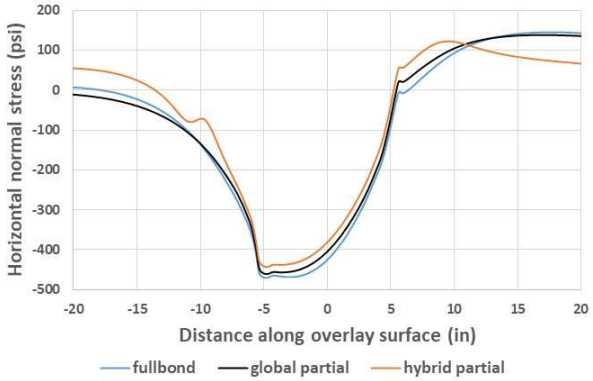


(c) HOR normal stress: overlay surface

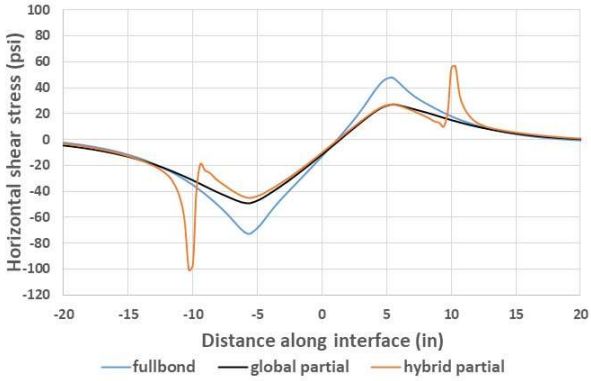


(d) HOR shear stress: interface

Figure 4-15 Effect of scabbing on stress distribution in plane strain models (braking).

## 4.5 Concluding Remarks

Finite element models with a hybrid interface representation were developed for investigating the effect of key factors on critical pavement responses including scab size. A summary of key findings from the model development effort is presented as follows.

- Axisymmetric and three-dimensional finite element pavement models were developed for obtaining pavement responses under the free-rolling and braking conditions, respectively.
- The interface model implemented in the LS-DYNA program was appropriate for simulating the behavior of a partial bond under both the free-rolling and braking loads.
- The localized partial bond condition clearly led to more critical responses than both global full bond and global partial bond conditions. Therefore, a sensitivity study was

warranted for pavement scabbing analysis with the hybrid interface representation (Chapter 5).

In addition, the plane strain models generally produced similar trends in critical responses at the locations of interest as those from the 3-D models. As a more efficient alternative while retaining sufficient accuracy, a plane strain model appeared to be promising for further study on responses of pavement sections under impact loading (Chapter 6).

# CHAPTER 5
# PAVEMENT SCABBING ANALYSIS WITH FINITE ELEMENT METHOD

A total of eighteen cases were simulated for this part of the study, including three scab sizes (2.5-inch radius and 0.25-inch thickness for a small size, 10-inch radius and 0.5-inch thickness for an intermediate size, and 25-inch radius and 0.75-inch thickness for a large size), three levels of interface reaction modulus (1, 10, and 100 N/mm$^3$), three levels of overlay thickness (1.0, 1.5, and 2.0 inch), and three levels of overlay stiffness (200, 400, and 800 ksi). Axisymmetric and three-dimensional finite element models with a hybrid interface representation were employed for investigating the effects of key factors on critical pavement responses under free-rolling and braking conditions, respectively. The pavement section with intermediate values of scab size (10-inch radius and 0.5-inch thickness), reaction modulus (10 N/mm$^3$), overlay thickness (1.5 inch), and with an overlay stiffness identical to that of the underlying AC (800 ksi) was employed as the reference case throughout the analysis. Appendix B included three mesh designs for three-dimensional pavement models with a large, an intermediate, and a small scab, respectively.

## 5.1 Effect of Scab Size

### 5.1.1 Results of analysis for free-rolling condition

Figure 5-1 presents the results of stress distribution at locations of interest for pavement sections with varying scab size under the free-rolling condition. Compared to the medium-size scab, the large-size scab (with a radius of about five times the radius of the wheel load) resulted in a significant reduction in tension and in shear below the edge of the scab (see Figure 5-1b and 5-1d, respectively), while small reduction occurred in tension at the upper interface below the center of the load (Figure 5-1a) and at the surface of the overlay (Figure 5-1c). The small-size scab, which has a radius of about half of the radius of the load, resulted in a stress reversal (i.e., a change from tension to compression) at the upper interface under the center of the load (Figure 5-1a) and a significant reduction in tension at the lower interface below the edge of the scab (Figure 5-1b). Although higher shear occurred at the interface below the edge of the load, the stress state was not critical for debonding due to presence of high confinement at the same

location. It appeared that a scab with the intermediate size (with a radius of about two times the radius of the load) had the most critical stress state. When the scab increased to a large size of about five times the radius of the load, the stress distributions became almost identical to those from the global partial bond condition (see Figure 4-8). The stress distributions became like those from the full bond condition when the scab decreased to a small size of about half of the radius of the load (see also Figure 4-8).

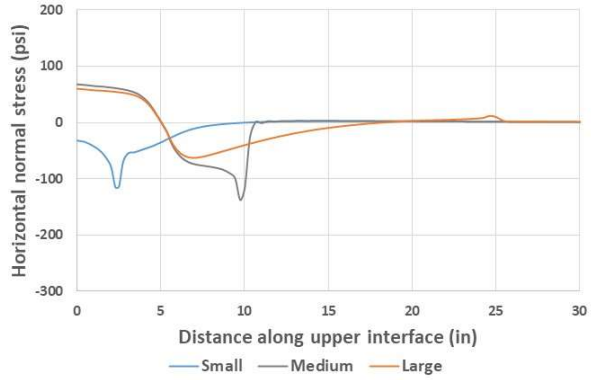


(a) HOR normal stress: upper interface

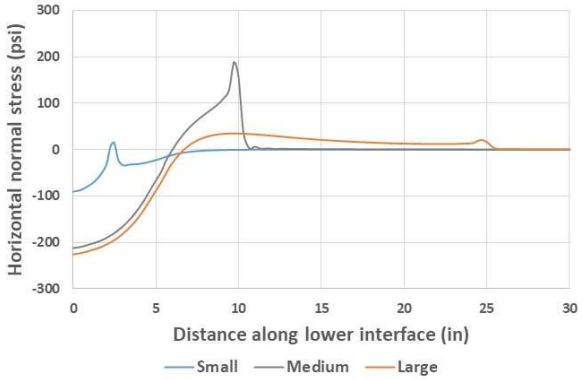


(b) HOR normal stress: lower interface

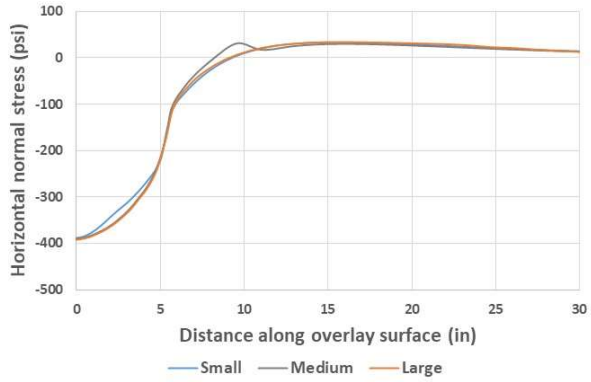


(c) HOR normal stress: overlay surface

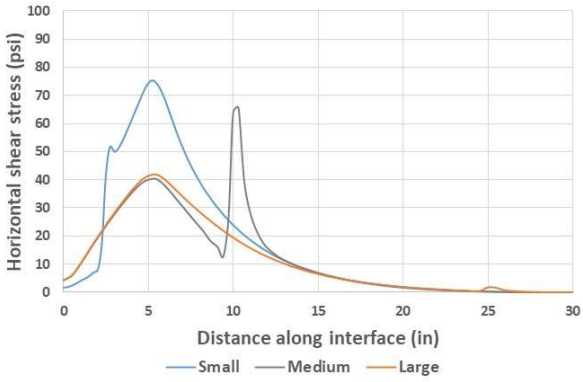


(d) HOR shear stress: interface

Figure 5-1 Effect of scab size on stress distribution (free-rolling).

### 5.1.2 Results of analysis for braking condition

Figure 5-2 presents the results of stress distribution for pavement sections with varying scab size under the braking condition. Compared to the results under the free-rolling condition, the addition of a horizontal load in the braking zones resulted in higher tension at the surface of the overlay and at the upper and the lower interfaces as well as higher shear stresses. The increase in surface tension was most significant. The peak value in the range of 89 to 158 psi occurred right behind the wheel load (Figure 5-2c). The peak tension at the upper interface increased to 132 psi,

which occurred below the back edge of the load in the section with the intermediate-size scab (Figure 5-2a). The peak tension at the lower interface increased to 284 psi, which occurred below the back edge of the scab (Figure 5-2b). The peak horizontal shear increased to 94 psi, which occurred below the front edge of the load in the section with the small-size scab (Figure 5-2d). Like the trend observed from the results under the free-rolling condition, a scab with the intermediate size (about two times the radius of the load) appeared to have the most critical stress state. When the scab increased to a large size of about five times the radius of the load, the stress distributions became almost identical to those from the global partial bond condition (see Figure 4-14). However, the stress distributions were clearly different from those from the full bond condition when the scab decreased to a small size of about half of the radius of the load (see also Figure 4-14). High tension was observed at both the upper and lower interfaces below the edge of the scab.

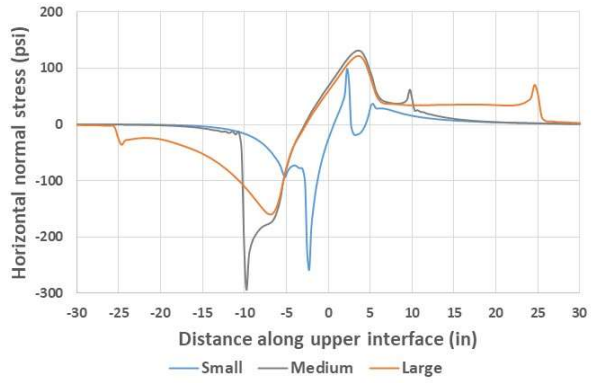


(a) HOR normal stress: upper interface

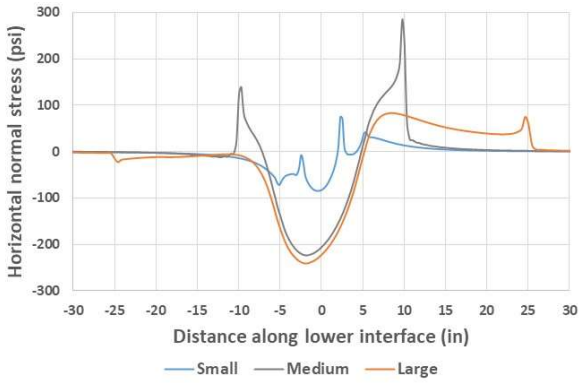


(b) HOR normal stress: lower interface

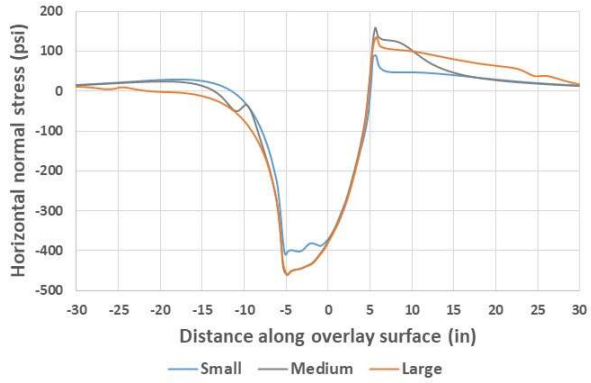


(c) HOR normal stress: overlay surface

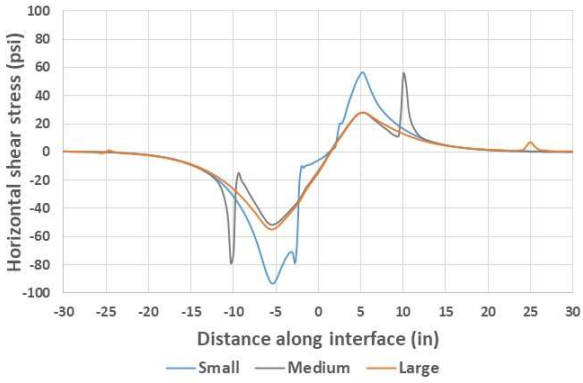


(d) HOR shear stress: interface

Figure 5-2 Effect of scab size on stress distribution (braking).

## 5.2 Effect of Interface Reaction Modulus

Figure 5-3 presents the resulting stress distribution in pavement sections under the free-rolling condition for scabbed layers with varying interface reaction modulus. An increase in the degree of weakness in the bond condition (i.e., a reduction in K value) resulted in an increase in tension at the upper interface below the center of the load in Figure 5-3a (higher fatigue cracking potential), at the lower interface below the edge of the scab in Figure 5-3b (higher reflective cracking potential), and at the surface of the overlay in Figure 5-3c. Also, a decreased reaction modulus led to higher shear at the edge of the scab in Figure 5-3d (higher debonding potential).

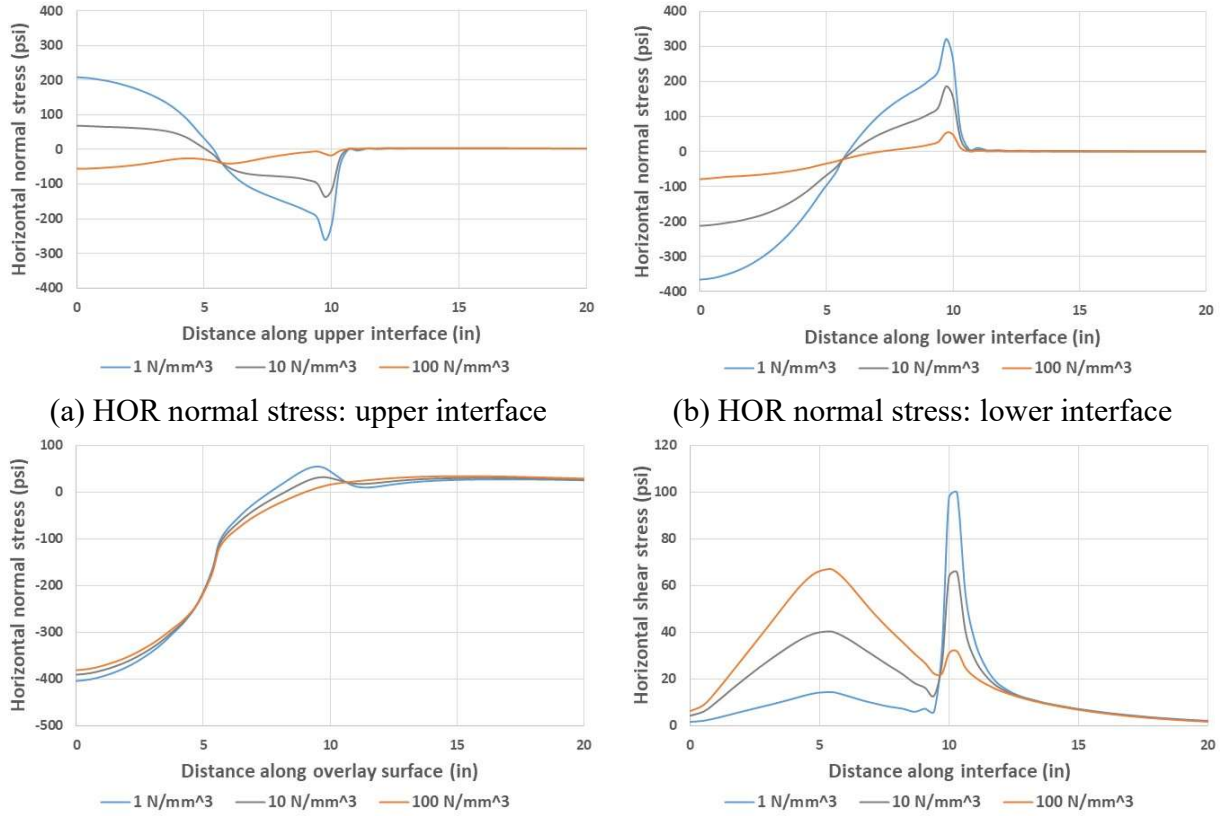


(a) HOR normal stress: upper interface

(b) HOR normal stress: lower interface

(c) HOR normal stress: overlay surface

(d) HOR shear stress: interface

Figure 5-3 Effect of interface reaction modulus on stress distribution (free-rolling).

Figure 5-4 presents the resulting stress distribution in pavement sections under the braking condition for scabbed layers with varying interface reaction modulus. Compared to the results under the free-rolling condition, the addition of a horizontal load in the braking zones resulted in higher tension at the surface of the overlay and at the upper and lower interfaces as well as

higher shear stresses. The increase in surface tension was most significant. The peak value in the range of 136 to 182 psi occurred right behind the wheel load (Figure 5-4c). The peak tension at the upper interface increased to 245 psi, which occurred below the back edge of the load in the section with a K of 1.0 N/mm$^3$ (Figure 5-4a). The peak tension at the lower interface increased to 355 psi, which occurred below the back edge of the scab (Figure 5-4b). The peak horizontal shear increased to 123 psi, which occurred below the front edge of the scab (Figure 5-4d).

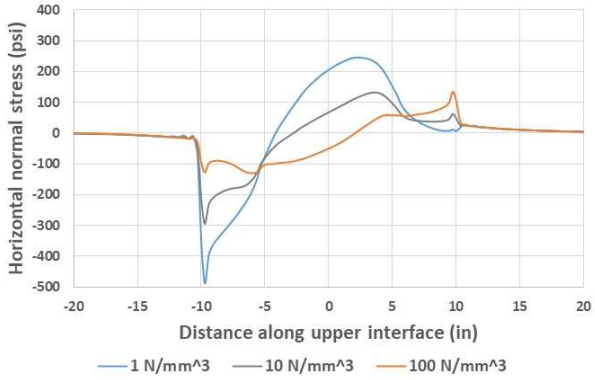


(a) HOR normal stress: upper interface

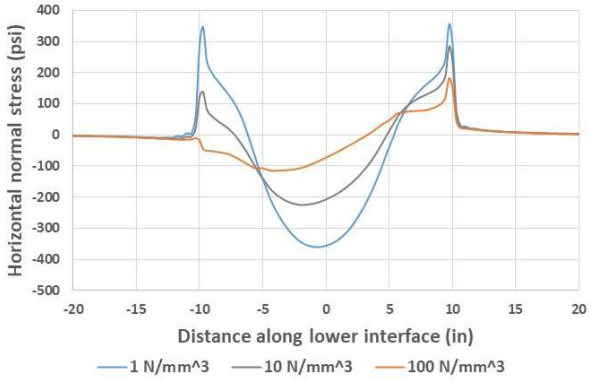


(b) HOR normal stress: lower interface

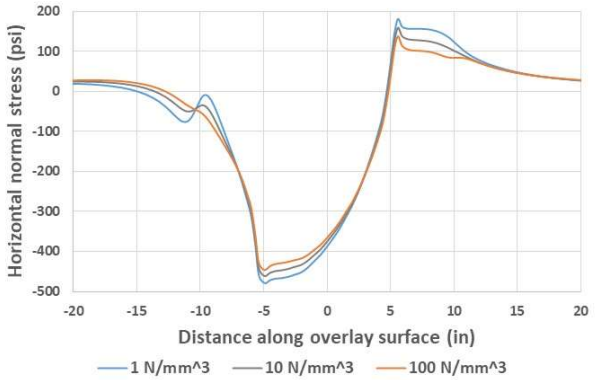


(c) HOR normal stress: overlay surface

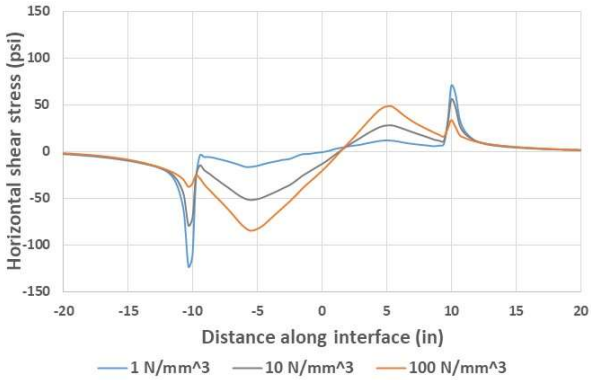


(d) HOR shear stress: interface

Figure 5-4 Effect of interface reaction modulus on stress distribution (braking).

### 5.3 Effect of Overlay Thickness

Figure 5-5 presents the resulting stress distribution for pavement sections with varying overlay thickness under the free-rolling condition. Increasing overlay thickness resulted in a reduction in tension at the lower interface below the edge of the scab in Figure 5-5b (lower reflective cracking potential) and at the surface of the overlay in Figure 5-5c. However, an increased overlay thickness resulted in higher tension at the upper interface below the center of the load (Figure 5-5a) and slightly higher shear at the edge of the scab (Figure 5-5d).

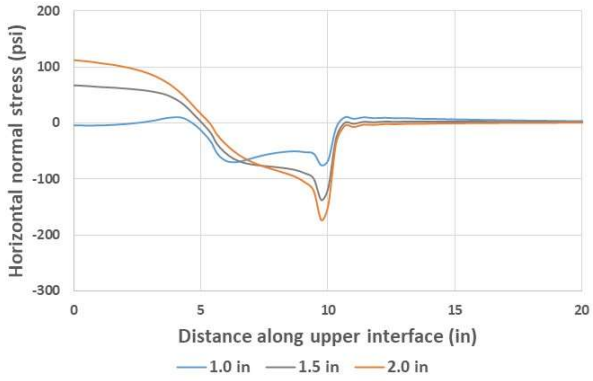


(a) HOR normal stress: upper interface

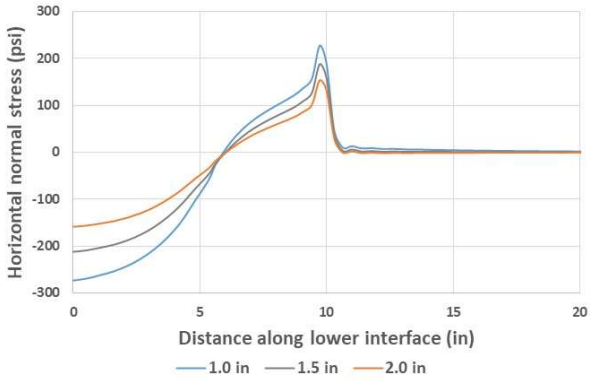


(b) HOR normal stress: lower interface

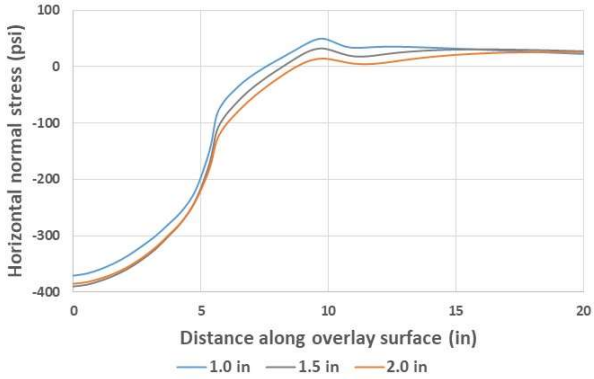


(c) HOR normal stress: overlay surface

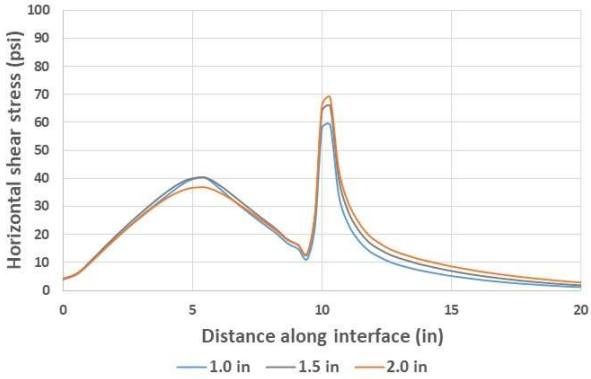


(d) HOR shear stress: interface

Figure 5-5 Effect of overlay thickness on stress distribution (free-rolling).

Figure 5-6 presents the resulting stress distribution for pavement sections with varying overlay thickness under the braking condition. Compared to the results under the free-rolling condition, the addition of a horizontal load in the braking zones resulted in higher tension at the surface of the overlay and at the upper and the lower interfaces as well as higher shear stresses. The increase in surface tension was most significant. The peak value in the range of 115 to 231 psi

occurred right behind the wheel load (Figure 5-6c). The peak tension at the upper interface increased to 176 psi, which occurred below the back edge of the scab in the section with the thin overlay (Figure 5-6a). The peak tension at the lower interface increased to 368 psi, which occurred below the back edge of the scab (Figure 5-6b). The peak horizontal shear increased to 83 psi, which occurred below the front edge of the scab in the section with an overlay thickness of 2.0 inch (Figure 5-6d).

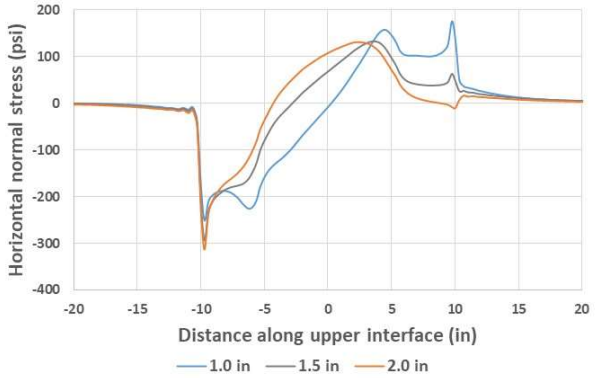


(a) HOR normal stress: upper interface

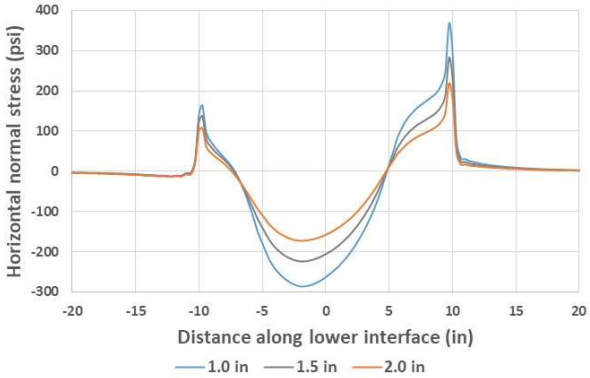


(b) HOR normal stress: lower interface

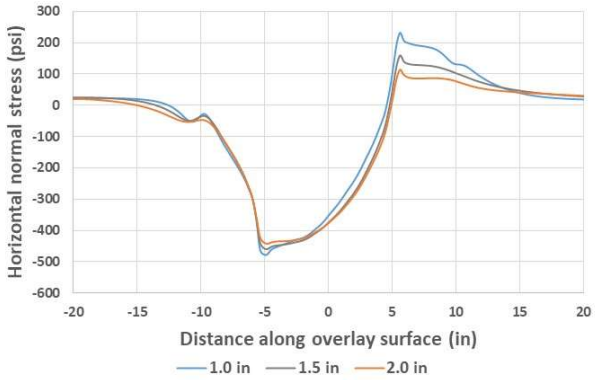


(c) HOR normal stress: overlay surface

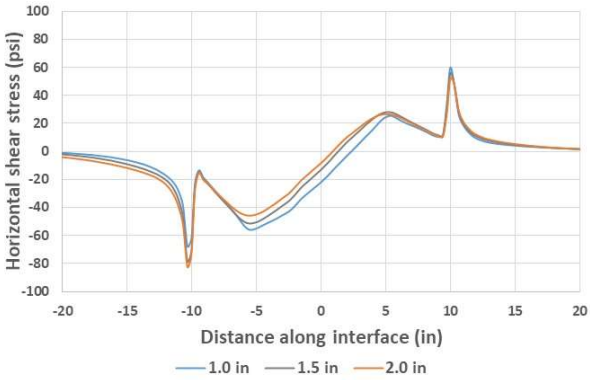


(d) HOR shear stress: interface

Figure 5-6 Effect of overlay thickness on stress distribution (braking).

## 5.4 Effect of Overlay Stiffness

Figure 5-7 shows the resulting stress distribution for pavement sections with varying overlay stiffness under the free-rolling condition. A less stiff overlay mixture resulted in a reduction in tension at the upper interface below the center of the load in Figure 5-7a (lower fatigue cracking potential) and at the surface of the overlay (Figure 5-7c) and lower shear at the edge of the scab (Figure 5-7d). A reduced overlay stiffness led to slightly higher tension at the lower interface below the edge of the scab (Figure 5-7b).

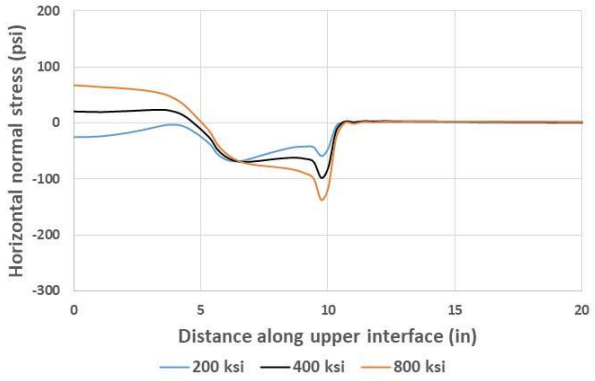


(a) HOR normal stress: upper interface

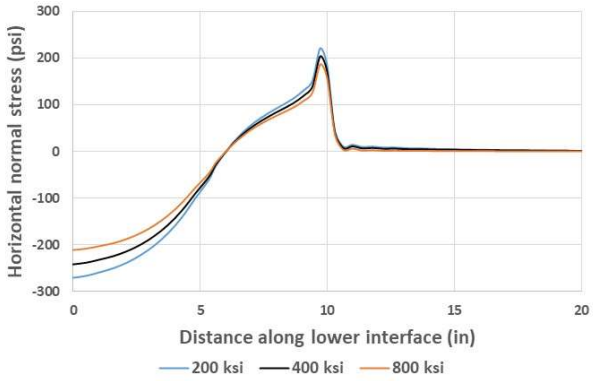


(b) HOR normal stress: lower interface

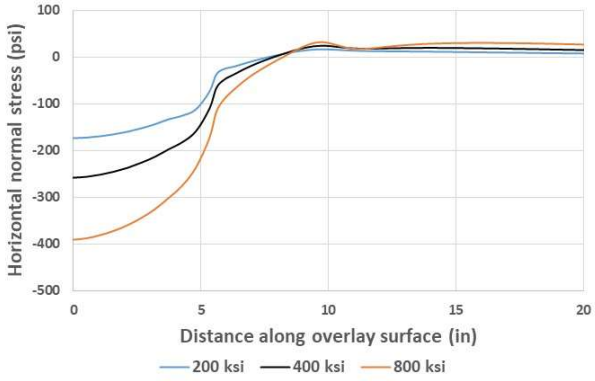


(c) HOR normal stress: overlay surface

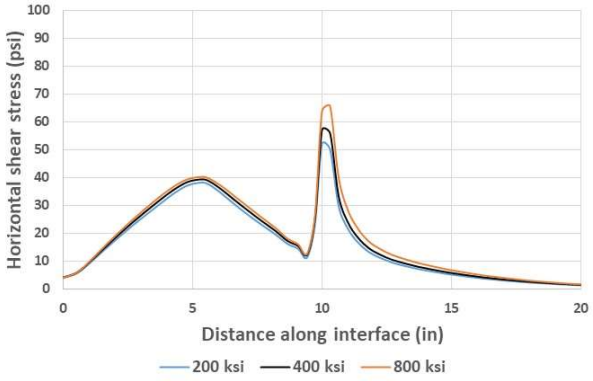


(d) HOR shear stress: interface

Figure 5-7 Effect of overlay stiffness on stress distribution (free-rolling).

Figure 5-8 shows the resulting stress distribution for pavement sections with varying overlay stiffness under the braking condition. Compared to the results under the free-rolling condition, the addition of a horizontal load in the braking zones resulted in higher tension at the surface of the overlay and at the upper and the lower interfaces as well as higher shear stresses. The increase in surface tension was most significant. The peak value in the range of 141 to 158 psi occurred right behind the wheel load (Figure 5-8c). The peak tension at the upper interface increased to 290 psi, which occurred below the back edge of the scab in the section with the low-stiffness overlay (Figure 5-8a). The peak tension at the lower interface increased to 398 psi, which occurred below the back edge of the scab (Figure 5-8b). The peak horizontal shear increased to 79 psi, which occurred below the front edge of the scab in the section with an overlay stiffness of 800 ksi (Figure 5-8d).

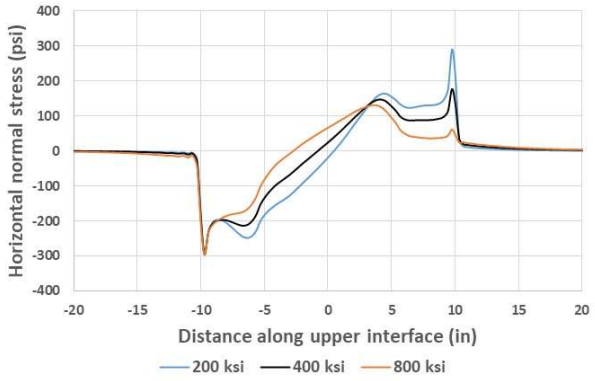


(a) HOR normal stress: upper interface

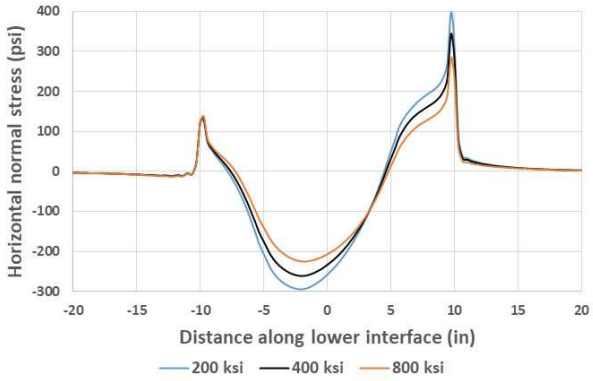


(b) HOR normal stress: lower interface

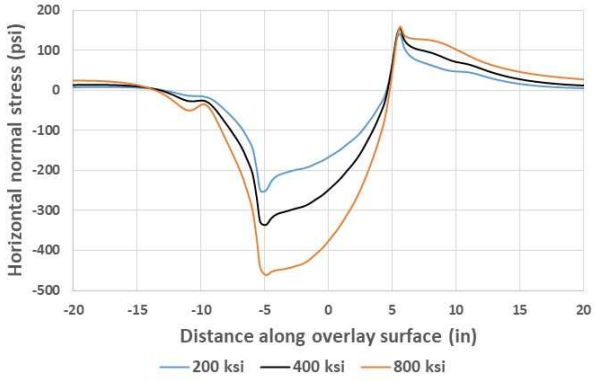


(c) HOR normal stress: overlay surface

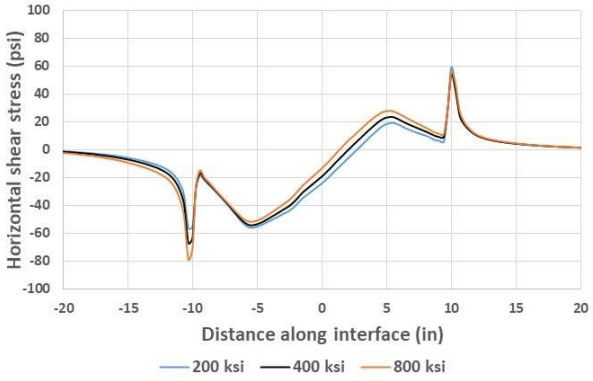


(d) HOR shear stress: interface

Figure 5-8 Effect of overlay stiffness on stress distribution in 3-D models (braking).

## 5.5 Concluding Remarks

Pavement scabbing analysis was conducted with the hybrid interface (scabbing) representation for a combination of 18 cases based on five key factors: scab size, interface reaction modulus, overlay thickness, overlay stiffness, and rolling condition. A summary of findings regarding effects of these key factors on stress distribution near the scabbed area is presented as follows.

- An intermediate scab size (in the range of one to two times the radius of the load) appeared to induce the most critical responses.
    - When the scab size increased to about five times the radius of the load, the stress distributions became almost identical to those from the global interface representation for partial bond under both free-rolling and braking conditions.
    - When the scab size reduced to less than the radius of the load, the stress distributions became like those from the global interface representation for full

bond condition under free-rolling condition. High tension was present in the section with the small-size scab under the braking condition.

- An increase in the degree of weakness in the bond condition led to significant increase in tension at the upper and lower interfaces and at the surface of overlay. Also, a weaker bond resulted in a significant increase in shear at the interface.
- Increasing overlay thickness generally resulted in lower tension at the lower interface and at the surface of the overlay. A thicker overlay had slightly higher shear at the edge of the scab.
- A less stiff overlay mixture resulted in slightly lower tension at the surface of the overlay and lower shear at the edge of the scab. Lower overlay stiffness generally led to higher tension at the lower interface.
- The addition of a horizontal load in the braking zones consistently resulted in much higher tension at the surface of the overlay. Also, the brake loading condition led to higher tension at the upper and the lower interfaces as well as higher shear stress.

Overall, the finite element models with the hybrid interface (scabbing) representation were helpful for investigating effects of a range of key factors on pavement responses including scab size.

# CHAPTER 6
# EFFECTS OF ROLLER COMPACTION ON RESPONSES OF INTERFACE BOND BELOW THE SCABBED LAYER

Prior research effort (Chapters 3-5) showed that weakly-bonded scabbed areas in the overlay had the potential to cause slippage and longitudinal cracking under repeated traffic load. This part of the study investigated whether compaction on overlay would weaken the bond between the thin scabbed layer and the underlying AC layer. Compaction of overlay with scabbing was simulated as an impact process, where a drum impacted the pavement structure at an initial velocity selected based on a typical range of roller vibration frequencies and amplitudes.

## 6.1 Methods for Roller Compaction Analysis

### 6.1.1 Simulation of vibratory roller compaction

Vibratory rollers introduced in the late 1950s provide compaction force by a combination of weight and vibration of steel drums. The roller drum moves up and down as it vibrates. As shown in Figure 6-1, vibration amplitude is the greatest movement of a drum from its position at rest. The frequency of vibration depends on the number of cycles per minute that the eccentrics rotate within the drum. The faster the rotation of the eccentrics, the higher the frequency of vibration. Impact spacing is the distance between two drum impacts, which depends on vibration frequency and roller travel speed. To ensure smoothness under vibratory compaction, the frequency and roller speed should be controlled so that there will be at least ten impacts per foot of travel of the roller, which is equivalent to a maximum impact spacing of 0.1 feet (AI, 2003). The speed of drum impact under a vibration mode (Figure 6-2a) can be estimated based on vibration frequency and amplitude. For a typical range of frequencies (2400 to 4200 vibrations per minute or 40 to 70 Hz) and amplitudes (0.01 to 0.04 inch), the average impact speed was estimated to be in the range of 0.8 to 5.6 inch per second. A drum moving toward a pavement section at an initial velocity (V) in the direction normal to the pavement surface was employed for simulation of drum impact from a vibratory roller (Figure 6-2b).

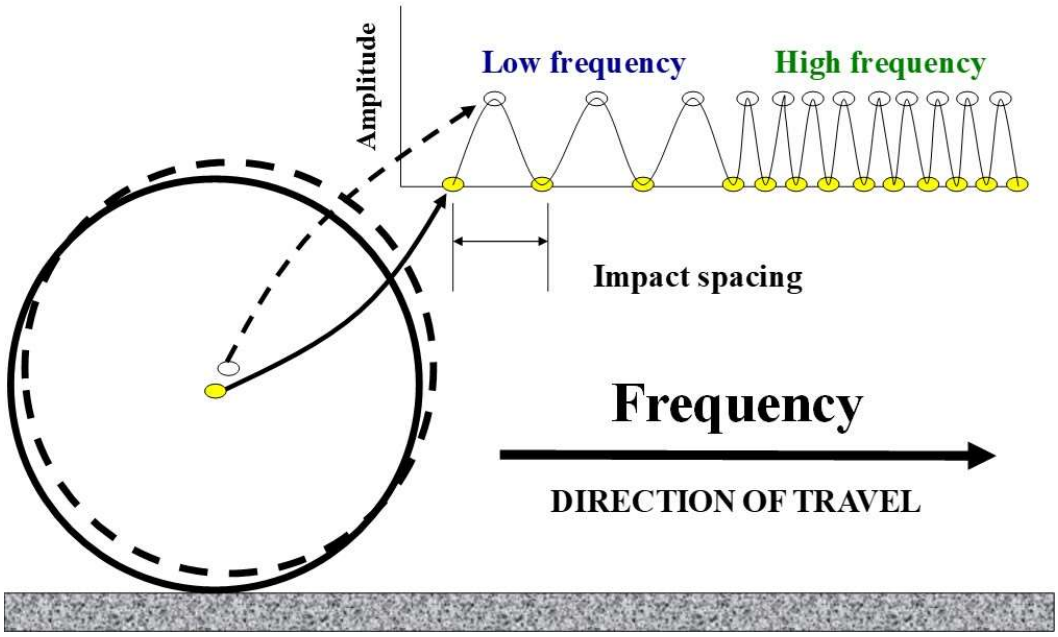


Figure 6-1 Vibratory roller: amplitude, frequency of vibration, and impact spacing.

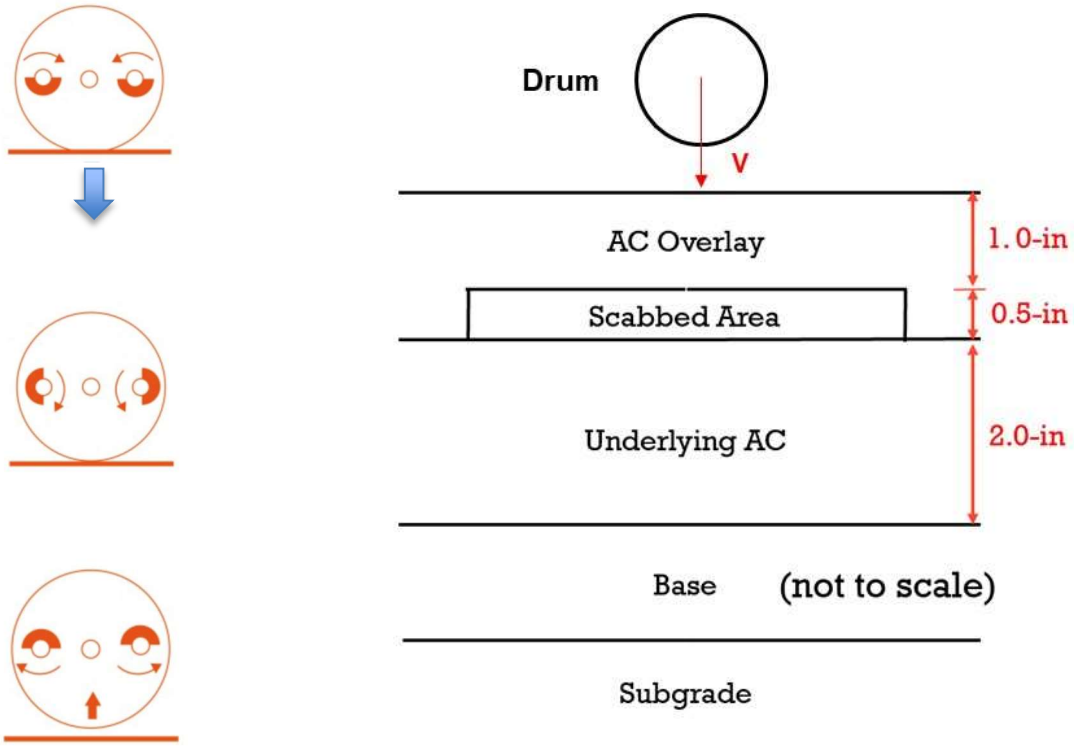


(a) Schematic for vibration motion

(b) Drum impact at an initial velocity of V normal to the pavement surface

Figure 6-2 Drum impact for simulation of vibratory roller compaction.

### 6.1.2 Simulation of oscillatory roller compaction

The oscillatory roller was developed in Germany in 1983 and introduced in the United States in early 2003. Unlike the vibratory roller, the drum does not bounce (i.e., lift off the pavement surface). As a result, damage to underground utilities, nearby buildings, or bridges is minimized (Kearney, 2006). The oscillatory system uses dual, opposed, eccentric weights rotating in the same direction to create a rocking motion. The rocking motion produces horizontal and downward forces that achieve compaction by "massaging" the hot mix asphalt (Figure 6-3a). Therefore, an impact angle (θ) was introduced to simulate the drum impact from an oscillatory roller at an initial velocity inclined to the normal of the pavement surface (Figure 6-3b). Two impact angles were selected (22.5° and 45.0°) for oscillatory roller along with the 0° impact angle defined for the vibratory roller to evaluate the effect of impact angle on pavement responses, while magnitude of the impact velocity (i.e., the impact speed) was kept the same.

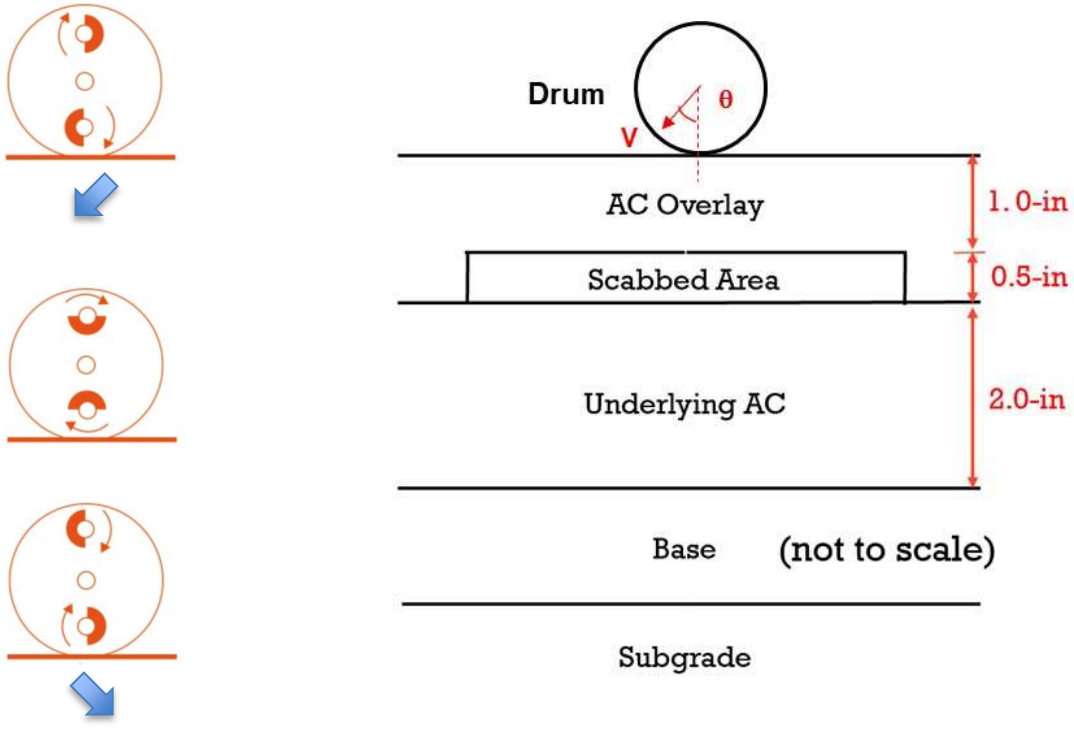


(a) Schematic for rocking motion

(b) Drum impact at an initial velocity of V inclined to the normal of the pavement surface

Figure 6-3 Drum impact for simulation of oscillatory roller compaction.

## 6.2 Plane Strain Finite Element Model

As mentioned in Chapter 4, a plane strain model was a more efficient alternative to a 3-D finite element pavement model, while generally retaining sufficient accuracy. Therefore, plane strain models were developed to predict responses of pavement sections with scabbing under drum impact. Figure 6-4 shows the pavement model with an intermediate-size scab adopted for this part of the study, which has the same mesh design (8,400 elements) as the model used in the prior chapter. The pavement structure was composed of AC overlay, underlying AC, granular base, and subgrade. A scabbed layer of 20-inch width and 0.5-inch thickness was introduced on top of the underlying AC layer. Table 6-1 summarizes layer thickness and material properties. It is important to note that the scabbed layer and underlying AC layer were assumed to be fully bonded to investigate whether drum impact on overlay would weaken the bond. Figure 6-5 shows the mesh design for the drum model containing 512 elements. The drum model was assumed to have a diameter of 3 feet, a modulus of 29,000 ksi, and a Poisson's ratio of 0.30.

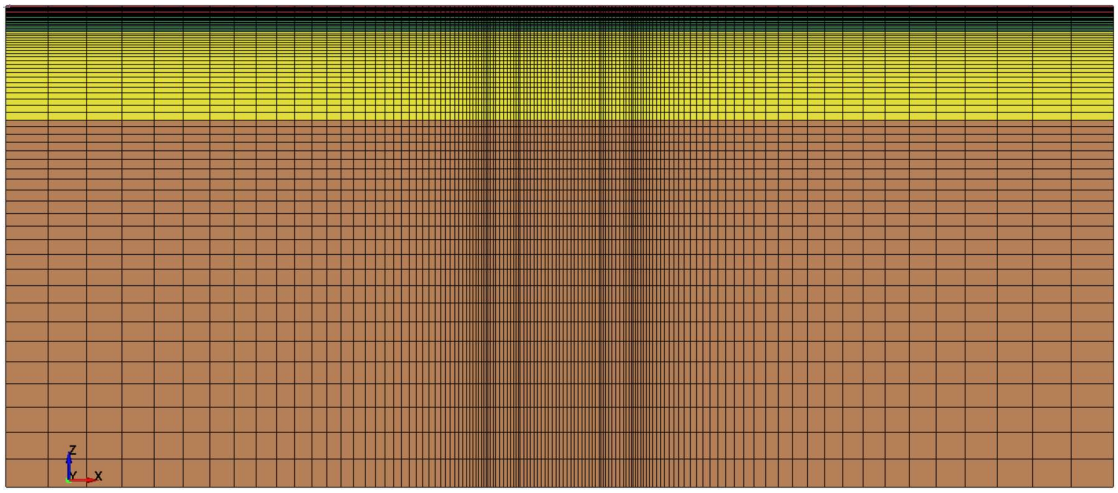

Figure 6-4 Plane strain finite element pavement model with a medium scab.

Table 6-1 Layer thickness and material properties of pavement structure

| Pavement layers | Thickness (in.) | Modulus (ksi) | Poisson's ratio |
|---|---|---|---|
| AC overlay | 1.5 | 800 | 0.35 |
| Scabbed layer (20-in wide) | 0.5 | 800 | 0.35 |
| Underlying AC | 2 | 800 | 0.35 |
| Base | 12 | 25 | 0.40 |
| Subgrade | – | 15 | 0.45 |

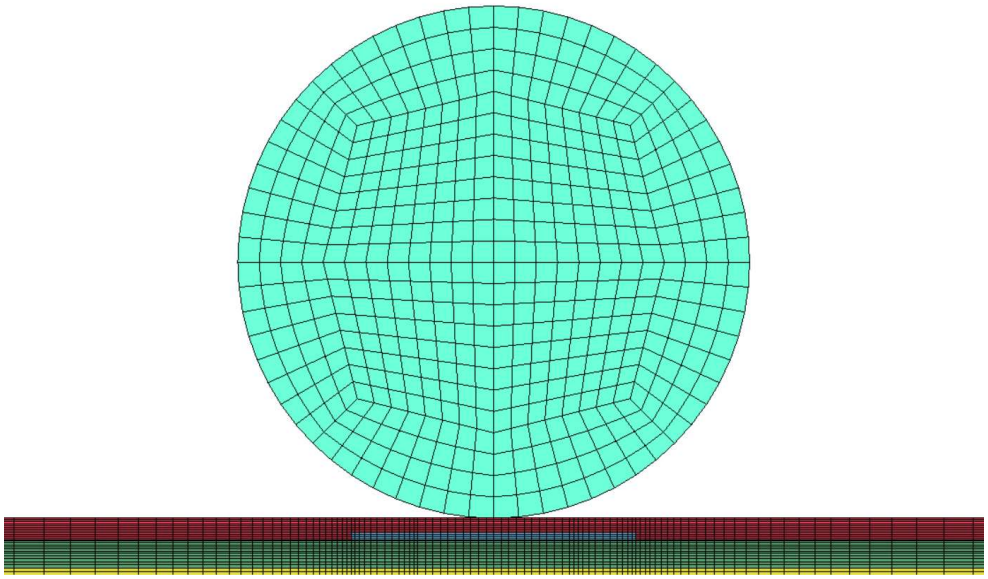

Figure 6-5 Drum model on top of the pavement model (zoom-in view).

## 6.3 Example Simulation and Results

### 6.3.1 Effect of impact angle

Example simulations were conducted to compare the effects of vibratory and oscillatory rollers on stresses in the overlay with scabbing. Drum impact from a vibratory roller was represented by a velocity normal to the surface of the pavement, i.e., a velocity at a 0-degree impact angle. Two levels of impact angles (22.5 and 45 degrees) were employed to simulate drum impact from oscillatory rollers. The magnitude of the velocity adopted was 5 inch per second. This impact speed was determined in a separate analysis to produce a maximum bending stress similar to the level of stress from a 9-kip wheel load at the bottom of the underlying AC layer.

Figure 6-6 presents impact load time history determined for the impact process. For all three impact angles, the resulting impact loads lasted about 25 milliseconds. As expected, the drum impact from a vibratory roller (i.e., at a 0-degree impact angle) led to a vertical impact load only, which peaked at about 400 pound at the midpoint of the impact period. The negative sign denotes the downward direction of the vertical load.

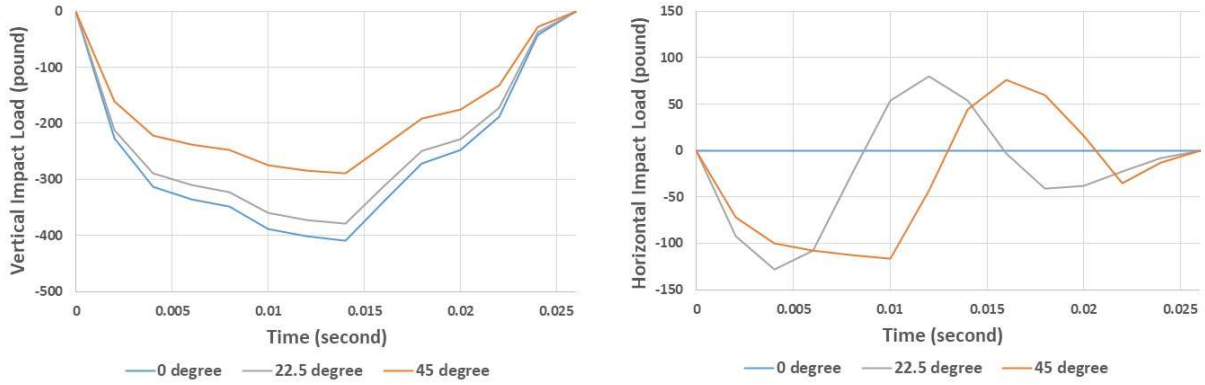


(a) Vertical impact load (b) Horizontal impact load

Figure 6-6 Drum impact load time signatures.

The drum impacts from oscillatory rollers (i.e., at 22.5-degree and 45-degree impact angles) had lower vertical impact loads than that from the vibratory roller compaction. However, both drum impact angles resulted in horizontal impact loads. As shown in Figure 6-6b, the horizontal impact load resulting from a 22.5-degree impact angle exhibited double stress reversals. Specifically, it had a negative sign for the first one-third of the impact duration, followed by a positive sign for the second one-third, and then returned to be negative for the rest of the time. The negative sign refers to the forward direction of the horizontal load (i.e., toward the left side of the drum). This phenomenon is consistent with the concept of "massaging" described in the literature for an oscillatory system to achieve compaction. Compared to the 22.5-degree impact angle, a 45-degree impact angle resulted in a smaller vertical load. With respect to the horizontal impact load, although the peak value was almost identical to that from the 22.5-degree impact, it occurred later in the impact process. As a result, the horizontal load from a 45-degree impact stayed in the forward direction for the first one-half of the impact duration.

Figure 6-7 shows the horizontal shear stress contour when peak shear was reached for all three cases, including 0-degree, 22.5-degree, and 45-degree drum impacts. The peak shear from the 0-degree impact occurred at 12 milliseconds (Figure 6-7a). Due to the symmetry of the drum impact velocity with respect to the central plane, horizontal shear to the left side of the drum (forward shear with a negative sign) and to the right side (backward shear with a positive sign) reached the peak simultaneously. The peak shear from the 22.5-degree impact also occurred at 12 milliseconds (Figure 6-7b). However, the backward shear was dominant for this case because a combination of downward vertical load and backward horizontal load resulted in the peak shear

(see Figure 6-6). The peak shear induced from the 45-degree impact occurred at 8 milliseconds (Figure 6-7c). In this case, the forward shear was dominant because a combination of downward vertical load and forward horizontal load resulted in the peak shear (see also Figure 6-6).

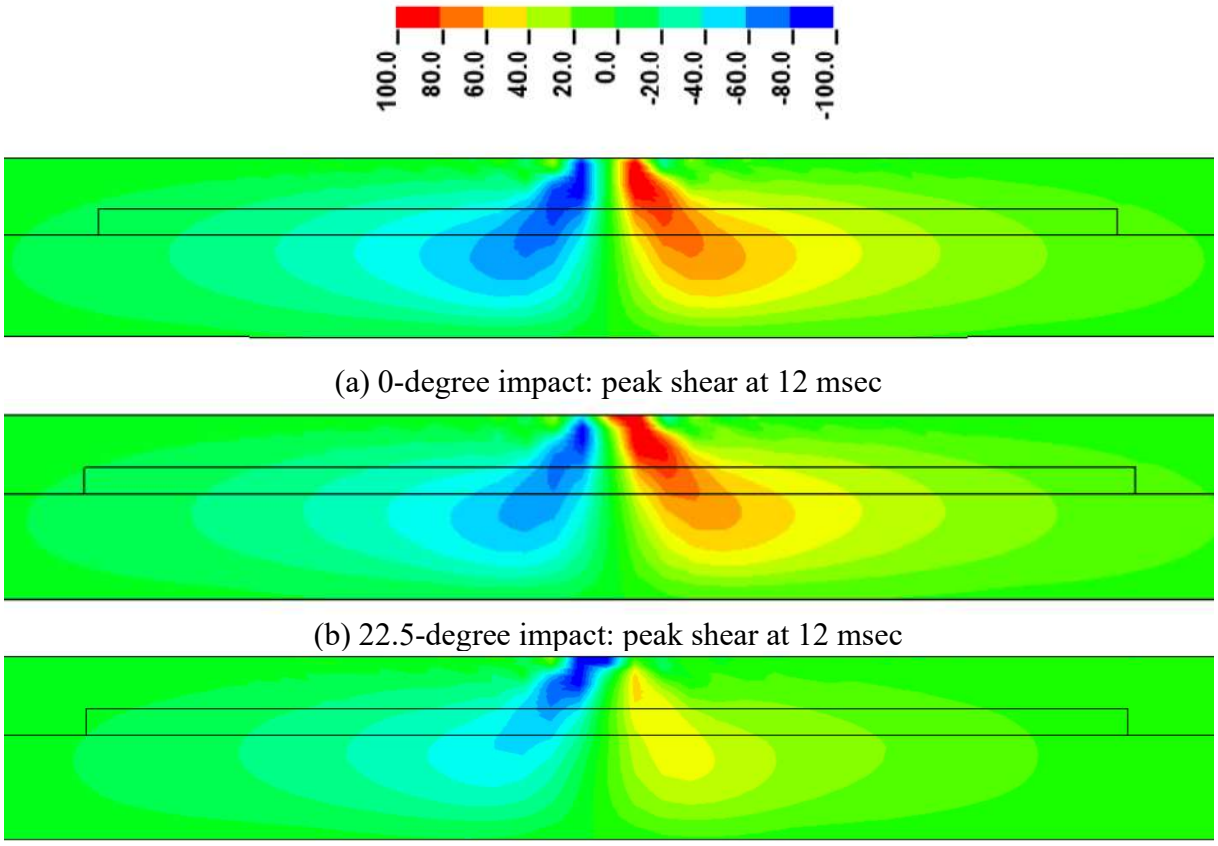


(a) 0-degree impact: peak shear at 12 msec

(b) 22.5-degree impact: peak shear at 12 msec

(c) 45-degree impact: peak shear at 8 msec

Figure 6-7 Horizontal shear stress contours (zoom-in view).

Figures 6-8a to 6-8c show horizontal shear stress and confinement distribution along the interface when peak shear was reached for 0-degree impact, 22.5-degree impact, and 45-degree impact, respectively. In general, both horizontal shear and confinement decreased with increasing distance from the center of the impact load. However, the reduction in confinement was much faster than the reduction in horizontal shear. This trend resulted in critical stress states at the interface in the vicinity of the load represented by a combination of relatively high shear with low confinement. For example, at 2.1 inch from the center of the load, the horizontal shear was 63.9 psi while the confinement was only 10.7 psi under the 0-degree impact. At the same distance, a combination of 62.4 psi in shear and 13.4 psi in confinement was identified for the 22.5-degree impact, and a combination of 49.6 psi in shear and 12.5 psi in confinement was

determined for the 45-degree impact. These stress states indicated a potential of interface debonding under repeated compaction loads. It was clear that the 0-degree impact resulted in more critical conditions for debonding to occur along the interface than the other two cases. Figure 6-8d shows that the 0-degree impact also led to the highest bending stress at the bottom of the underlying AC layer.

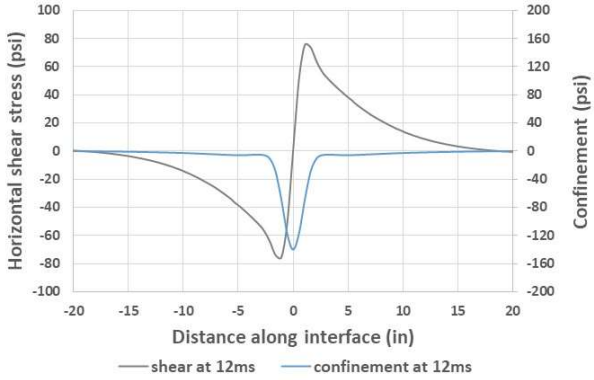


(a) 0-degree impact: shear and confinement

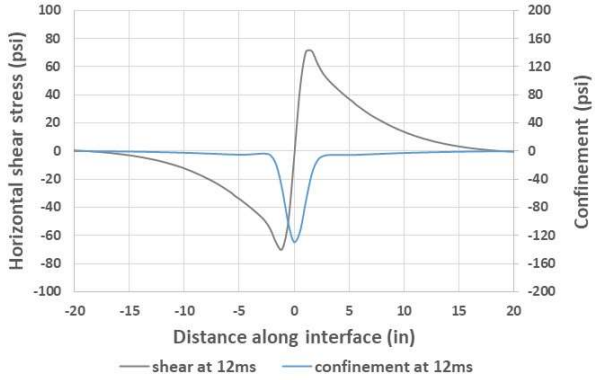


(b) 22.5-degree: shear and confinement

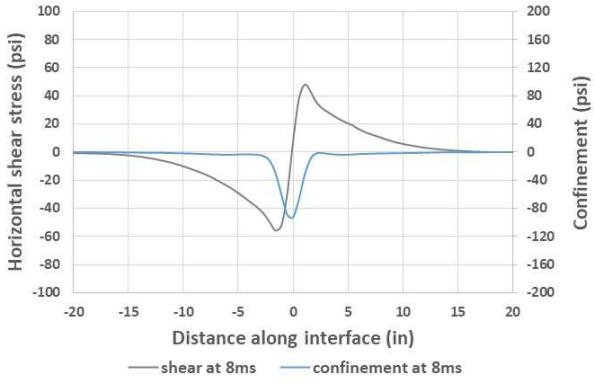


(c) 45-degree: shear and confinement

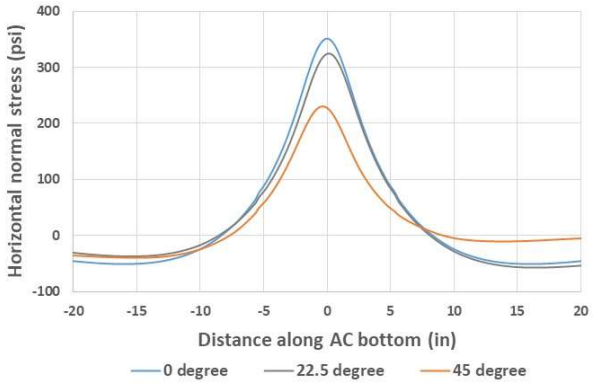


(d) Bending stress

Figure 6-8 Snapshots for shear stress, confinement, and bending stress distribution.

## 6.4 Analysis of Scabbed Sections under Drum Impact

It was determined in Section 6.3 that the 0-degree impact (i.e., the vibratory roller impact) resulted in the most critical conditions. Therefore, it was employed for investigating the effects of key factors on critical pavement responses under drum impact, including three levels of overlay thickness (1.0, 1.5, and 2.0 inch) and three levels of overlay stiffness (200, 400, and 800 ksi).

### 6.4.1 Effect of overlay thickness

Figures 6-9a to 6-9c present the resulting stress distribution for pavement sections with varying overlay thickness under the drum impact. Increasing overlay thickness resulted in a reduction in peak shear and peak confinement along the interface. The confinement reduced to about 10 psi at 1.6-inch, 2.1-inch, and 2.7-inch from the center of the load for the thin, medium, and thick overlay, respectively. The corresponding horizontal shear was 70.8 psi, 63.9 psi, and 55.9 psi. It was clear that a thicker overlay led to a less critical condition for potential interface debonding. Also, a thicker overlay led to lower maximum bending stress at the bottom of the underlying AC layer. Figure 6-9d shows impact load time history. Generally, all impact loads arrived at a similar peak value of 410 psi. The impact load on a thicker overlay appeared to reach its peak earlier.

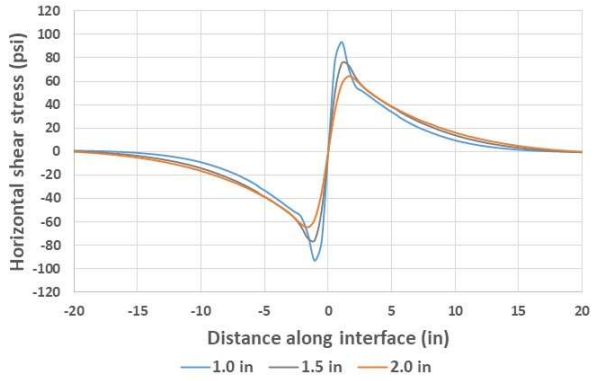


(a) Horizontal shear

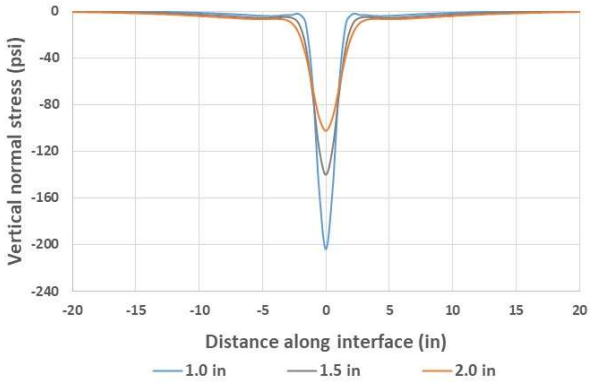


(b) Confinement

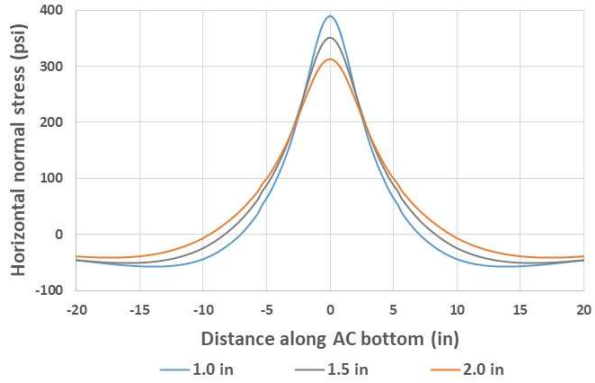


(c) Bending stress

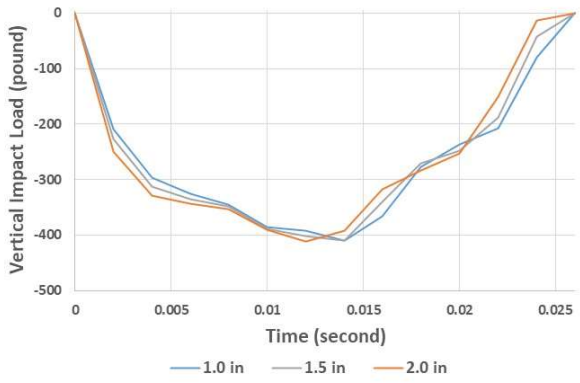


(d) Impact load

Figure 6-9 Effect of overlay thickness on stress distribution and impact load.

### 6.4.2 Effect of overlay stiffness

Figures 6-10a to 6-10c present the resulting stress distribution for pavement sections with varying overlay stiffness under the drum impact. Decreasing overlay stiffness had almost no effect on peak shear at the interface, while it caused the shear to reduce more rapidly with increasing distance from the center of the load (Figure 6-10a). A less stiff overlay mixture resulted in a slight increase in peak confinement at the interface (Figure 6-10b). Therefore, it appeared that a lower stiffness might lead to less critical condition for potential interface debonding. It is important to note that a less stiff overlay resulted in lower peak load which occurred later in the impact process (Figure 6-10d), which likely overshadowed the sensitivity of the responses to overlay stiffness.

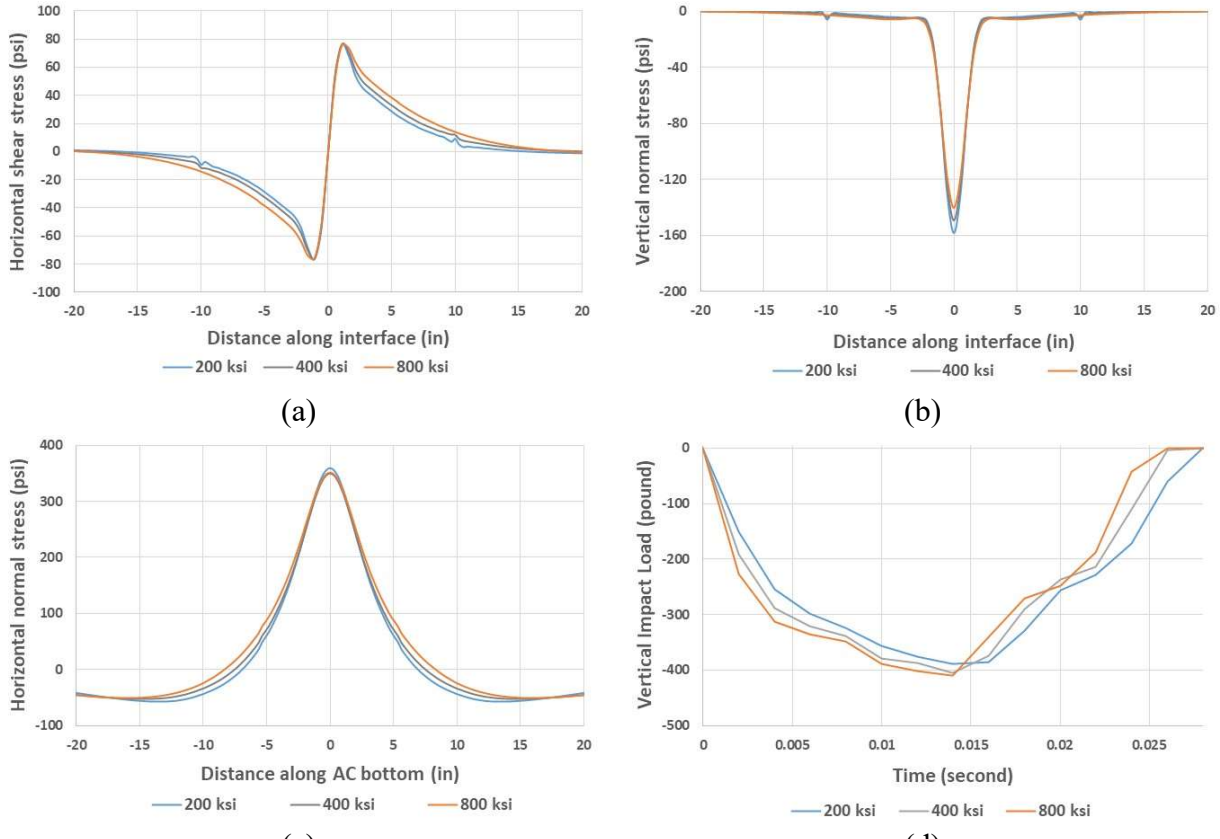


Figure 6-10 Effect of overlay stiffness on stress distribution and impact load.

## 6.5 Concluding Remarks

A preliminary investigation of the effect of compaction on asphalt overlay with scabbing was performed. Roller compaction was approximated by drum impact on the pavement structure at an initial velocity. A total of seven cases were presented: three impact angles (0-degee, 22.5-degree, and 45-degree), three levels of overlay thickness (1.0, 1.5, and 2.0 inch), and three levels of overlay stiffness (200, 400, and 800 ksi). The pavement section with intermediate scab size and overlay thickness and a high value of overlay stiffness subjected to the 0-degree impact was selected as the reference case throughout this analysis. The scabbed layer and underlying AC layer were assumed to be fully bonded to investigate whether drum impact on overlay would weaken the bond. A summary of findings regarding effects of these key factors on potential interface debonding under the drum impact is presented as follows.

- The 0-degree drum impact representing vibratory roller compaction appeared to induce the most critical stress state, i.e., a combination of high shear and low confinement along the interface. Both 22.5-degree impact and 45-degree impact, representing oscillatory roller compaction, caused less critical stresses along the interface. This is generally consistent with the statement of less damage to underground utilities, nearby buildings, or bridge induced by oscillatory roller compaction reported in the literature.
- Increasing overlay thickness resulted in less critical condition for potential interface debonding under drum impact. All impact loads arrived at a similar peak value and the impact load on a thicker overlay appeared to reach its peak earlier.
- A less stiff overlay mixture helped to reduce the potential for interface debonding under drum impact. The lower stiffness in the overlay resulted in a lower peak load occurred later in the impact process.

Overall, the approach using drum impact captured the rocking motion of compaction associated with the oscillatory roller. Drum impact analysis showed that vibratory rollers were potentially more harmful than oscillatory rollers. Compaction of asphalt overlay with scabbing would potentially weaken the bond between the scabbed layer and the underlying AC layer and likely cause debonding along the interface.

# CHAPTER 7
# CLOSURE

## 7.1 Summary of Findings

Field investigation in Florida indicated that there was a potential link between weakly bonded scabbed areas and slippage failure in the braking zones (FDOT, 2015). Also, evidence from NCAT test track studies suggested that localized interface debonding might lead to surface cracking under free-rolling traffic (Willis and Timm, 2007). The primary objective of this research was to determine critical responses and potential distress in asphalt overlay associated with the presence of scabbing. In order to achieve the objective, both conventional analysis assuming a global interface representation and finite element analysis with a hybrid interface representation were conducted to evaluate the effect of weakly-bonded scabbed layer on pavement responses and potential distress. Furthermore, impact analysis was performed to investigate whether compaction of overlay would weaken the bond below the scabbed layer. A summary of findings based on results of simulations and analyses is presented as follows:

- The conventional analysis with the global interface (scabbing) representation provided an efficient tool to access the effect of weakly-boned scabbed layer on pavement responses without considering scab size. Results showed that a higher AC-to-base stiffness ratio and a thinner underlying AC generally resulted in more critical responses.
- The finite element analysis with the hybrid interface representation allowed more comprehensive evaluation of the effect of weakly-boned scabbed layer on pavement responses. Results showed that a localized partial bond condition clearly led to more critical responses than a global partial bond condition.
- Results from both conventional analysis and finite element analysis showed that a weak bond led to more critical responses. The addition of a horizontal load in the braking zones consistently resulted in significantly higher tension at the surface of the overlay and higher tension and shear at the interface.
- Further analysis with the finite element approach showed an intermediate scab size (with a radius in the range of one to two times the radius of the load) appeared to induce the most critical responses. When the scab size increased to about five times the radius of the

load, the stress distributions became almost identical to those from the global partial bond condition under both free-rolling and braking loads.

- Increasing overlay thickness generally resulted in lower tension at the lower interface and at the surface of the overlay. A thicker overlay had slightly higher shear at the edge of the scab.
- A less stiff overlay mixture resulted in slightly lower tension at the surface of the overlay and lower shear at the edge of the scab. Lower overlay stiffness generally led to higher tension at the lower interface.
- The approach using drum impact successfully reproduced the rocking motion of compaction associated with oscillatory rollers. Further analysis with drum impact showed that compaction of asphalt overlay with scabbing induced critical stress states that may lead to debonding at the interface between the scabbed layer and the underlying AC layer.

## 7.2 Conclusions and Guidelines for Dealing with Scabbed Sections

Based on the findings of this study, the following conclusions were drawn:

- Under the free-rolling condition, the presence of weakly-bonded scabbed area has the potential to cause near-surface cracking initiated at the upper interface below the center of the load for intermediate and large size scabs, and reflective cracking at the lower interface below the edge of the scab and further interface debonding at the edge of the scab for intermediate size scab.
- Under the braking condition, the presence of poorly-bonded scabbed area would most likely cause slippage at the overlay surface behind the back edge of the wheel load for intermediate and large size scabs. It would increase the potential of further interface debonding ahead of the front edge of the scabbed area for intermediate size scab. Also, it would increase the potential of near-surface cracking at the upper interface below the center of the load and reflective cracking at the lower interface below the edge of the scab regardless of scab size.
- Roller compaction would likely weaken the bond below the scabbed area if it was fully bonded to the underlying AC layer before the compaction. Vibratory rollers would induce more critical conditions than oscillatory rollers.

It is important to note that although this study showed a small size scab (2.5-inch radius and 0.25-inch thickness) did not cause critical responses under free-rolling condition, a recent HVS study (Kwon et al., 2023) reported that surface cracks were observed in pavement sections with moderate scabbing involving multiple scattered small scabs (0.25-inch thickness). Therefore, the following guidelines are provided for dealing with scabbed sections:

- Make every effort to set the milling depth to minimize scabbing during resurfacing
- Loose scabbing should be removed prior to resurfacing
- Consider removing isolated scabbed areas or scabbed areas adjacent to critical locations such as intersections and other braking areas

### 7.3 Recommendations and Future Work

Based on evaluations performed in this study, recommendations for further investigation are provided below:

- In addition to a single scabbed area, the existence of multiple weakly-bonded scabs should be considered for further modeling and analysis to have a better understanding of the effect of scabbing on pavement responses and potential distress.
- Simulation of the milling operation is recommended to determine whether the remaining scabbed layer would potentially have a weaker bond than prior to the milling process.

# LIST OF REFERENCES


Asphalt Institute. (2001). Construction of Hot Mix Asphalt Pavements. Manual Series No. 22 (MS-22), Second edition. The Asphalt Institute, Lexington, KY.

Asphalt Institute. (2008). Basic Asphalt Emulsion Manual. Manual Series No. 19 (MS-19), Fourth edition. The Asphalt Institute, Lexington, KY.

Canestrari, F.; Santagata, E. (2005). Temperature Effects on the Shear Behavior of Tack Coat Emulsions Used in Flexible Pavements. International Journal of Pavement Engineering, Vol. 6 (1), pp. 39–46.

Canestrari, F.; Ferrotti, G.; Lu, X.; Millien, A.; Partl, M. N.; Petit, C.; Phelipot-Mardelé, A.; Piber, H.; Raab, C. (2013). Mechanical Testing of Interlayer Bonding in Asphalt Pavements. In Advances in Interlaboratory Testing and Evaluation of Bituminous Materials, State-of-the-Art Report, International Union of Testing and Research Laboratories for Materials and Structures, Paris, Vol. 9, pp. 303–360.

Cho, S.; Karshenas, A.; Tayebali, A. A.; Guddati, M. N.; Kim, Y. R. (2017). A Mechanistic Approach to Evaluate the Potential of the Debonding Distress in Asphalt Pavements. International Journal of Pavement Engineering, Vol. 18 (12), pp. 1098-1110.

Choi, Y.; Collop, A.; Airey, G.; Elliott, R. (2005). A Comparison between Interface Properties Measured Using the Leutner Test and the Torque Test. Journal of the Annual Meeting of the Association of Asphalt Paving Technologists, Vol. 74, 29p.

Das, R.; Mohammad, L. N.; Elsefi, M.; Cao, W.; Cooper, S. B. (2017). Effects of Tack Coat Application on Interface Bond Strength and Short-Term Pavement Performance. Transportation Research Record, Vol. 2633, pp. 1–8.

De Jong, D. L.; Peutz, M. G. F.; Korswargen, A. R. (1979). BISAR, External Report AMSR.0006.73. Koninklijke/Shell-Laboratorium, Amsterdam.

Deysarkar, I. (2004). Test Set-up to Determine Quality of Tack Coat. Master Thesis, University of Texas at El Paso.

Diakhaté, M.; Millien, A.; Petit, C.; Phelipot-Mardelé, A.; Pouteau, B. (2011). Experimental Investigation of Tack Coat Fatigue Performance: Towards an Improved Lifetime Assessment of Pavement Structure Interfaces. Construction and Building Materials, Vol. 25, pp. 1123–1133.

Hallquist, J. O. (1976). Procedure for the solution of finite-deformation contact-impact problems by the finite element method: California University, Livermore (USA). Lawrence Livermore Lab.

Hasiba, K. I. Q. (2012). Development of a Testing Approach for Tack Coat Application Rate at Pavement Layer Interfaces. Master Thesis, University of Illinois at Urbana-Champaign, Urbana, IL.

Hernando, D. (2017). Localized Interface Debonding as a Potential Mechanism of Near-Surface Longitudinal Cracking in Asphalt Pavements. Ph.D. Dissertation, University of Florida, Gainesville, FL.

Hernando, D.; Waisome, J. A. M.; Zou, J.; Roque, R. (2018). Identification of Potential Location and Extent of Localized Interface Debonding in the Wheelpath of Asphalt Pavements. Transportation Research Record, Vol. 2672, pp. 371–381.

Isailovic, I.; Falchetto, A. C.; Wistuba, M. (2017). Fatigue Investigation on Asphalt Mixture Layers' Interface. Road Materials and Pavement Design, Vol. 18 (sup4), pp. 514-534.

Karshenas, A.; Cho, S.; Tayebali, A. A.; Guddati, M. N.; Kim, Y. R. (2014). Importance of Normal Confinement to Shear Bond Failure of Interface in Multilayer Asphalt Pavements. Transportation Research Record, Vol. 2456, pp. 170–177.

Leng, Z.; Ozer, H.; Al-Qadi, I. L.; Carpenter, S. H. (2008). Interface Bonding between Hot-Mix Asphalt and Various Portland Cement Concrete Surfaces. Transportation Research Record, Vol. 2057, pp. 46–53.

LS-DYNA User's Manual, r:14226. Livermore software technology (LST), Livermore, CA, 2021.

Kwon, O.; Greene, J.; Sholar, G. A.; Moseley, H. (2023). Impact of the Interlayer Scabbing on Asphalt Pavement Performance. Transportation Research Record, In Press.

Maina, J. W.; De Beer, M.; Matsui, K. (2007). Effects of Layer Interface Slip on the Response and Performance of Elastic Multi-layered Flexible Airport Pavement Systems. Maintenance and rehabilitation of pavements and technological control, 5th International Conference, Utah, USA, August 8-10, pp. 145–150.

McGhee, K. K.; Clark, T. M. (2009). Bond Expectations for Milled Surfaces and Typical Tack Coat Materials Used in Virginia. VTRC 09-R21, Virginia Transportation Research Council, Charlottesville, VA.

Mohammad, L. N.; Elseifi, M. A.; Bae, A.; Patel, N.; Button, J.; Scherocman, J. A. (2012). Optimization of Tack Coat for HMA Placement. National Cooperative Highway Research Project (NCHRP) Report 712. Transportation Research Board, Washington, D.C.

Mohammad, L. N.; Raqib, M. A.; Huang, B. (2002). Influence of Asphalt Tack Coat Materials on Interface Shear Strength. Transportation Research Record, Vol. 1789, pp. 56–65.

Muench, S. T.; Moomaw, T. (2008). De-Bonding of Hot Mix Asphalt Pavements in Washington State: An Initial Investigation. Report No. WA-RD 712.1. Washington State Department of Transportation, Olympia, WA.

Ozer, H.; Al-Qadi, I. L.; Leng, Z. (2008). Fracture-Based Friction Model for Pavement Interface Characterization. Transportation Research Record, Vol. 2057, pp. 54–63.

Ozer, H.; Al-Qadi, I. L.; Wang, H.; Leng, Z. (2012). Characterisation of Interface Bonding between Hot-Mix Asphalt Overlay and Concrete Pavements: Modelling and In-situ Response to Accelerated Loading. International Journal of Pavement Engineering, Vol. 13 (2), pp. 181–196.

Ozer, H.; Al-Qadi, I. L.; Hasiba, K. I.; Wang, H.; Salinas, A. (2013). Pavement Layer Interface Shear Strength Using a Hyperbolic Mohr-Coulomb Model and Finite Element Analysis. Proceedings of the Airfield and Highway Pavement Conference, Los Angeles, CA, 9-12 June.

Raab, C.; Partl, M. N. (2004). Effect of Tack Coats on Interlayer Shear Bond of Pavements. Proceedings of the 8th Conference on Asphalt Pavements for Southern Africa, Sun City, South Africa, 12-16 September.

Romanoschi, S. A.; Metcalf, J. B. (2001a). Characterization of Asphalt Concrete Layer Interfaces. Transportation Research Record, Vol. 1778, pp. 132–139.

Romanoschi, S. A.; Metcalf, J. B. (2001b). Effects of Interface Conditions and Horizontal Wheel Loads on the Life of Flexible Pavement Structures. Transportation Research Record, Vol. 1778, pp. 123–131.

Roque, R.; Chun, S.; Zou, J.; Lopp, G.; Villiers, C. (2011). Continuation on Superpave Projects Monitoring. Final report BDK-75-977-06. Florida Department of Transportation (FDOT), Tallahassee, FL.

Roque, R.; Hernando, D.; Park, B.; Zou, J.; Waisome, J. A. M. (2017). Evaluation of Asphalt Pavement Interface Conditions for Enhanced Bond Performance. Final report BDV31-977-37. Florida Department of Transportation (FDOT), Tallahassee, FL.

Sangiorgi, C.; Collop, A. C.; Thom, N. H. (2002). Laboratory Assessment of Bond Condition Using the Leutner Shear Test. Proceedings of the 3rd International Conference on Bituminous Mixtures and Pavements, Thessalonkiki, Greece, pp. 315–324.

Sholar, G. A.; Page, G. C.; Musselman, J. A.; Upshaw, P. B.; Moseley, H. L. (2004). Preliminary Investigation of a Test Method to Evaluate Bond Strength of Bituminous Tack Coats. Journal of the Annual Meeting of the Association of Asphalt Paving Technologists, Vol. 73, pp. 771–806.

Tashman, L.; Nam, K.; Papagiannakis, T.; Willoughby, K.; Pierce, L.; Baker, T. (2008). Evaluation of Construction Practices that Influence the Bond Strength at the Interface between Pavement Layers. Journal of Performance of Constructed Facilities, Vol. 22 (3), pp. 154–161.

Tozzo, C.; D'Andrea, A.; Cozzani, D.; Meo, A. (2014). Fatigue Investigation of the Interface Shear Performance in Asphalt Pavement. Modern Applied Science, Vol. 8 (2), pp. 1-11.

Tran, N. H.; Willis, R.; Julian, G. (2012). Refinement of the Bond Strength Procedure and Investigation of a Specification. NCAT Report No. 12–04, National Center for Asphalt Technology, Auburn, AL.

Uzan, J. (1976). Influence of the Interface Condition on Stress Distribution in a Layered System. Transportation Research Record, Vol. 616, pp. 71–73.

Uzan, J.; Livneh, M.; Eshed, Y. (1978). Investigation of Adhesion Properties between Asphaltic Concrete Layers. Journal of the Annual Meeting of the Association of Asphalt Paving Technologists, Vol. 47, pp. 495–521.

Waisome, J. A. M. (2017). Evaluation of Asphalt Layer Interface Resistance to Bond Degradation through Repeated Load. Ph.D. Dissertation, University of Florida, Gainesville, FL.

West, R.; Zhang, J.; Moore, J. (2005). Evaluation of Bond Strength between Pavement Layers," NCAT Report No. 05–08, National Center for Asphalt Technology, Auburn, AL.

West, R.; Willis, J. R.; Marasteanu, M. (2013). Improved Mix Design, Evaluation, and Materials Management Practices for Hot Mix Asphalt with High Reclaimed Asphalt Pavement Content. National Cooperative Highway Research Project (NCHRP) Report 752. Transportation Research Board, Washington, D.C.

Willis, J. R.; Timm, D. H. (2007). Forensic Investigation of Debonding in Rich Bottom Pavement. Transportation Research Record, Vol. 2040, pp. 107–114.

Wilson, B.; Scullion, T.; Faruk, A. (2015). Evaluation of Design and Construction Issues of Thin HMA Overlays. Report No. FHWA/TX-15/0-6742-1. Texas A&M Transportation Institute (TTI), College Station, TX.

Wilson, B.; Seo, A. Y.; Sakhaeifar, M. (2016). Performance Evaluation and Specification of Trackless Tack. Report No. FHWA/TX-16/0-6814-1. Texas A&M Transportation Institute (TTI), College Station, TX.

# APPENDIX A

# COMPARISON OF 3-D AND PLANE-STRAIN FINITE ELEMENT RESULTS

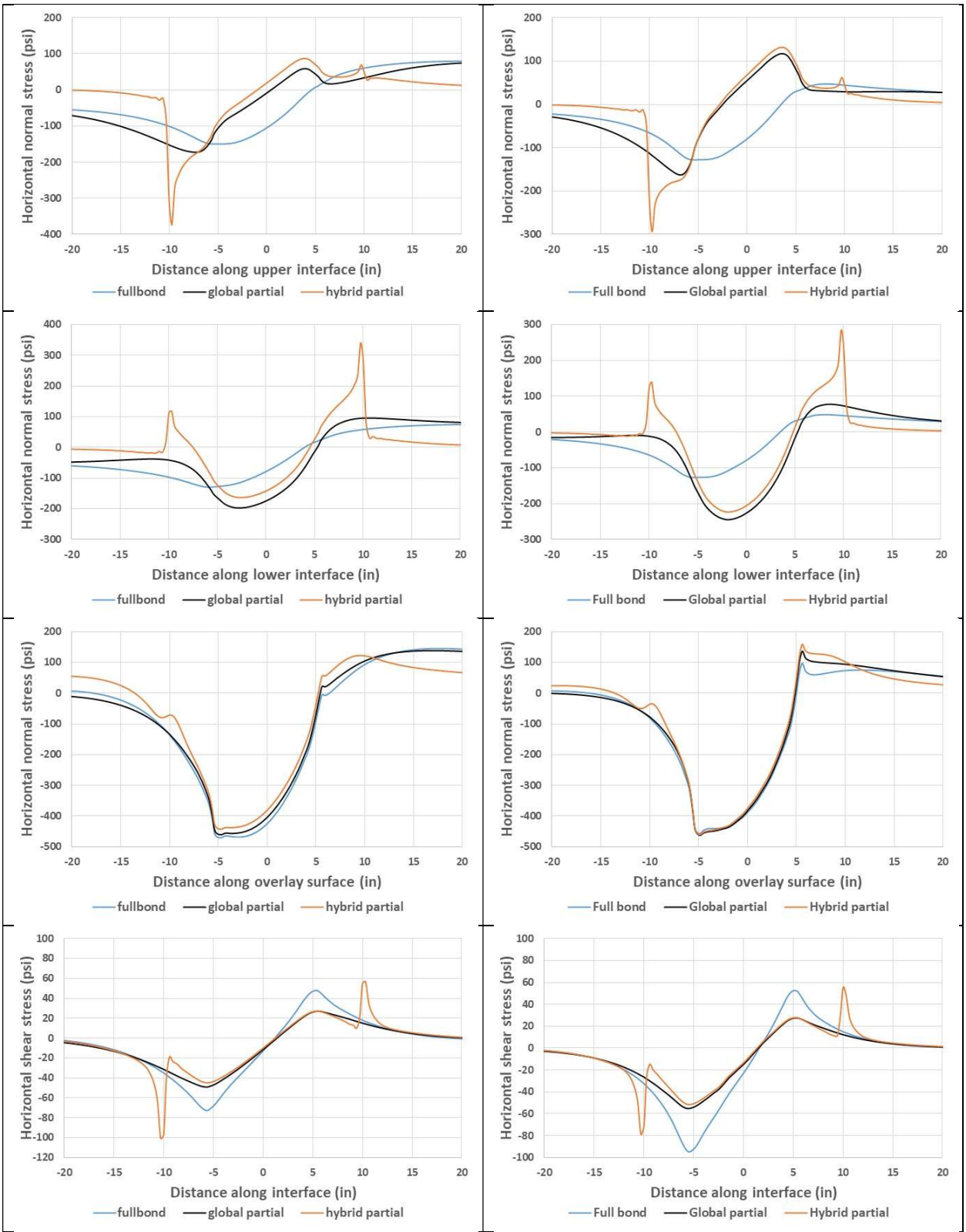


| Plane Strain | 3-D |
|---|---|

Figure A-1 Effect of scabbing (full bond vs. global partial bond vs. hybrid partial bond).

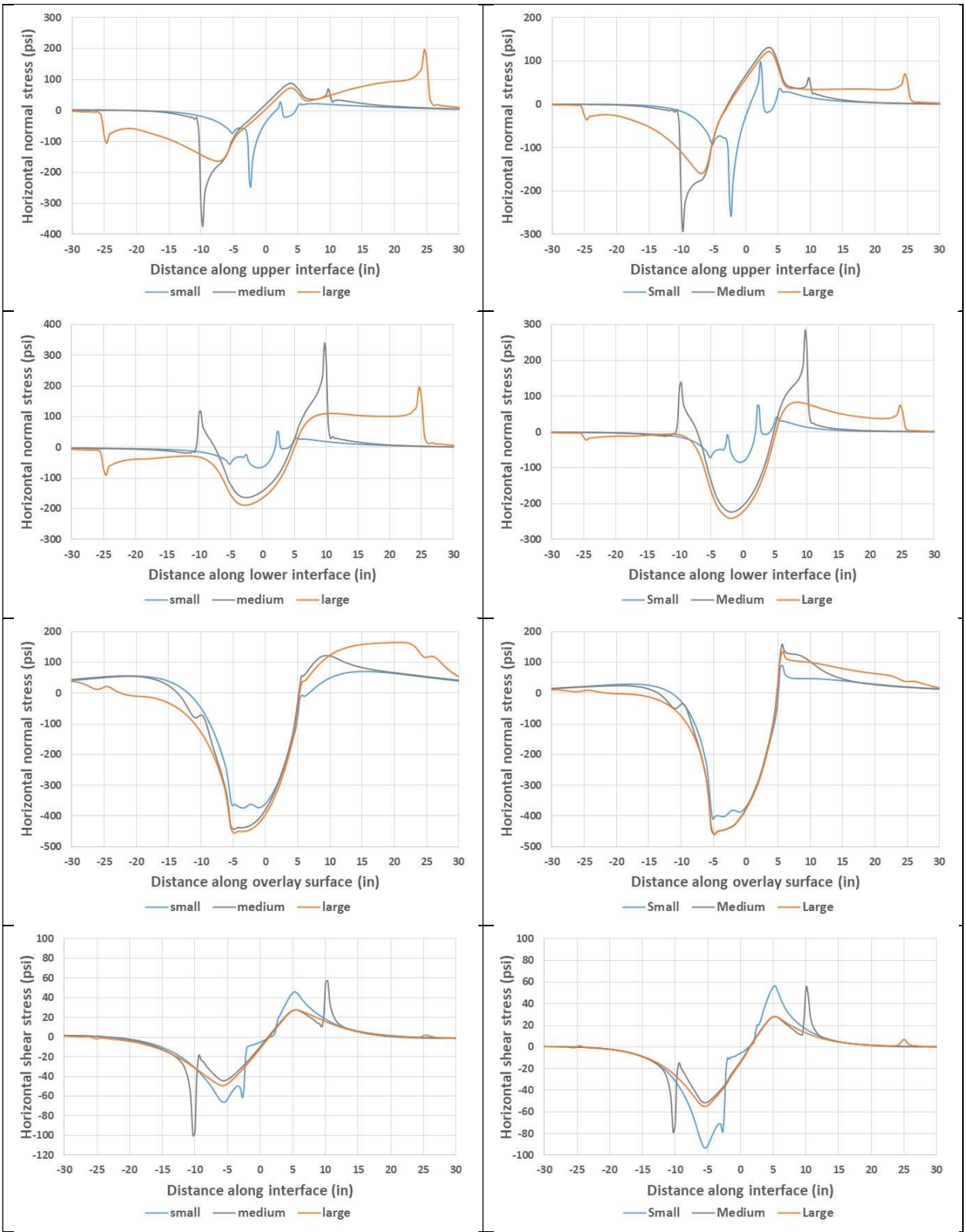


| Plane strain | 3-D |
|---|---|

Figure A-2 Effect of scab size.

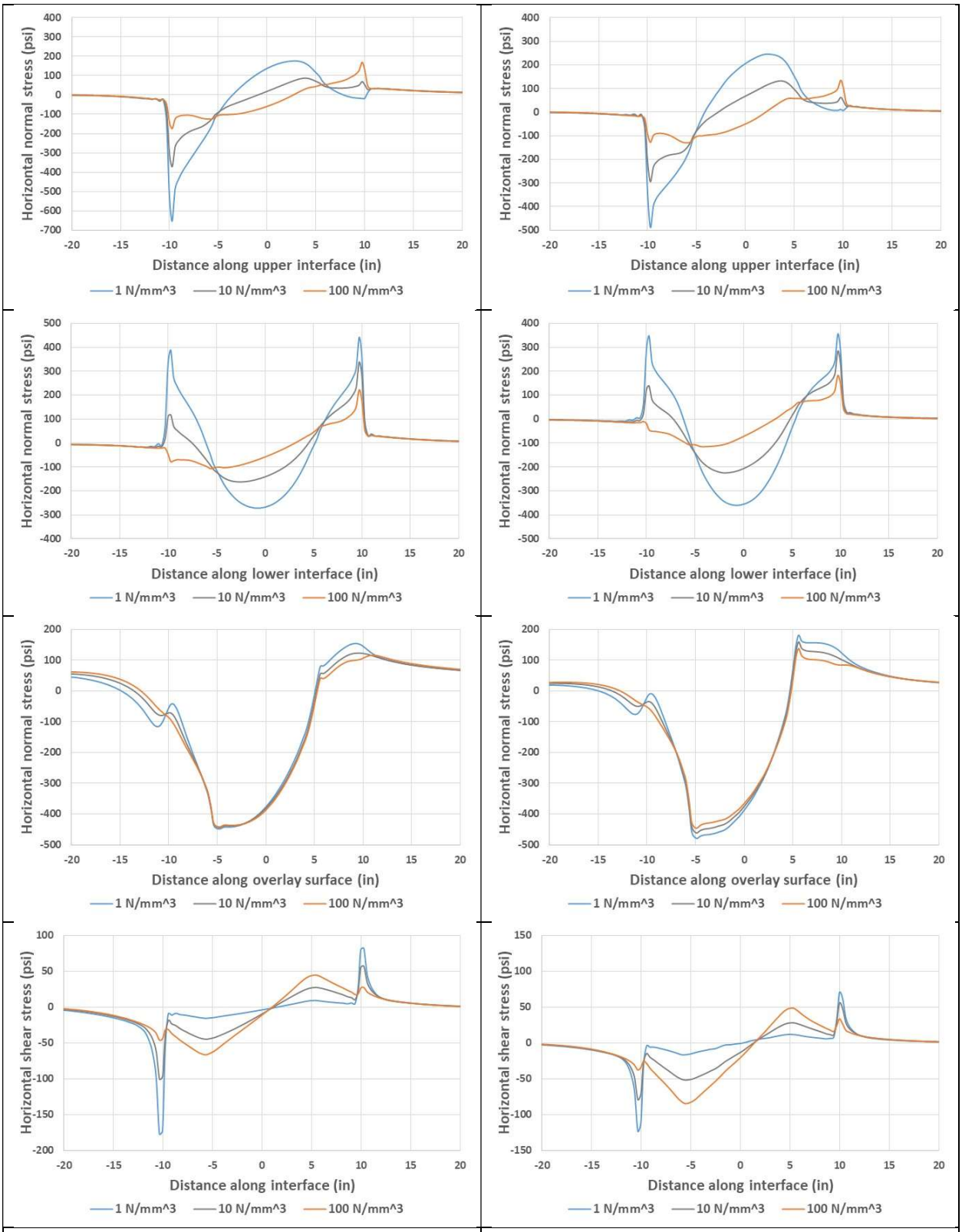


| Plane strain | 3-D |
|---|---|

Figure A-3 Effect of interface reaction modulus.

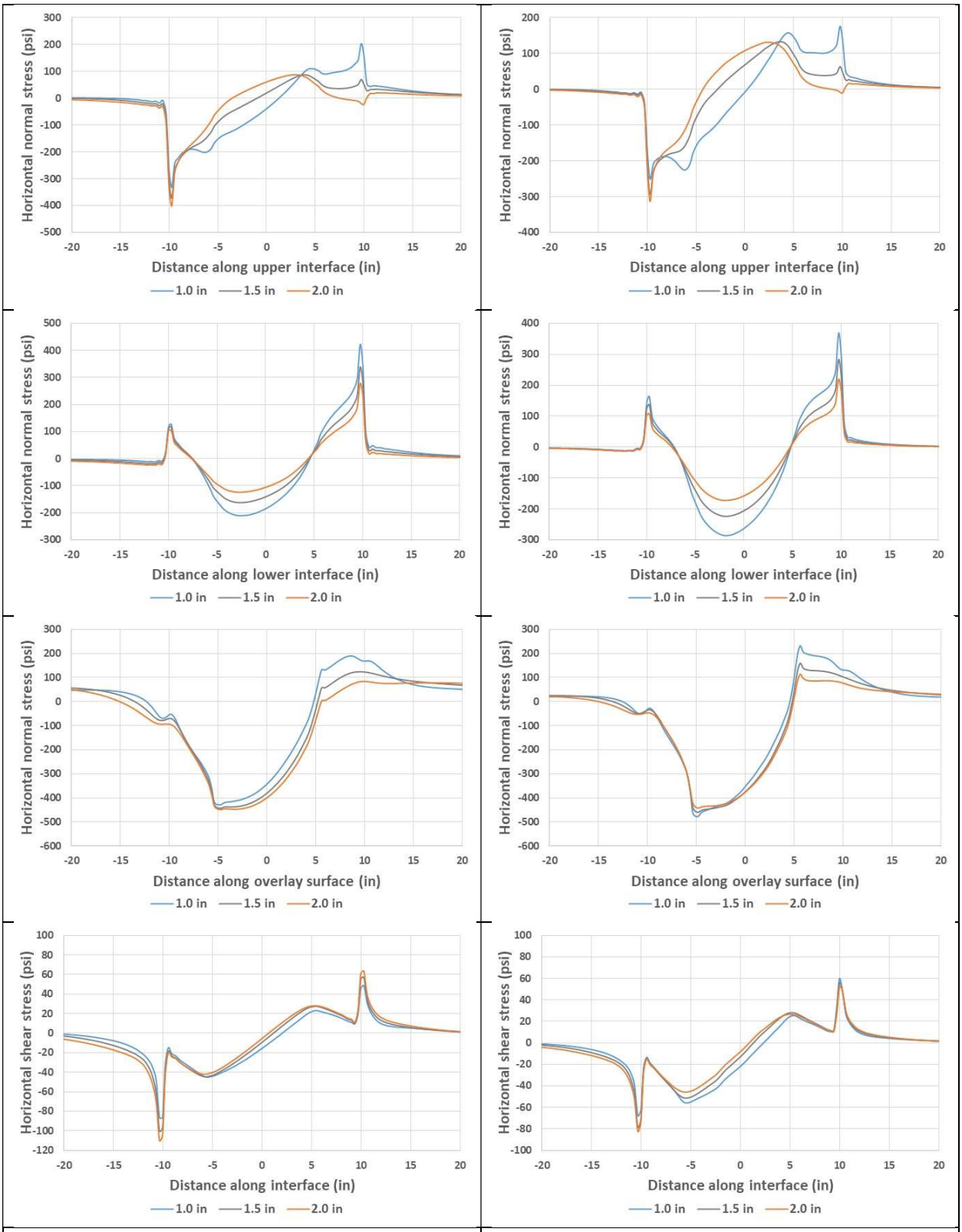


| Plane Strain | 3-D |
|---|---|

Figure A-4 Effect of overlay thickness.

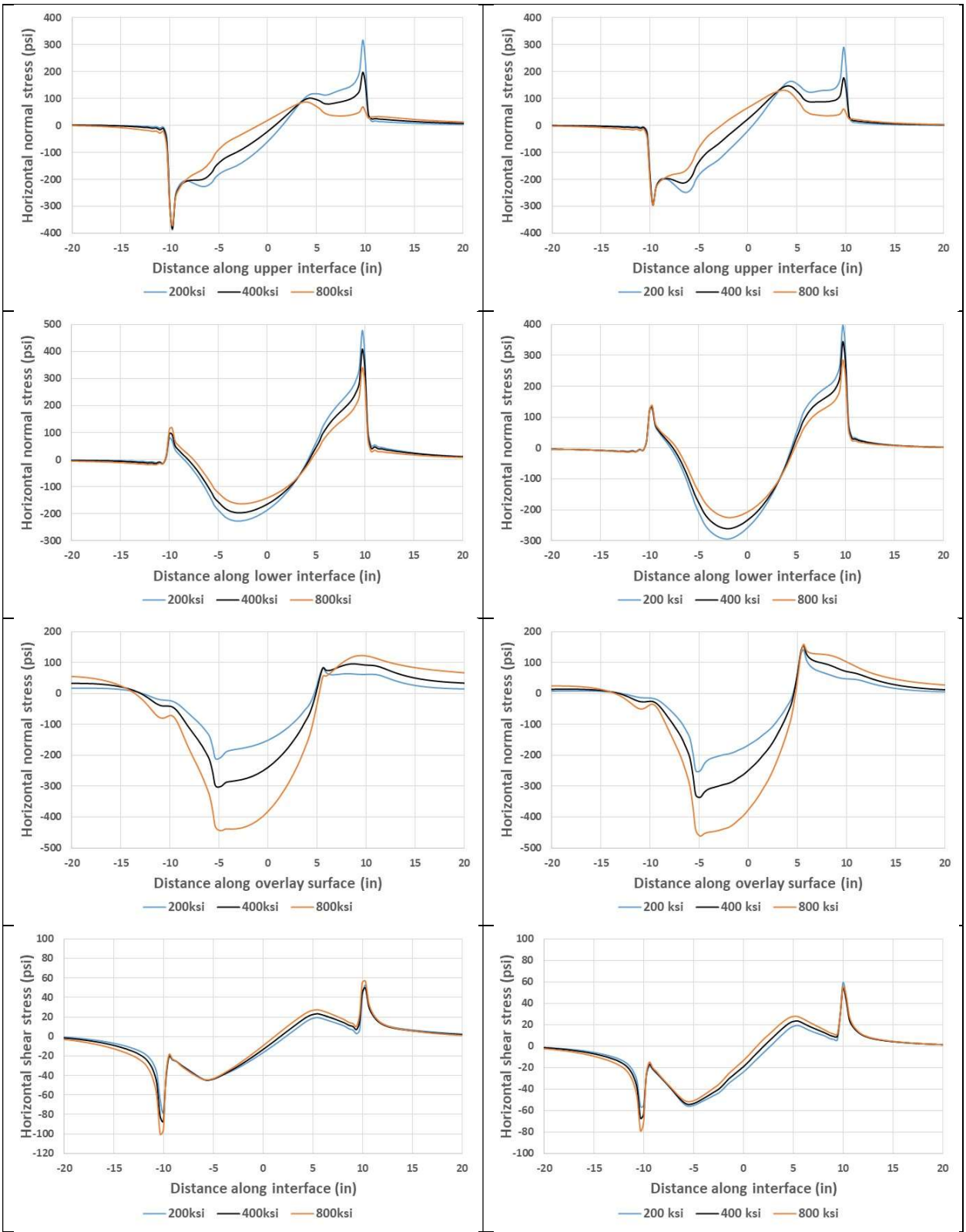


| Plane Strain | 3-D |
|---|---|

Figure A-5 Effect of overlay stiffness.

# APPENDIX B

# THREE-DIMENSIONAL FINITE ELEMENT MESH DESIGNS

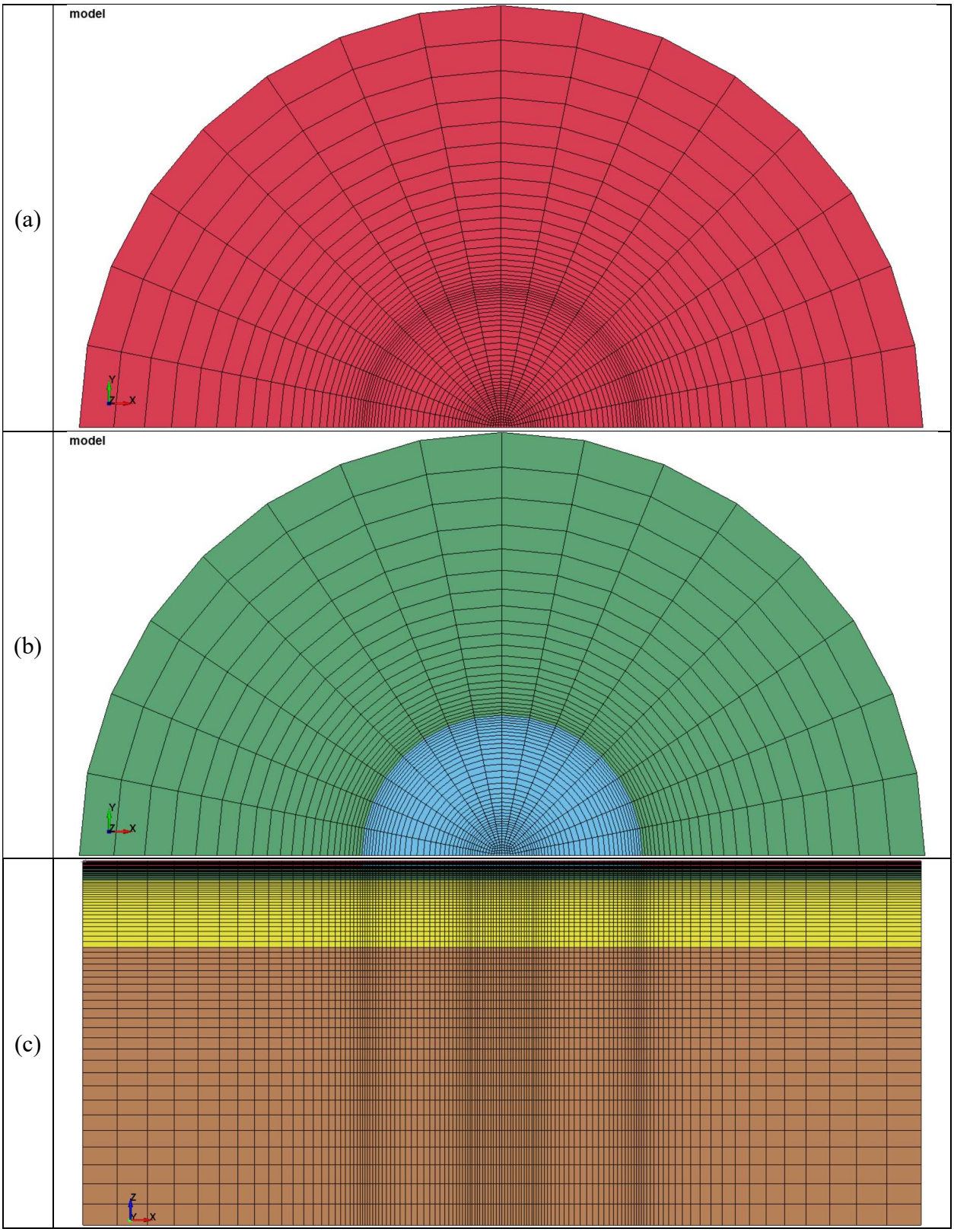


Figure B-1 Three-dimensional finite element pavement model with a large scab (25-inch): a) plan view (overlay), b) plan view (scab and underlying AC), c) front view.

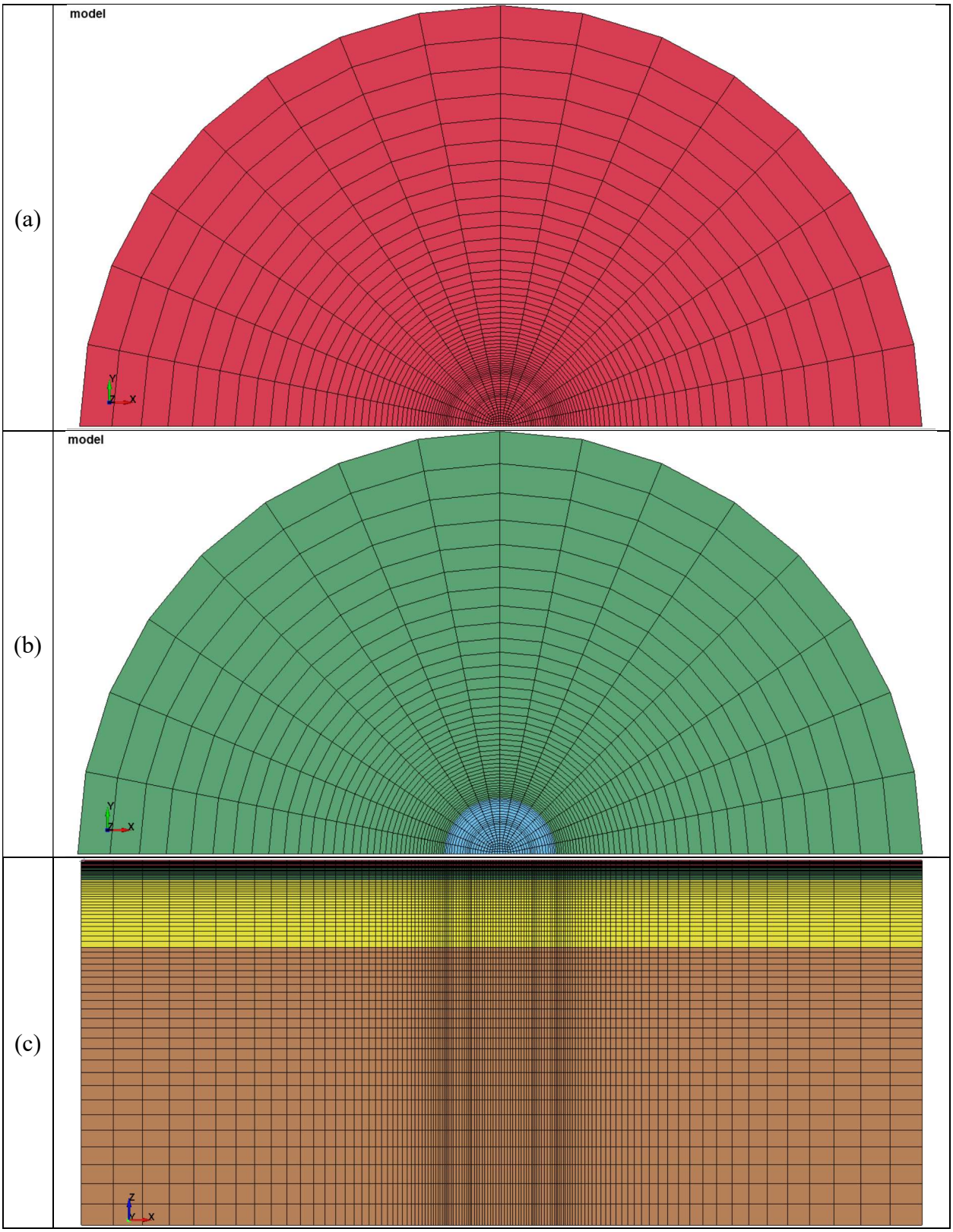

Figure B-2 Three-dimensional finite element pavement model with a medium scab (10-inch): a) plan view (overlay), b) plan view (scab and underlying AC), c) front view.

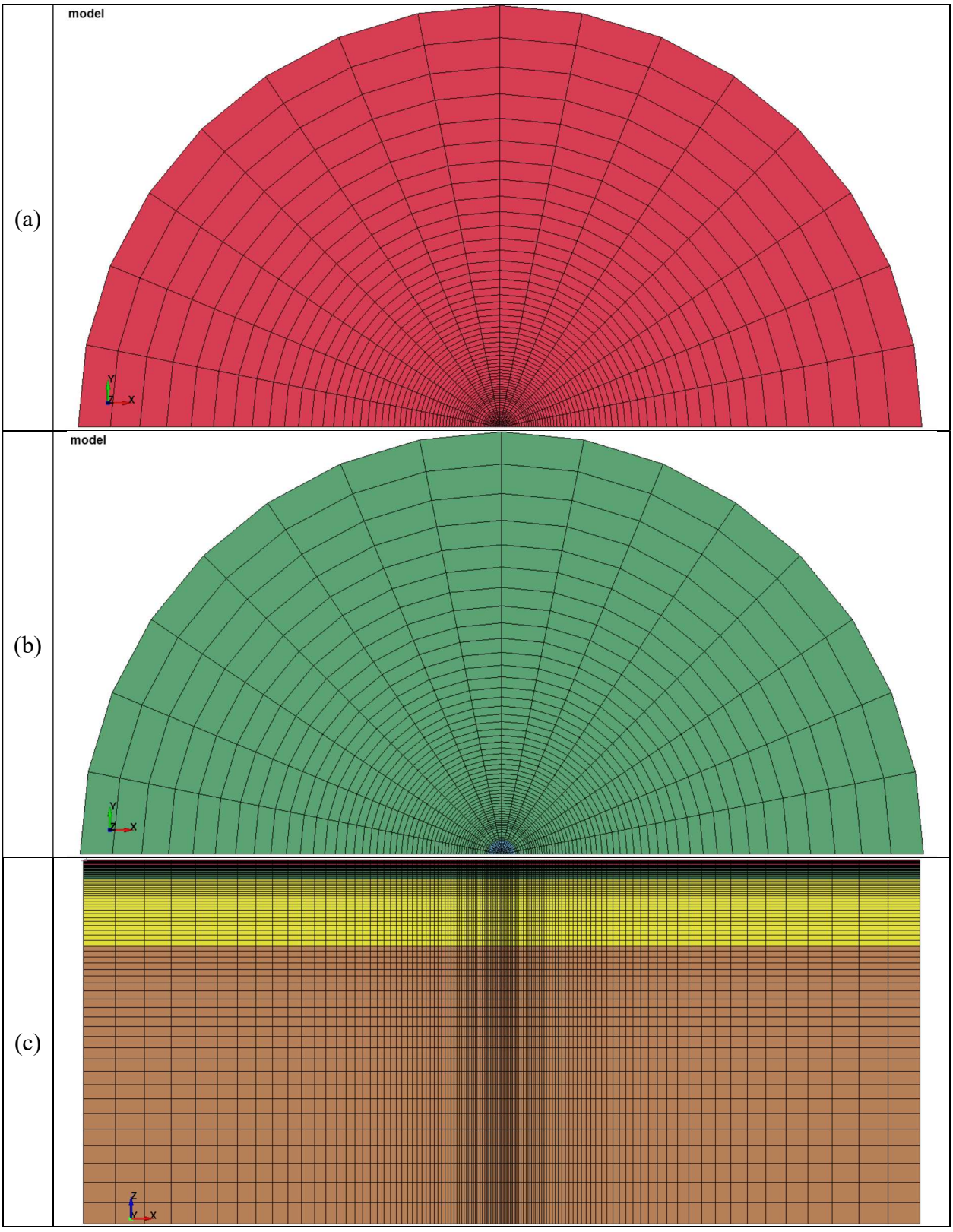

Figure B-3 Three-dimensional finite element pavement model with a small scab (2.5-inch): a) plan view (overlay), b) plan view (scab and underlying AC), c) front view.